2022

Development of Novel Intracavitary Intensity Modulated Brachytherapy Applicators for Optimizing the Target Coverage in Gynecologic Malignancies, Monte Carlo Simulation Dosimetry

Moeen Meftahi

Development of Novel Intracavitary Intensity Modulated Brachytherapy Applicators for Optimizing the Target Coverage in Gynecologic Malignancies, Monte Carlo Simulation Dosimetry

A dissertation submitted in partial fulfillment of the requirements for the degree of Doctor of Philosophy at Virginia Commonwealth University.

By

Moeen Meftahi

Master of Science in Medical Physics

Virginia Commonwealth University, United States, April 2020

Master of Science in Nuclear Engineering

Amirkabir University of Technology, Iran, February 2009

Bachelor of Science in Physics

Bu-Ali Sina University, Iran, August 2006

Director: William Y. Song, Ph.D.

Professor, Department of Radiation Oncology

Virginia Commonwealth University

May 2022

Dedication

I would like to dedicate this very little to my loved ones, particularly my parents, from whom I have everything.

ACKNOWLEDGEMENTS

I would like to sincerely thank all my instructors in the VCU medical physics graduate program for all the best they did to teach, provide feedback, and support me during my education. I am particularly grateful to my advisor, Dr. William Song, for all his scientific insights, directions, encouragements, accommodations, supports, etc., he did to advance my research capability. In addition, I would like to sincerely thank my research committee members, Dr. Siyong Kim, Dr. Frank Corwin, and Dr. Christopher Guy, for all the feedback and support they provided me to improve my research work. I am also very grateful to Dr. Emma Fields for her excellent mentoring during my research work.

I am very grateful to my former teachers who taught and prepared me very well for such a fantastic academic opportunity.

I am also thankful to the former and present members of the Medical Physics graduate program: Dr. Laura Padilla (my excellent teacher), Katherine Goracke, Collin Wade, Mitchell Polizzi, Gabrielle Seymore, Areej Aljabal, Brittany Morgan, Anusha Liyanage, Siqiu Wang, Matthew Riblet, Nicky Mahon, Sarah Holler, Dylan Richeson, and Suman Gautam for all the help, guidance, supports, and constructive feedback I received from them.

I am the most indebted to my parents, who did their best to raise and support me throughout my life. I am very thankful for the love I received from them. I am also grateful to my siblings for their extraordinary role in my life.

I would like to state my deepest thank to my wife, who was incredibly supportive during this academic journey.

Table of Contents

Table of Figures

List of Tables

ABSTRACT

Development of Novel Intracavitary Intensity Modulated Brachytherapy Applicators for Optimizing the Target Coverage in Gynecologic Malignancies, Monte Carlo Simulation Dosimetry

By Moeen Meftahi

A dissertation submitted in partial fulfillment of the requirements for the degree of Doctor of Philosophy at Virginia Commonwealth University.

Virginia Commonwealth University, 2022
Director: William Y. Song, Ph.D.
Professor, Department of Radiation Oncology

Gynecologic brachytherapy (GYN-BT) is essential for treating cervical and endometrial cancers, the most prevalent female reproductive cancers. This technique enables high radiation doses to a target with rapid dose fall-off to protect adjacent healthy organs. This dissertation aims to address some of the limitations of intracavitary GYN-BT using an intensity modulated brachytherapy (IMBT) technique and Monte Carlo (MC) simulations. First, a novel non-invasive shielded vaginal cylinder (VC) applicator was designed to provide optimized radiation coverage for the target volume at vaginal apex, site of most recurrences without BT, for endometrial cancer BT. Physical limitations of current applicators and their resulting treatment plans, such as the cold spots in the dose distribution due to BT radiation source design and presence of air gaps/suture materials can cause significant loss of coverage in this region. The new IMBT VC was designed using GEANT4 Monte Carlo (MC) simulation, by embedding a detachable high-density metal inside a standard VC applicator to directionally modulate the radiation beam and help the optimized coverage at the region.

Second, the effect of the VC heterogeneity on dose calculation for different commercial VCs was investigated. BrachyVision Acuros (BVA), a model-based dose calculation

commercial treatment planning system capable of accounting for any inhomogeneity, was also benchmarked against MC simulations. Unlike BVA dose calculation, MC simulations showed the heterogeneity could reduce the target coverage and notably increase uncertainty when prescribing to the surface of the applicator.

Third, a novel IMBT tandem applicator was designed for BT of cervical cancer. This non-invasive approach can provide coverage for non-symmetric targets which present a big challenge in clinical applications. The novel applicator utilizes high-density iridium wires that can easily move inside a tandem base. Therefore, dynamic directional modulation of the radiation beam is achievable in any desired direction, through active insertion/removal of iridium wires in a multichannel base.

Finally, a benchmark study was implemented for another novel IMBT tandem applicator to help the ongoing clinical research. The applicator has been recently modeled in BVA TPS and has shown promising results for coverage of nonsymmetric targets in cervical cancer. Results indicated that the accuracy of the TPS in dose calculations depends notably on the phantom (and hence patient) size.

In summary, non-invasive solutions for coverage of big/nonuniform targets in cervical and endometrial cancers were successfully introduced and implemented, through applications of IMBT. Manufacturing of the applicator prototypes and development of required software/hardware would be the next steps for the advancement of the research. In addition, BVA was thoroughly benchmarked for GYN-BT dose calculations. The results may further be available for correlation with known clinical outcome.

Chapter 1. Introduction

1.1 BACKGROUND

Gynecologic (GYN) cancer is any cancer that starts in a woman's reproductive organs. Cancer is always named for the part of the body where it starts. For instance, cervical cancer begins in the cervix, which is the lower, narrow end of the uterus. GYN cancers begin in different places within a woman's pelvis, which is the area below the stomach and in between the hip bones [1]. Approximately 100,000 women are diagnosed with GYN cancer in the United States each year [2], with incidence rates of about 52.6% and 12.3% for endometrial and cervical cancers, respectively [3]. Although surgery is a primary treatment for GYN malignancies, in the case of cervical and endometrial cancers, often disease is locally advanced such that surgery is precluded or surgical pathology reveals disease extent that mandates adjuvant treatment. Brachytherapy (BT) is an integral tool for both definitive and adjuvant treatment of these two leading cancers. BT allows delivery of high radiation doses to a target with rapid fall-off to protect adjacent normal structures. BT is now mostly practiced with remotely controlled after-loading machines that allow instant loading/unloading of radioactive sources (e.g., ^{192}Ir for high dose rate (HDR) BT) inside the patient body through GYN applicators (intracavitary) or needles/catheters (interstitial). New advances in imaging techniques, 3D adaptive treatment planning, and dose-volume reporting has added precision and versatility to this powerful treatment modality in the curative treatment for cervical and endometrial cancers [3,4].

Intracavitary (IC) BT is usually preferred to interstitial (IS) BT due to being non-invasive and easier implementation. However, there are a few main challenges with this modality that could impact its efficacy and/or applications. These issues would include the target coverage and dose calculations in heterogeneous environment and will be discussed in detail as follows.

1.2 COVERAGE OF NON-UNIFORM/BIG TARGETS IN ICBT

The coverage of nonuniform/big targets is challenging with ICBT and falls inside the realm of ISBT. The latter is very painful for the patients and can lead to severe side effects, such as bleeding and trauma. It also needs extensive training for the physicians to be able to implement it. This issue has been discussed in more detail based on the cancer type in the following sections.

1.2.1 Endometrial cancer: loss of coverage in vaginal cylinder (VC) BT

Complete coverage of the cuff is critical for the patients who receive VCBT, since about 70% of the recurrences occur in this region without BT. Therefore, vaginal cuff BT using VC applicators is an integral part of patient treatment. Loss of coverage, however, can happen due to the anisotropy effect caused by the heterogeneity of the ^{192}Ir HDR BT sources (density= 22.56 g/cc) and presence of the airgaps/suture material that can restrict access to the cuff. Possible solutions to address this problem are to use needles (ISBT) or multichannel vaginal cylinders. However, both can cause severe side effects in the patients, including severe radiation toxicity due to overdosage of the targets and organ at risks (OARs) as well as trauma/pain [5]. A possible non-invasive approach to address these issues could be the intensity modulated brachytherapy (IMBT) technique, in which a shielding material would be inserted inside the standard IC applicators to allow intensity/direction modulated brachytherapy (IMBT/DMBT). Consequently, this technique provides at least one additional degree of freedom in the dose-delivery process, being the directionality of the dose distribution during treatment [14].

1.2.2 Cervical cancer: coverage of the non-symmetric target

The coverage of the non-symmetric target with the radiation field is one of the critical challenges in cervical cancer BT, brought up by the EMBRACE II clinical study. This issue demands developing state-of-the-art IC/IS (hybrid) applicators. However, the ISBT is complicated to be implemented and can cause severe side effects as mentioned above [11]. On the other hand, the capability of the standard IC applicators such as the tandem applicator for coverage of lateral extension of the tumor is significantly limited since the

dose distribution achievable with these IC applicators is symmetric. Therefore, complete coverage of the nonuniform target with these applicators will result in delivering a huge amount of dose to the OARs nearby. Alternatively, IMBT technique may be able to provide a non-invasive solution for this challenging issue.

1.3 HETEROGENEITIES IN DOSE CALCULATION

The IC applicators are usually fabricated from high density plastic materials. Some of the applicators of the kind might also have shielding materials (i.e., high-density metals) embedded in their structures. Therefore, relying on treatment planning systems (TPS) which consider all the environment around the radiation source as water based on the TG43 formalism could end up with notable inaccuracy. The following sections review two cases of the heterogeneity int ICBT that could impact the dose calculations.

1.3.1 Heterogeneity of the VC applicator

Most of the current treatment planning systems (TPS) for BT consider all material surrounding the radiation source as water to benefit from pre-calculated dose matrices for the radiation dosimetry [6]. This assumption is based on the formalism recommended by the AAPM working group TG43. However, the commercial VC applicators are made of plastic materials such as PEEK and PPSU with a significantly higher density (~1.3g/cc) than the water density (1g/cc) [7]. This inconsistency could affect the coverage of the target volume for multiple dwell positions inside a VC for a standard plan as opposed to one dwell position. This issue could be more complicated by taking the prescription point, either the surface or 5mm beyond the VC surface [8], into account. A solution to this problem could be Monte Carlo (MC) simulations. However, this approach is very slow in nature and can be very complicated to be used for clinical applications. Model-base dose calculation algorithms (MBDCA) would also offer such a capability to account for different kinds of heterogeneities. However, clinical applications of such TPS require validation of their accuracy using reference dosimetry (such as MC simulations) for each anatomical site. Such data, then, could allow transition from TG43 formalism in clinical applications [9,10].

1.3.2 The heterogeneity effect of shielding materials

A non-invasive IMBT tandem applicator, known as DMBT tandem, has been introduced previously, which offers promising results regarding the coverage of non-symmetric targets and OAR sparing for cervical cancer [12]. Nonetheless, since the applicator is made of a high-density tungsten alloy (density= 18.0 g/cc), the clinical application of this technology needs TPS capable of accounting for the metal heterogeneity, namely MBDCA. The latter also takes a robust validation of the TPS against reference dosimetry for different clinical scenarios [13].

1.4 STATEMENT OF PURPOSE

This dissertation aims to address the abovementioned problems to improve the intracavitary GYN BT for endometrial and cervical cancers. As a result, four main projects were defined and conducted as follows:

1. Design of a novel single-channel shielded applicator to optimize the coverage at the apex

   This project aims to provide a noninvasive solution for VCBT to:

   1. remove anisotropy dip
   2. minimize the effect of the air gaps/suture when present
   3. allow deep access when needed
   4. avoid overdosing the periphery sides while optimizing the coverage

2. Design of a novel shielded tandem applicator for cervical cancer to provide optimized coverage for non-symmetric target:

   This project aims to help optimized lateral coverage of the tumor extension, through an effective shielding design. To this end, a dosimetry study will be performed using the different materials (with different shielding characteristics) to determine an optimal design for fabrication of the prototype.

3. A comprehensive study on the impact of VC heterogeneity on dose calculations

This project aims to benchmark the accuracy of a commercial MBDCA in accounting for the VC heterogeneity on dose calculation and includes the following considerations:

1. the prescription point
2. study on commercial models and based on standard plans

4. Benchmarking a commercial MBDCA in modeling an IMBT tandem applicator

   The novel DMBT tandem applicator has been recently incorporated in a commercial MBDCA. This project is going to thoroughly benchmark the accuracy of the TPS in modeling of this shielded applicator.

In summary, this dissertation is going to address some of the limitations/challenges relevant to intracavitary brachytherapy. It further includes the design of two novel applicators that can improve the coverage of the target in endometrial and cervical cancers, taking advantage of the DMBT (IMBT) technique. In addition, this research project investigates the treatment planning side and benchmarks the accuracy of a commercial MBDCA, in dose calculations, which may further assist in the plan optimization processes and advancing the available innovation in ongoing clinical research.

Chapter 2. The design of a novel direction modulated brachytherapy vaginal cylinder applicator for optimizing coverage of the apex

BACKGROUND AND MOTIVES

Vaginal cylinder brachytherapy (VCBT), an effective adjuvant therapy, aims to reduce risk of recurrence for endometrial cancer patients after the surgery (primary treatment) is done. Since most of recurrences occur at the vaginal apex, complete dosimetric coverage of the target is of high importance, particularly for the patient with high-intermediate risk criteria. Providing deep access to this critical region is another challenging issue for VCBT.

In this study, some of the factors that can cause poor dosimeric coverage at the vaginal apex were identified (e.g., anisotropy effect causing up to 30% underdosage). In addition, the potential solutions to this issue as well as how to provide deep access were reviewed. The solutions would suffer from either being invasive (e.g., ISBT), being complicated to be implemented (e.g., 3D printer applicators), causing radiation toxicity (e.g., multichannel applicators), or providing limited deep access (e.g., multichannel and 3D printer applicators).

A novel concept-design VC applicator for IMBT was then introduced, which provides a non-invasive approach for the optimized target coverage and offers deep access without the abovementioned limitations as follows.

Abstract

Purpose: High-dose-rate (HDR) vaginal cuff brachytherapy (VCBT) is an effective adjuvant therapy for women with stage I endometrial cancer. Although infrequent, failures do occur, most frequently at the vaginal vault. A potential cause of failure is insufficient dosimetric coverage at the vaginal apex due to cold spots from the anisotropic dose distribution of the source. Here we propose a novel Direction Modulated Brachytherapy (DMBT)-concept vaginal cylinder (VC) applicator that resolves this dosimetric issue.

Methods and Materials: The novel DMBT-VC applicator was designed and simulated with the GEANT4 Monte Carlo (MC) code. The outer cylinder material chosen was PPSU plastic, and the central part was a detachable rod, housing a single lumen made of either PEEK plastic or an MR-compatible tungsten alloy. The PPSU-based outer cylinder, together with the inner PEEK rod provides the dose distribution of a conventional VC applicator. The PEEK rod is then replaced with an MR-compatible tungsten alloy rod of the same dimensions to generate directional pencil beams to compensate for the anisotropic cold spots. Two widely used ^{192}Ir HDR sources, VS2000 and GammaMedPlus, were simulated.

Results: The novel DMBT-VC applicator was able to remove the underdosage at the apex due to the anisotropy effect regardless of the HDR sources without unnecessarily increasing the dose to the periphery of the applicator. Also, further directional modulation to reach deeper in the apex by up to 14 mm beyond the VC surface was achievable, again without increasing the peripheral doses. Total treatment dwell times increased only by 7-13%.

Conclusions: The novel DMBT-VC applicator provides improved dose coverage at the vaginal apex by overcoming the classical anisotropy issue ubiquitous to all HDR brachytherapy sources. The next step in development of the device is manufacturing a prototype for clinical testing.

Keywords

Direction Modulated Brachytherapy Vaginal Cylinder Applicator, Apex Optimization, Monte Carlo Simulations

2.1 INTRODUCTION

Endometrial carcinoma is the most common gynecologic malignancy in the United States, comprising 6% of female cancers and 3% of all cancer deaths in women. Most women present with early-stage disease and are cured with hysterectomy and nodal staging. However, there are known risk factors that increase the risk of tumor recurrence. Of these recurrences, the primary site is the vaginal cuff [8,15–17].

In women who meet the Post-Operative Radiation Therapy in Endometrial Carcinoma (PORTEC) or the Gynecological Oncology Group (GOG) trials' high-intermediate risk criteria, vaginal brachytherapy has been shown to decrease the risk of recurrence with considerably less radiation toxicity in comparison to pelvic external beam radiotherapy [8,18,19]. Although rates of recurrence after vaginal brachytherapy are very low, there are some limiting factors in the application of vaginal cylinder brachytherapy (VCBT) that can result in underdosage of the target [20,21].

Factors that may affect dose to the vaginal mucosa include air gaps, suture material, and altered anatomy after hysterectomy, all of which cause poor contact between the cylindrical applicator and the vaginal mucosa. Additionally, dosimetric anisotropy caused by the common single channel applicator geometry and standard source designs affect the dose as well, particularly at the apex. That is, dose distributions produced by the high-dose-rate (HDR) ^{192}Ir sources are inherently anisotropic due to self-attenuation of the emitted radiation by the high-density core of the source, oblique filtration by the source capsule, and asymmetric geometry of the source capsule [22]. Consequently, the anisotropy dip can cause underdosage of the vaginal apex by as much as 30% [15]. This phenomenon more commonly affects single-channel applicators, which are the most widely used vaginal applicators. Although anisotropy can be mitigated to some extent using a multichannel applicator combined with inverse planning (e.g., the Miami applicator), this modification can cause loss of coverage at the other parts of the apex or give an unnecessary dose to the surrounding tissue, notably the lateral mucosa, leading to potentially increased radiation toxicity as target volume is also an organ at risk [23,24]. Deeper coverage of the tumors located in the apex of the vaginal cuff may also lead to increased dose to overlying sigmoid colon or bowel when treated with multichannel applicators such as the Capri™ [25]. Additionally, 3D printable patient-specific applicators

have recently been introduced to improve coverage along the length of the applicator [26]. These applicators have shown to be beneficial for better target coverage and OAR sparing in certain cases. However, there are limited options for printable shielding materials, which can restrict deep access, and that additional plan optimization steps with inhomogeneity-corrected dose calculations are necessary, consequently.

In this research, we aim to find a novel solution to remedy the anisotropy of the source for a single channel VC applicator and to provide flexible deep access at the apex when air gaps, sutures, and/or deep-seated legions may be present to improve dosimetric coverage, without introducing excessive dose to the peripheral surface. To do this, we benefit from the concept of Direction Modulated Brachytherapy (DMBT), which has been used for the design of other applicators for sites such as rectum and cervix [27–29]. The classical DMBT applicators utilize embedded shielded components to direct the radiation to a specified target while reducing dose to normal structures. Utilizing this concept, we propose a novel DMBT-type VC applicator design that addresses the aforementioned issues of anisotropy and presence of air gaps/sutures/deep legions.

2.2 METHODS AND MATERIALS

2.2.1 HDR sources

The GEANT4 MC Simulation Code Toolkit 10.06 was used for all simulations. Two widely used Varian ^{192}Ir HDR sources, namely VS2000 and GammaMedPlus (GMP), were modeled into GEANT4 using Boolean operations. Figure 2. 1 shows the physical dimensions and fabricating materials of the two sources [7] and the simulated source constructions in GEANT4. As depicted, we accounted for 2 mm of wire at the distal end of the HDR sources. The ^{192}Ir source was defined based on all its significant gamma-ray and X-ray radiations [30–32]. To get the typical dose distribution, the two HDR sources were then virtually placed inside a standard water phantom, and the deposited dose was recorded, as will be discussed in the section "*Planning and Optimization*".

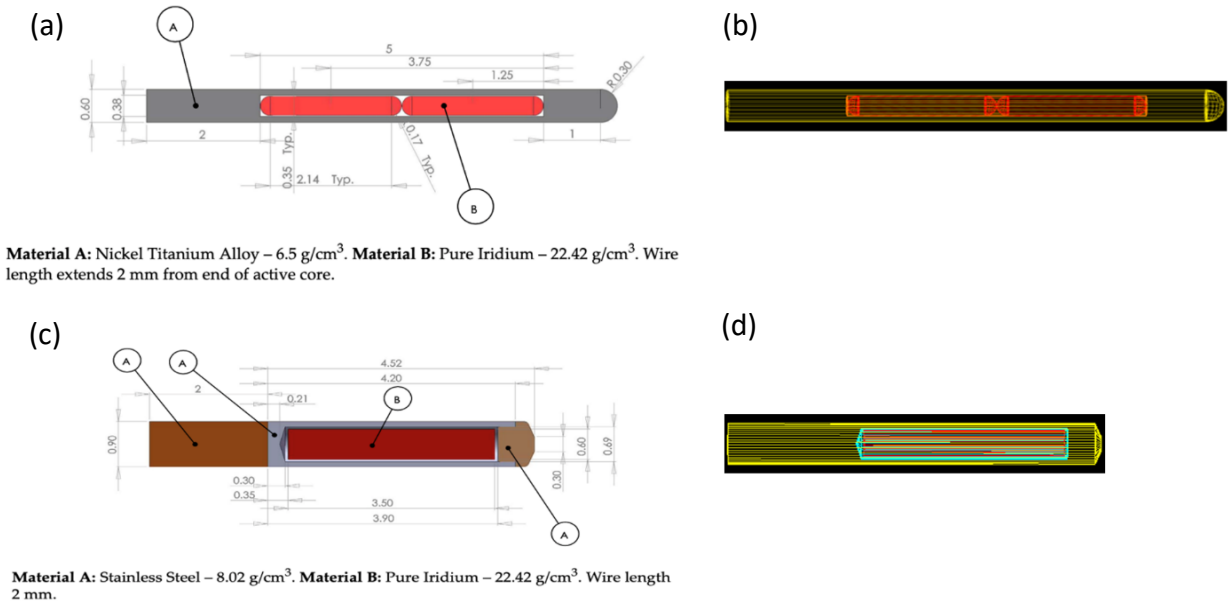

Figure 2. 1 VS2000 source (a) 17, simulated VS2000 source in GEANT4 (b), GMP source (c) 17, and simulated GMP source in GEANT4 (d). The unit for the dimensions is in millimeters [mm].

2.2.2 Anisotropy effect

To show how the anisotropy effect can cause lack of coverage at the apex, we assessed the size of the anisotropy dips for the two VC designs as described by Kim *et al* [33] based on the MC simulation results. These two VCs have diameters of 30 mm but two different top thicknesses (TT) of 5.8 mm and 9.2 mm (i.e., distance from the end of lumen to the tip of the applicator), for older and latest models, respectively. Optimal standard plans prescribed to 5 mm beyond the cylinder surface were obtained using the two simulated HDR sources. Detailed information about simulations and planning is given in the section 2.2.4.

2.2.3 Design of the DMBT-VC applicator

The novel DMBT-VC applicator was modeled in GEANT4 using Boolean operations, to be a 30 mm diameter with 3 mm of TT, a single lumen, polyphenylsulfone (PPSU) plastic solid cylinder, with a density of 1.31 g/cm^3. The inner central part of the applicator, which includes the lumen of 1.5 mm diameter at the center, was a detachable 8 mm diameter rod made of polyether ether ketone (PEEK) plastic, with a density of 1.30 g/cm^3. The

PPSU and PEEK plastics are readily used by Varian for the fabrication of their VC applicators, and detailed information about them can be found in the AcurosBV® Algorithm Reference Guide (Varian, A Siemens Healthineers Company, Palo Alto, CA) [7]. In order to provide directional modulation, an *MR-compatible* tungsten alloy rod [29,34] with same dimensions as that of the detachable PEEK rod and a density of 18.0 g/cm^3 was incorporated into the DMBT-VC design. A GEANT4-simulated virtual applicator design is shown in Figure 2. 2.

The applicator works in two steps: (1) the PPSU-based outer cylinder is used together with the inner PEEK rod in place to provide the dose distribution of a conventional VC applicator, and (2) the central PEEK rod is replaced with the MR-compatible tungsten alloy rod of the same diameter by simply sliding them in and out of the outer PPSU cylinder, which is placed in the patient and held stationary by a table-mounted clamp. With the inner tungsten alloy rod in place, the applicator generates a directional “pencil-like” beam to help optimize the coverage at the apex. There are scatter contributions to the beam due to various interactions inside the tungsten rod, however, this pencil-like beam shape mainly arises from the ^{192}Ir’s primary radiation directed along the lumen. Therefore, the anisotropy dip can be removed and, in addition, the dosimetric effect of the air gaps/sutures minimized at the high-risk region of the vaginal cuff through inverse optimization of available dwell times and positions between the PEEK and tungsten alloy applicator configurations.

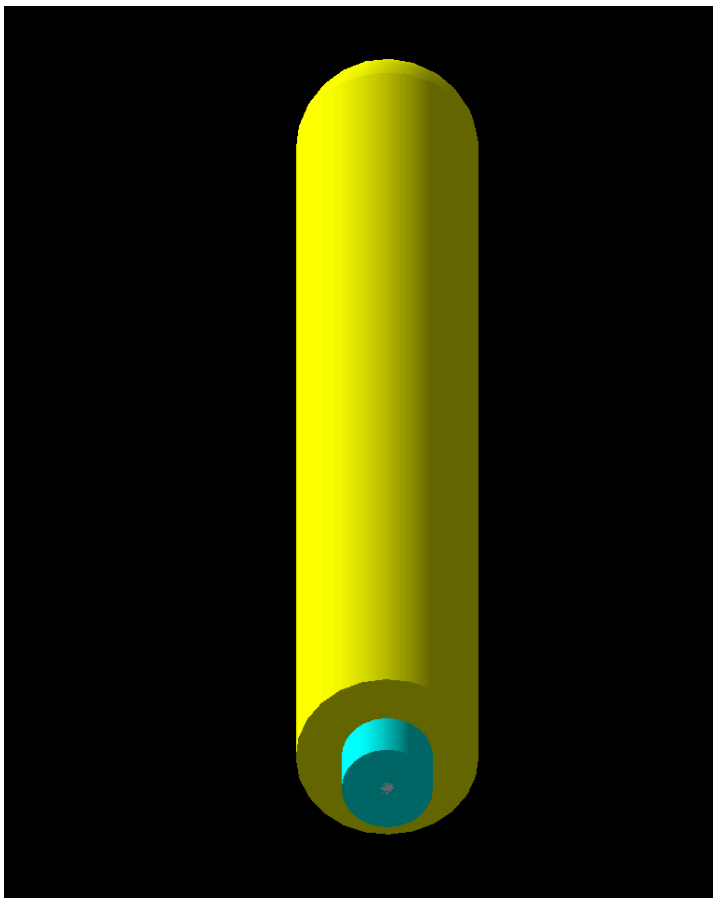

Figure 2. 2 The DMBT-VC applicator designed in GEANT4. The PPSU-based outer cylinder (yellow) and the detachable PEEK rod (blue), with built-in central lumen where a HDR source can traverse, are shown.

2.2.4 Planning and optimization

2.2.4.1 Removal of the anisotropy dip

Based on standard plans obtained from the commercial BrachyVision® Treatment Planning System (TPS), the two sources were separately placed inside a 30 mm diameter solid VC applicator with the inner detachable PEEK rod with a central lumen. The applicator was placed inside a virtual water phantom with the dimension of 30×30×30 cm^3, with the tip of the applicator at the center of the phantom for all dose calculations. We then repeated the MC dose calculations with the detachable tungsten alloy rod in the place of the PEEK rod. These steps were performed using both simulated VS2000 and GMP ^{192}Ir HDR sources at 5 mm dwell position spacing throughout the single central

lumen. For each dwell position, 10^9 particle histories were generated and dose deposition inside the water phantom was scored with a uniform mesh size of 1 mm. Due to the radial symmetry of the sources, only 2D data acquisition along the source/applicator axis was necessary for all simulations. The final dose distributions for each source dwell position and for both PEEK and tungsten inserts were given as input to an in-house-written inverse optimizer. Optimal plans were generated by balancing the weighted contributions from the individual dose distributions with the goal of minimizing the anisotropy at the apex without altering the dose to the remaining vaginal mucosa.

2.2.4.2 Deep dosimetric access at vaginal cuff

The ability of the applicator to mitigate the dosimetric underdosage at the vaginal cuff due to the presence of air pockets, sutures, or simply deep-seated targets was also investigated. Here we studied a clinical case in which a significant amount of localized suture prevented optimal coverage, subsequently leading to underdosage of the target [35]. Three scenarios were considered with the goal of seeing how far the prescription isodose line could be extended locally in the apex direction without increasing the dose at the periphery: (1) to reach 5 mm beyond the prescription line around the area covering the suture, (2) to reach the maximum possible coverage at that region, and (3) to provide 5 mm uniform extension beyond the prescription line at the apex. The apex optimization was performed using the in-house-developed inverse optimization algorithm for all three cases.

2.3 RESULTS

2.3.1 The HDR sources

The typical dose distributions of the simulated VS2000 and GMP ^{192}Ir sources inside the water phantom are shown in Figure 2. 3, illustrating the differences in the anisotropy effect at the apex between the two source models. The normalization point is 10 mm away from the center of the iridium core perpendicular to the source axis. The results show that the anisotropy dip of the VS2000 source (Figure 2. 3a) is more conspicuous than the GMP (Figure 2. 3b).

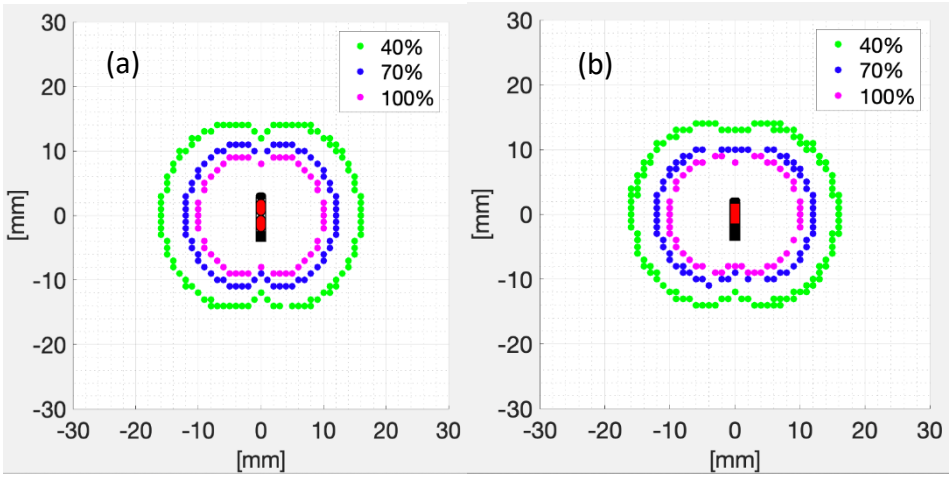

Figure 2. 3 Coronal views of the normalized isodose lines (color dots) are shown for VS2000 (a), and GMP (b), 192Ir sources. The normalization point is 10 mm away from the center of the iridium core perpendicular to the source axis with the prescription dose of 700 cGy × 3 fractions.

2.3.2 Anisotropy effect based on the VC design

The 100% isodose lines prescribed to 5 mm beyond the applicator body are given in Figure 2.4 for different VCs with different HDR sources and the TTs. The distance from the lowest 100% dose point at the apex in the dip to the 5-mm-prescription-line was 6 mm and 4 mm for the VS2000 source with the TTs of 9.2 mm (Figure 2. 4a) and 5.8 mm (Figure 2. 4c), respectively. This distance was also 4 mm and 3 mm for the GMP source with the TTs of 9.2 mm (Figure 2. 4b) and 5.8 mm (Figure 2. 4d), respectively. As illustrated, the underdosage to the prescribed area (i.e., within 5 mm from the applicator surface) due to the anisotropy effect is greatest for the VC applicator with the TT of 9.2 mm and using the VS2000 source.

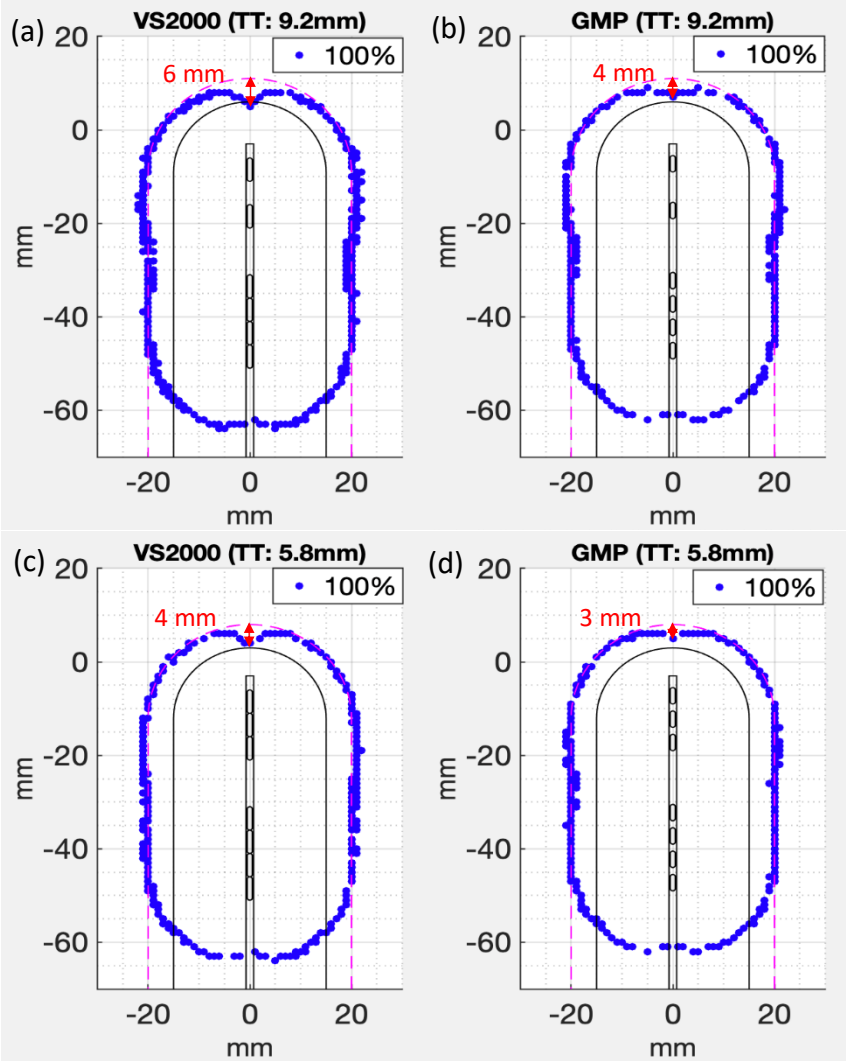

Figure 2. 4 100% isodose line (blue dots) prescribed to 5 mm beyond the surface of 30 mm diameter VCs using VS2000 and GMP sources. The top thickness (TT) is 9.2 mm for the upper row and 5.8 mm for the lower row. Note the size of the anisotropy dips are significantly different based on the source design and TTs. The maximum distance from the isodose lines to the prescription line (pink dashed line) is 6 mm and 4 mm for VC with the TT of 9.2 mm and VS2000 (a), and GMP (b), respectively. Also, the distance is 4 mm and 5 mm for the TT of 5.8 mm and VS2000 (c), and GMP (d), respectively. Note the volume not receiving the prescription dose due to anisotropy effect is the most for the VC with the TT of 9.2 mm and VS2000 source (a). The outline of the VCs, central lumen, and dwell positions are shown in solid black lines.

2.3.3 The DMBT-VC applicator

The dose distributions of the simulated HDR sources using both the PEEK and tungsten alloy inserts are shown in Figures 2. 5 & 2. 6. The 100% isodose lines in Figure 2.6 represent the prescription dose of 2100 cGy (700 cGy × 3 fractions). As illustrated, the apical and peripheral dose fall-off are significantly different between the HDR sources inside the PEEK rod compared to when they are inside the tungsten alloy rod but appear to be mutually compensatory, especially at the apex.

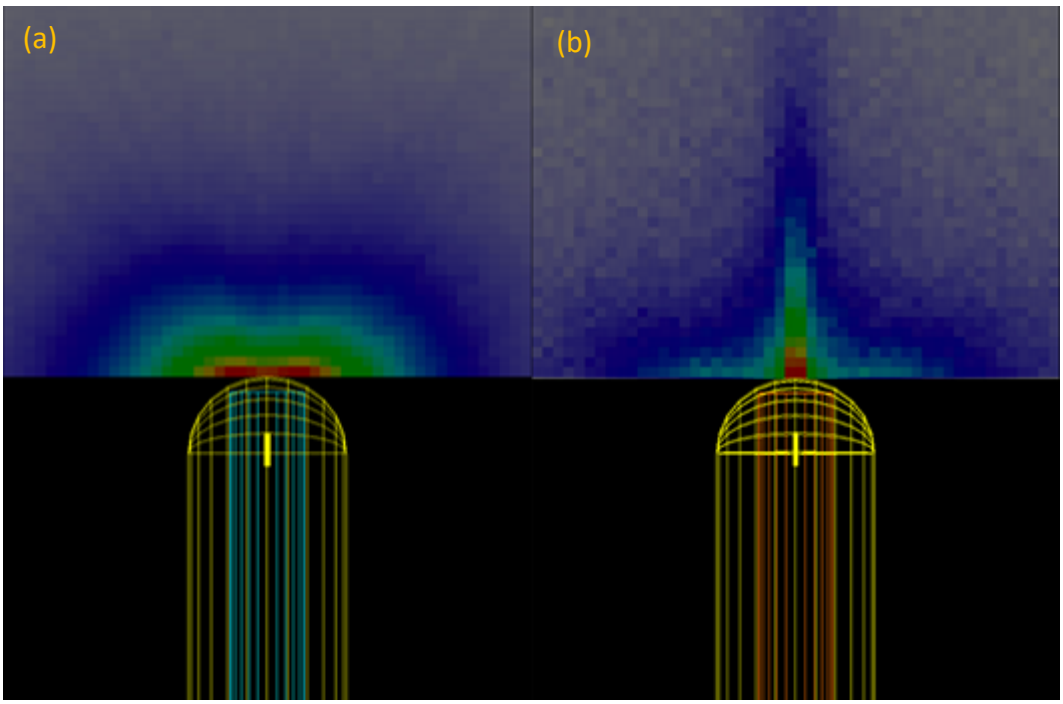

Figure 2. 5 Apical dose distribution of the DMBT-VC applicator simulated in GEANT4. Applicator with the PEEK rod in place (a), displaying a clear anisotropy effect at the apex. Applicator with the tungsten alloy rod in place (b), generating a pencil-like beam.

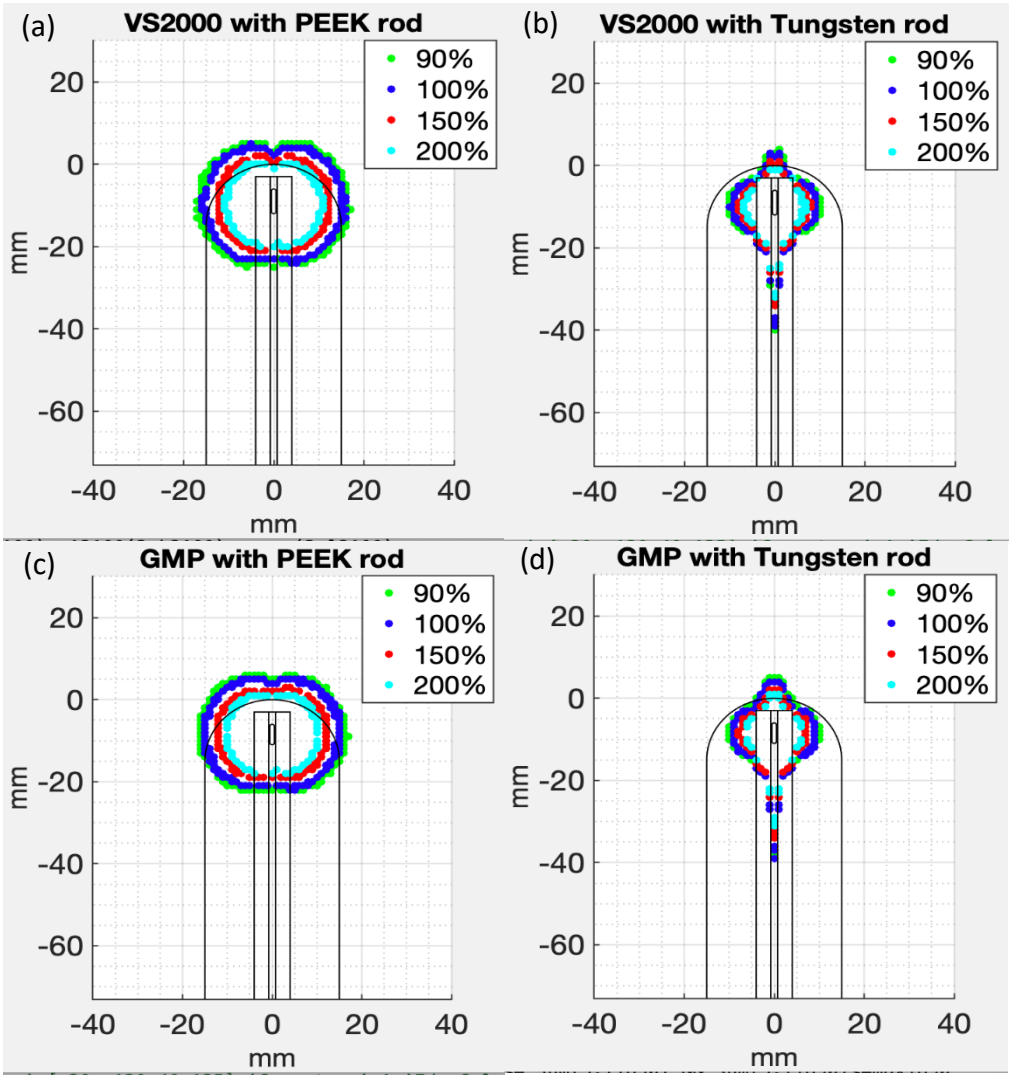

Figure 2. 6 Normalized isodose lines (color dots) at its first dwell position in the applicator are shown. 100% dose indicates a dose of 2100 cGy. VS2000 source with the PEEK (a) and tungsten alloy rods (b). Also, GMP source with the PEEK (c), and tungsten alloy rods (d). Solid black lines illustrate the outline of the outer PPSU cylinder, detachable rods, central lumen, and the dwell positions of the HDR sources.

2.3.4 Removal of the anisotropic dips

The optimized dose distributions produced by the DMBT-VC applicator, which are the weighted sums of the dose distributions from the PEEK and tungsten alloy rods to effectively remove the anisotropy at the apex, are illustrated in Figure 2. 7, for the two sources. In the case of the PEEK insert, the 100% isodose line prescribed to 5 mm beyond the applicator surface dips due to anisotropy with maximum differences in distance between the desired and actual isodose line of 3 mm and 2 mm for the VS2000 and GMP sources at the apex, respectively. However, using the pencil-like beam generated through the tungsten alloy insert and with subsequent inverse optimization of the dwell times for both the PEEK and tungsten alloy inserts, the ubiquitous anisotropic dips at the critical apex region were essentially eliminated, all without increasing the dose to the peripheral surfaces along the prescription line. The total treatment dwell times needed for the removal of the anisotropy dip showed an increase of 13% and 7% for the VS2000 and GMP sources, respectively, compared to the standard plans with the PEEK rod (Figures 2. 7a & 2. 7c).

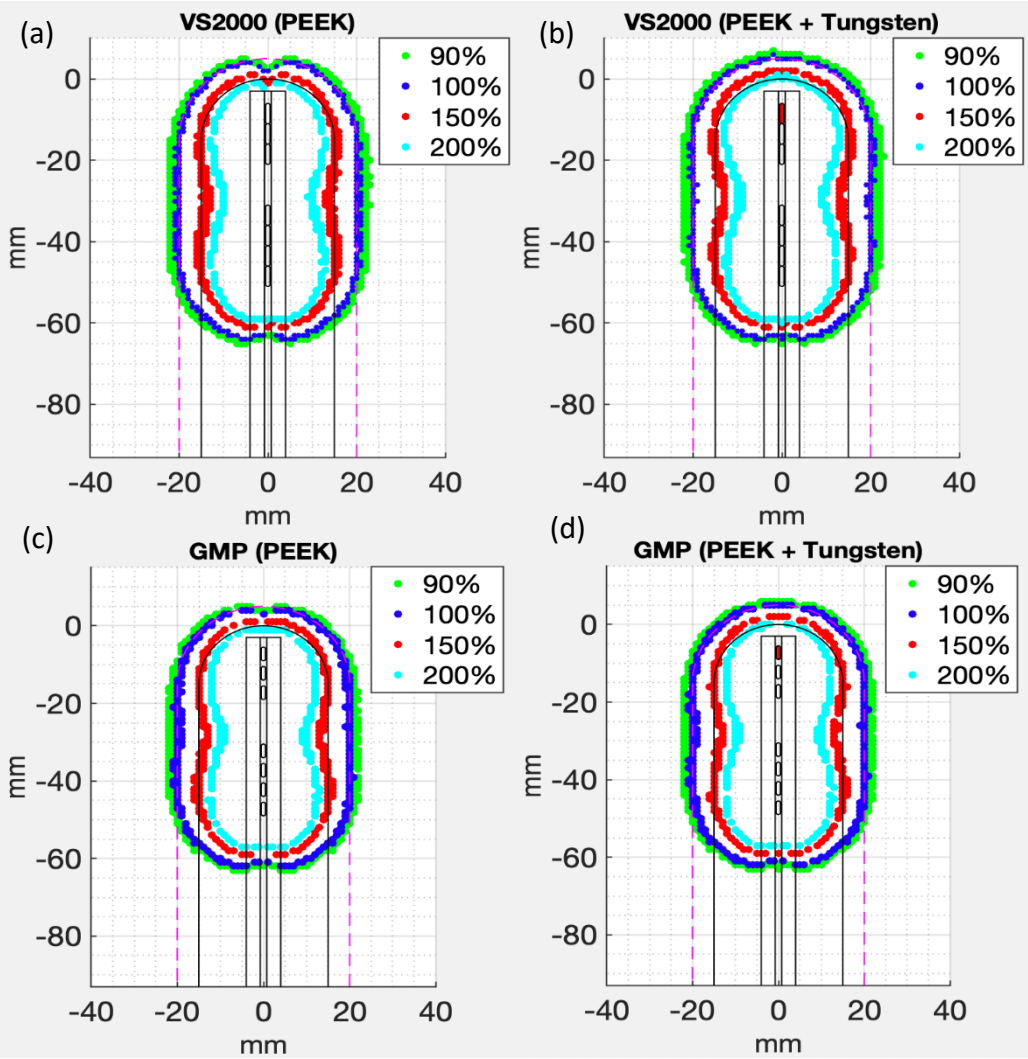

Figure 2. 7 Standard clinical plans with 100% isodose lines optimally covering the prescription to 5 mm beyond the applicator surface (pink dashed line), with the PEEK inner rod, using the VS2000 (a), and GMP (c), sources. An anisotropic dip of about 3 and 2 mm in magnitude are shown at the apical region, respectively. Inversely optimized plans with the DMBT-VC applicator, with the combined use of the PEEK and tungsten alloy inner rods, using the VS2000 (b), and GMP (d), sources. Note that an anisotropic dip is completely removed without increasing the dose to the periphery. The outline of the VCs, central lumen, and dwell positions are shown in solid black lines. Dwell positions inside the PEEK and tungsten rods are shown in black edge and red face, respectively. Colored dots are the isodose lines listed.

2.3.5 Deep dosimetric access at vaginal cuff

Figure 2. 8 shows that the 100% isodose line can be flexibly extended beyond the 5 mm prescription line (dash pink line) to cover up to 9 mm deeper (14 - 5 = 9 mm) at the apex. For the 5 mm (Figure 2. 8b) and 9 mm (Figure 2. 8c) isodose extensions would increase

the total treatment dwell times by 42% and 75%, respectively. Figure 2. 8d shows a scenario where the dose can also be extended uniformly in the apex direction by 5 mm beyond the prescription line without increasing the peripheral dose, demonstrating the additional flexibility of the DMBT-VC applicator. In this case, an increase of 28% was recorded for the overall treatment dwell times.

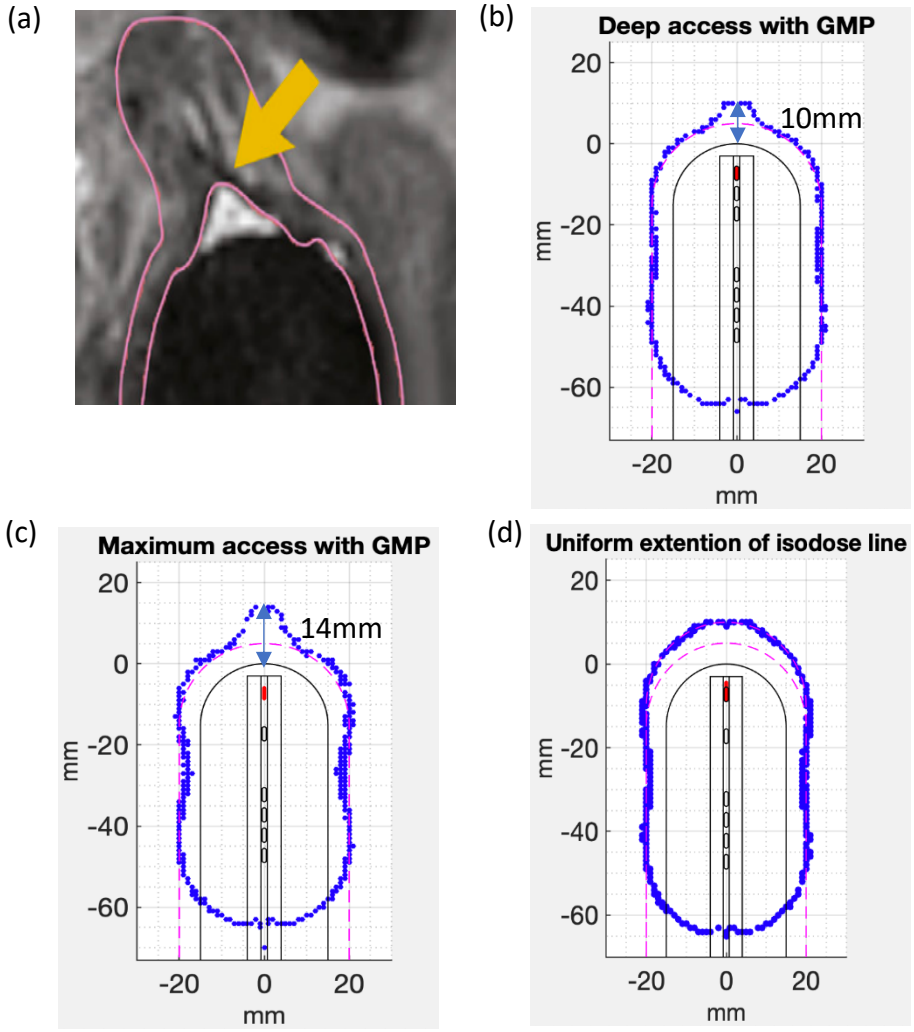

Figure 2. 8 An example clinical case showing a significant amount of suture material present at the apex 23 (a), and 5 mm extension of the 100% isodose line (blue dots) beyond the prescription line (pink dashed line) for target coverage at the apex while maintaining peripheral dose with the novel DMBT-VC applicator (b). The prescription isodose line can be extended up to 14 mm (maximum possible access) from the applicator's apical surface (c), as shown. Also, a maximum 5 mm uniform extension of the prescription isodose (d), beyond the prescription line at the apex is possible without increasing the peripheral dose. All cases shown are generated with the GMP source.

2.4 DISCUSSION

The goal of adjuvant vaginal cuff brachytherapy is to reduce the risk of vaginal vault recurrence in women with endometrial cancer. Here we show that using a novel DMBT-VC applicator design the ubiquitous underdosage phenomenon at the apex can be eliminated, which we hope can further improve the positive results associated with the treatment [33,36,37].

We simulated two widely used ^{192}Ir HDR sources with differing degrees of the anisotropy effect due to their different core and encapsulation designs (Figure 2. 3). The effect is more notable for the VS2000 source mainly due to more attenuation (oblique filtration) inside the longer iridium core (5 mm vs 3.5 mm) (Figure 2. 1a-b). Furthermore, we showed how some of the VC models (perhaps still in use) can significantly accentuate the anisotropy effect for standard plans at the critical apical region (Figure 2. 4). This is because the bigger the TT indicates longer distances from the source needs to be covered. At longer distances, the anisotropy dip is worsened due to the additional oblique filtration that occurs inside the applicator and the medium.

Nonetheless, the feasibility of the DMBT-VC applicator to remedy the anisotropy effect with standard cylinders/sources has been effectively demonstrated. The 3 mm of the TT in the DMBT-VC design allows better access to the target volume at the apex and reduces the size of the anisotropy dips with the PEEK rod in place (Figures 2. 7a & 2. 7c). Therefore, the removal of the anisotropy dips with the tungsten rod in place is readily achievable through inverse optimization (Figures 2. 7b & 2. 7d). This was all achieved with reasonable increase in the total treatment dwell times of 7-13%, translating to about 23-45 sec increase over 5.8 min, per fraction, assuming a 10 Ci ^{192}Ir HDR source, for our standard plans. There is, of course, an additional step needed to exchange the inner PEEK rod to the tungsten alloy rod during treatment, which may take few minutes for an experienced operator (i.e., interrupt treatment delivery, replace the inner rod, reconnect the channel, open/close the vault door, etc.). Otherwise, the rest of the treatment delivery steps should be identical between the conventional cylinder treatments to that of the DMBT-VC applicator.

Further, the applicator was able to provide coverage for deeper-seated targets (Figure 2. 8). This flexibility is allowed due to the penetrating pencil beam that is generated through

the tungsten alloy rod (Figure 2. 5b and Figures 2. 6b & 2. 6d), which offers fast dose fall-off laterally as well, offering synergistic and compensatory addition to the typical dose distributions generated in standard applicators (Figure 2. 5a and Figures 2. 6a & 2. 6c). This unique feature also allowed a uniform extension of the dose by 5 mm beyond the prescription line in the superior direction without increasing the peripheral dose (Figure 2. 8d). Such capability could be helpful when there is a uniform air gap that cannot be closed between the applicator tip and the vaginal cuff, for example. It is also worth mentioning that there are notable dose tails extending inferiorly inside the tungsten rod as shown in Figures 2. 6b & 2. 6d, resulting from dose deposited inside the lumen (i.e., in air). Here, we considered 2 mm cable length at the inferior side of the sources for the GEANT4 simulations. Consequently, the attenuation inside the full length of the cable was not accounted for. Additionally, because of the voxel size (1 mm^3), dose has been volume-averaged at the boundary of the lumen (diameter=1.5 mm) for the tungsten rod, resulting in slightly exaggerated values at that region. Since we only need the dwell positions close to the superior tip of the applicator, for the tungsten rod, this would not harm the integrity of the plans inferiorly (Figure 2. 8, for example), thus of no clinical consequence for our study.

A study by Sapienza *et al* [38] found that the incidence of the air gaps amongst a large pool of patients (n=675) was 67%, with more than half of the air gaps being located at apical part of the cylinder (i.e., one-third of all patients). They mentioned the mean dose reduction (cold spots) to the target associated with the air gaps varied from 9.2% to 29.3%. These reductions will likely be more when suture material is present. Certainly, the novel applicator has shown its flexibility in compensating for any random air gaps or sutures as demonstrated in Figure 2. 8.

The potential workflow for this universal DMBT-VC applicator would include an optional initial imaging (X-Ray/CT/MRI) of the patient with the PEEK inner rod in place. Therefore, there is no need for an additional dummy placeholder piece to facilitate the imaging for proper orientation verification of the tungsten alloy shield, as suggested elsewhere [26,39]. The next step would be to create a clinical plan through inverse optimization, which removes the anisotropy effect. This plan can be further modulated when air gaps/sutures are present or when simply clinical need warrants it. Then, the patient will receive the

treatment with the PEEK inner rod in place, first. At the end of the first treatment portion with the PEEK rod, the operator needs to interrupt the treatment delivery to go inside the vault to replace the PEEK rod with the tungsten alloy rod while the outer PPSU cylinder is steadfast held in place by an external clamp. The PEEK/tungsten rod tip position will then be secured using a groove mark on the rods while the external clamp holds the outer PPSU cylinder in place. This step may reasonably take few minutes. Finally, the patient will be treated with the tungsten alloy inner rod in place to complete the second portion of the treatment plan.

The proposed novel applicator is designed to compensate specifically for the ubiquitous anisotropy dip at the apex direction only. Thus, the main limitation of the design would be that it cannot provide flexible coverage to complex target shapes in general (e.g., with asymmetric extension laterally), unless combined with multi-channel cylindrical applicators (e.g., Miami applicator – this is a future work). In addition, the applicator needs a dedicated commissioning and QA procedures to ensure (1) the dosimetric accuracy compared with the TPS predictions, (2) verification of the applicator and shield dimensions, 3) handling of the applicator and sterilization processes. The extra tungsten alloy piece would eventually increase the cost of fabrication, as well. There is also no clear/known clinical benefit/indication for this applicator, requiring clinical studies to quantify. Furthermore, the application of this novel design in some clinical scenarios (for example, see Figure 2. 8) may increase treatment time somewhat significantly (e.g., increase by 42-75%, translating to about 2.4-4.4 min increase over 5.8 min).

Future design improvement considerations include (1) 3D printing of the applicator for prototyping and end-to-end dosimetric testing, (2) combining the single-channel design with a multi-channel applicator to explore dosimetric coverage to complex target shapes, and (3) exploring additional degrees of freedom such as beam directionality, shield material choice for MR imaging, and shield shape & mobility during treatment (e.g., static[12] vs dynamic[40] DMBT treatment delivery modes).

2.5 CONCLUSIONS

We have shown the utility of the novel DMBT-VC applicator to provide, in terms of treatment depth, dosimetric coverage to the vaginal apex by overcoming the classical

anisotropy issue ubiquitous to all current HDR brachytherapy sources. The next step in development of the device is manufacturing a prototype for clinical end-to-end testing.

Chapter 3. The effect of vaginal cylinder inhomogeneity on the HDR brachytherapy dose calculations using Monte Carlo simulations and a commercial model-based dose calculation algorithm

BACKGROUND AND MOTIVES

Vaginal cylinder (VC) applicators are usually made of high-density plastic materials with a density up to 30% higher than the water density. Consequently, this inconsistency could notably impact dose calculation. However, most of the current treatment planning systems (TPS) work based on the TG43 formalism, which assumes all the environment except radiation source as water, particularly when the radiation dose is prescribed to the surface of the VC, as a popular approach.

The motives for this project include the following points:

1. The high-density plastics, namely PEEK and PPSU, are widely used for fabrication of commercial VC applicators. These plastics were used for the design of DMBT-VC presented in chapter 2. Therefore, this study may be considered as a complementary part for chapter 2.
2. There was no study that has had the prescription point, being either the surface of the VC or 5 mm beyond the surface, in to account when investigating the VC heterogeneity effect on dose calculations.
3. There was no relevant study based on the standard plans (multiple dwell positions) and commercial VC models.

4. There was no analytical description on how VC heterogeneity may affect dose calculations.
5. There was no benchmark study focusing only on VC applicators. Other studies had worked on the shielded VC applicator.

Detail information of this study comes in the following sections.

Abstract

Purpose: Some of the commercial vaginal cylinder (VC) applicators are made of high-density plastic materials. When an HDR source is placed inside the applicator's lumen(s), these applicators create a heterogeneous environment around the source that could affect the dose distribution, contrary to the TG43 formalism. In addition, the prescription/normalization point, popularly placed either on the surface or 5 mm beyond the applicator's surface, can intensify this effect. This study utilizes Monte Carlo (MC) simulations to assess this heterogeneity effect and benchmarks the accuracy of a commercial model-based dose calculation algorithm (MBDCA) against the MC simulation results.

Methods and Materials: The GEANT4 MC code was used to simulate a commercial ^{192}Ir HDR source and a commercial VC, with diameters ranging from 20-35 mm, inside a virtual water phantom. Standard plans were generated from a commercial treatment planning system (TPS - BrachyVision ACUROS^{TM} (BVA)) optimized through two dose calculation approaches: (1) TG43 protocol assuming all environment as water and (2) MC & BVA approaches accounting for the heterogeneity of VC applicators. The dose and energy deposited profiles were extracted for analysis.

Results: The MC simulation results showed that the VC inhomogeneity can cause shrinkage of the isodose lines by up to 1 mm at the peripheral-lateral surfaces compared to TG43, leading to the reduction of the dose when prescribing to the surface. In addition, the BVA overestimated the dose on the surface of about 5.0% and 8.5% at the periphery and the apex, respectively, when prescribing to the surface. However, the difference between the BVA and MC simulations were negligible at the prescription point when prescribing to 5 mm beyond the surface.

Conclusion: The uncertainty due to the VCs' heterogeneity on dose calculations depends on the applicators' material/design, and the prescription point's location. The incident of the air bubbles around the applicators can add to the complexity, which needs further study.

Keywords

Vaginal Cylinder Applicator Heterogeneity, HDR Brachytherapy Dose Calculations, TG43, MBDCA, Monte Carlo

3.1 INTRODUCTION

Vaginal cylinders (VC) is the most common applicator type used for high-dose-rate (HDR) brachytherapy (BT) in the patients suffering from endometrial cancer after surgery [15,24,33]. Many of the commercial VCs are made of high-density plastic materials, such as polyether ether ketone (PEEK) and polyphenylsulfone (PPSU) with a density of about 1.3 g/cc [7]. Also, these applicators house at least one lumen inside for source positioning, which is filled with air. Therefore, these applicators create a heterogeneous environment around the HDR sources and could potentially influence the dose distributions, depending on the materials and their densities, the size, and the design of the VC applicator. In addition, the prescription point, either the surface or 5 mm beyond the surface of the VC, can magnify this effect [8]. However, most of the currently available brachytherapy treatment planning systems (TPS) and clinical practice take advantage of the AAPM Task Group 43 (TG43) formalism to estimate dose inside the patients' body using precalculated parameters obtained from single-dose distributions in an infinite water medium. As a result, this method cannot consider the effect of shapes and materials other than water, such as VCs [6,41–44].

To overcome these limitations, the model-based dose calculation algorithms (MBDCA) have been developed and since become available in commercial TPSs. These algorithms rely on CT imaging of the patients to account for scattering conditions different from that in the reference geometry for source dosimetric characterization, patient heterogeneities as opposed to a homogeneous water medium, and applicators [9]. However, TG229 emphasizes on a need for reference dosimetry data obtained in liquid water phantoms to evaluate the uniform clinical implementation and robustness of these advanced dose calculation algorithms [13].

The Monte Carlo (MC) simulations can be utilized for reference dosimetry and benchmarking the commercial MBDCAs, while accounting for the limitations related to the TG43 formalism for the absorbed dose calculations with a high accuracy [6,9,32,45–47]. In this study, we aim to assess the effect of VC heterogeneity on dose calculations and benchmark the accuracy of the commercial MBDCA (BrachyVision ACUROS™ (BVA), Varian, Palo Alto, CA) against MC simulations. To end this, we performed a comprehensive study on a set of commercial VC applicators modeled in the BVA TPS.

3.2 METHODS AND MATERIALS

3.2.1 Monte Carlo simulations

We utilized the GEANT4 MC package version 10.6 for all of the simulations. Detailed information about the GEANT4 MC package and its physics models can be found in the *Conseil Européen pour la Recherche Nucléaire (*CERN) documents and other literature [48–52]. We simulated the VS-2000 (Varian, Palo Alto, CA) ^{192}Ir HDR brachytherapy source model as described in the BVA algorithm reference guide [7]. The G4UniounSolid was used to define the source geometry in detail. A diagram of the source structure and its simulation model are shown in Figure 3. 1. For the TG43 parameters, including the 2D anisotropy factor, the radial dose function, and the dose rate constant, were obtained as described in the literature [52–55].

(a)

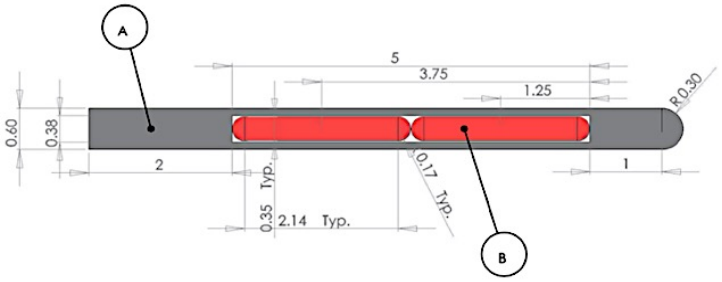

(b)

Material A: Nickel Titanium Alloy – 6.5 g/cm^3. **Material B:** Pure Iridium – 22.42 g/cm^3. Wire length extends 2 mm from end of active core.

Figure 3. 1 (a) 192Ir VS-2000 source diagram from the BVA algorithm reference guide 7. Unit is in [mm]. The white area inside the source is filled with air. (b) The simulated VS-2000 (2012) source constructed in our GEANT4 MC code.

For only-MC heterogeneity study, we modeled the Varian's VC applicators, model 11011160, with diameters of 20, 25, and 30 mm. The applicators have two parts, including the outer tube made of PPSU plastic (percentage weight: 95% H (4.2%), C (79.1%), O (16.7%)) and a detachable universal inner tube made of PEEK plastic (percentage weight: 95% H (4.0%), C (72.0%), O (16.0%), S (8%)) with densities of 1.31 g/cc and 1.3 g/cc, respectively [7]. The inner part is 6 mm in diameter, has a dome shape piece at the top with a thickness of 3.13 mm, and includes a 1.5 mm diameter central lumen for an HDR source

to travel through. The G4UnionSolid and G4Intersection were used to define the VCs' geometry. A diagram of the simulated 30 mm diameter VC is shown in Figure 3. 2.

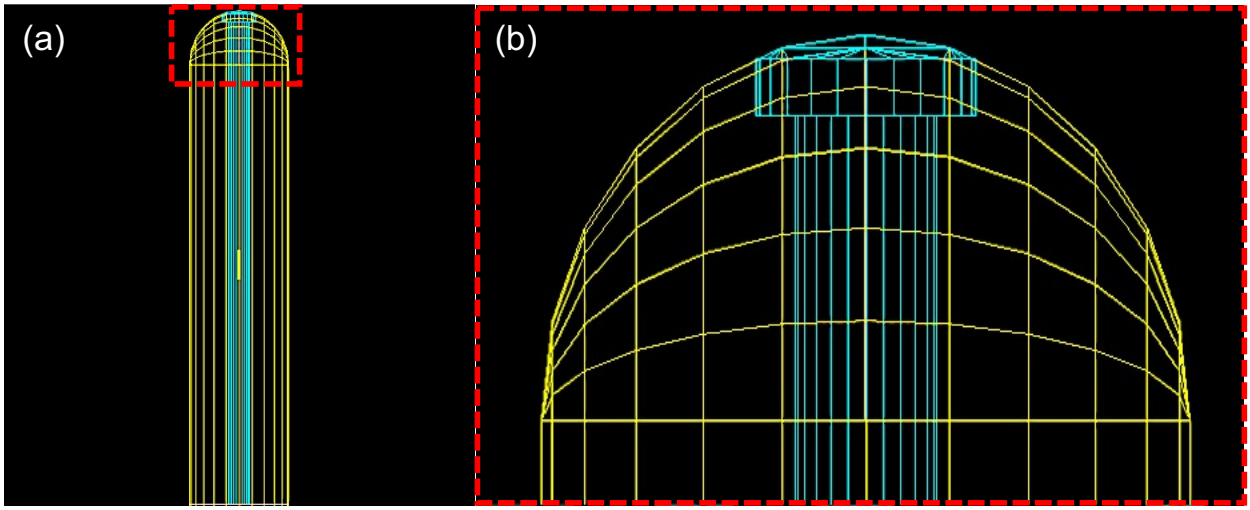

Figure 3. 2 A simulated 30 mm VC applicator in GEANT4. (a) The wholistic view of the VC, including the PPSU outer cylinder shown in yellow, and the inner PEEK rod shown in blue. (b) A zoomed view of the apical part of the VC applicator shown in the red dash rectangle in (a).

We considered two different scenarios to assess the effect of heterogeneity on the dose calculations for a set of plans fed from the BVA TPS, prescribed to 5 mm beyond the VCs' surface. First, we performed simulations for when the VCs are inside a 30×30×30 cm^3 virtual water phantom and accounted for the plastic materials and the single lumen (filled with air) heterogeneities to be in the MC model. Second, we repeated the simulations with all the heterogeneities (i.e., the plastics and air in the lumen) as water to represent the TG43 model. We ran the simulations for 10^9 particle histories, and scored dose and energy deposited for each dwell position using a mesh with a voxel size of 1 mm. The statistical uncertainty for the GEANT4 data was less than 1%, on average, in the area of interest.

3.2.2 BrachyVision ACUROS™ vs Monte Carlo simulations

In this study, the BVA version 16.1 was used. The BVA algorithm was developed to provide accurate and rapid dose calculations for HDR and pulsed-dose rate (PDR) brachytherapy treatments [7]. In the BVA implementation, a Linear Boltzmann Transport

Equation (LBTE) is deterministically solved using fine-discretized grid of spatial, angular, and energy variables and then the average photon energy-fluence distribution is obtained, which is then converted to a dose distribution [56]. Further explanation about the BVA algorithm can be found elsewhere [7,57–59].

For benchmarking of the BVA, we used the VC with a diameter of 35 mm and provided the same condition in both the GEANT4 MC simulations and the BVA. For BVA, after creating a digital phantom with a slice thickness of 1 mm, we inserted the VC from the Solid Applicator library and placed it along the Z-axis. Further, we created two standard plans for two normalization points: (1) the surface of the VC and (2) 5 mm beyond the surface of the applicator. A 3 mm gap for the first dwell position and a step length of 5 mm were also considered for each plan.

A grid size of 201×201×201 mm^3 with a voxel size of 1 mm^3 was used for the dose calculations under two conditions: (1) considering all the heterogeneities (i.e., the plastics and air in the lumen) as water (TG43) and 2) considering the effect of the VC heterogeneities (BVA vs MC). We ran 10^9 particle histories for MC simulations for each of the dwell positions inside the cylinder and scored the dose deposited.

3.3 RESULTS

3.3.1 Monte Carlo simulations

A coronal view of the VS2000 (2012) ^{192}Ir HDR source generated isodose lines and the 2D anisotropy function generated by the GEANT4 MC, compared to the consensus data from a previous study [13,60] are shown in Figure 3. 3. We chose a 2% error bar on the GEANT4 MC data for the anisotropy function data points for display. As shown, there was an overall good agreement between the two sets of data.

Table 3. 1 lists the numeric results between the GEANT4 MC and the consensus data [13,61] for the radial dose function, indicating a good overall agreement between the two. Furthemore, the dose rate constant obtained from the GEANT4 MC simulations, 1.109 ± 0.013 $cGy{\cdot}h^{-1}{\cdot}U^{-1}$, agreed well with the consensus data of 1.100 ± 0.006 $cGy{\cdot}h^{-1}{\cdot}U^{-1}$ [13].

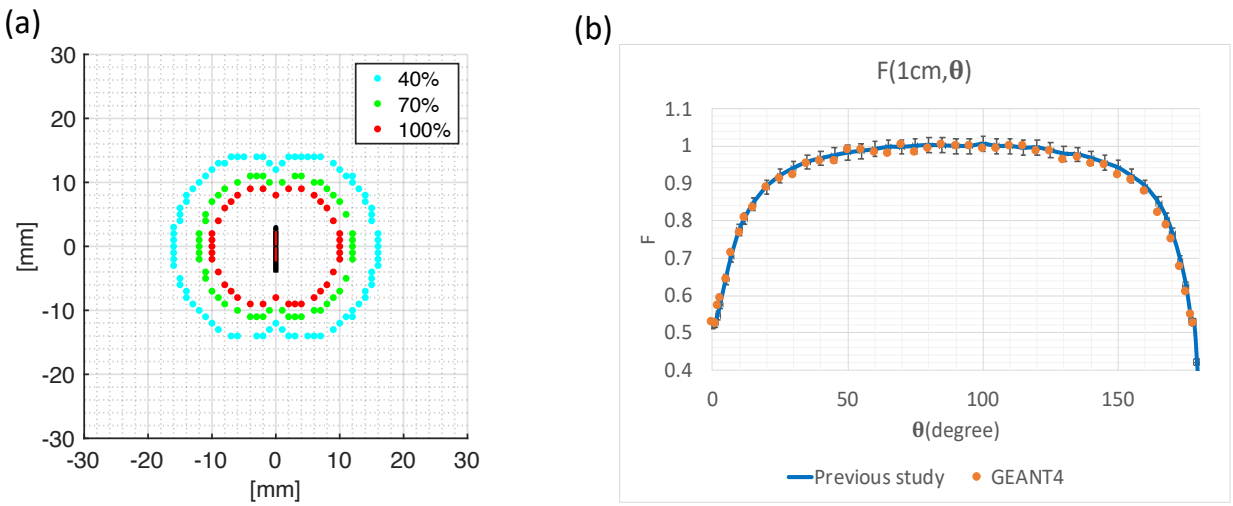

Figure 3. 3 (a) Isodose lines generated by the VS2000 (2012) source, in coronal view, derived from the GEANT4 MC results. Normalization point is 1 cm from the center of the Iridium core and perpendicular to the source axis. (b) The VS2000 (2012) 2D anisotropy function: comparison between a previous study versus GEANT4 MC results at r = 1 cm.

Table 3. 1 The VS2000 (2012) geometric function: comparison between the GEANT4 (G) and the previous study (PS) results.

r(mm)	G	PS	G/PS
2	0.99	0.98	1.01
5	0.99	0.99	1.00
7	0.99	0.99	1.00
10	1.00	1.00	1.00
15	0.99	1.00	0.99
20	1.00	1.01	0.98
30	1.00	1.01	0.99
40	1.01	1.01	1.00
50	0.99	1.01	0.98
60	0.98	1.00	0.98
80	0.97	0.98	0.99
100	0.95	0.95	1.00

The dose distributions generated by the MC and the TG43 protocol, and the related dose & energy profiles, are shown in Figure 3. 4, Figure 3. 5, and Figure 3. 6 for the 20-mm, 25-mm, and 30-mm diameter VCs, respectively. The 100% isodose line indicates a dose of 2,100 cGy (3 fxs × 700 cGy), prescribed to 5 mm beyond the surface. As shown, the comparison between the dose distributions of the TG43 model (Figures 3. 4a, 3. 5a, and 3. 6a) and the MC simulations (Figures 3. 4b, 3. 5b, and 3. 6b) showed a shrinkage of the isodose lines by up to 1 mm for the MC results at the lateral periphery of the applicators, mainly just inside the VCs where the boundary of the water-PPSU interface is located. The isodose lines shrinkage is most marked for the 30-mm diameter VC (Figure 3. 6), as supported by the energy and dose profiles plots. To better visualize this effect, the energy & dose profiles were plotted from the P1 lines (X profiles), which crosses the water-PPSU boundary. For all of the MC results, the energy deposition is significantly higher inside the VCs, ranging from 19-22%, than the TG43 protocol. However, the opposite is true for the dose deposition with values ranging from 6.15-8.5%. Moreover, although the dose at the boundary between the water-PPSU cannot be extremely accurate due to the volume-averaging effect (due to finite voxel size), all of the MC results do indicate a trend of lower doses at the applicators' surface (see ~150% isodose lines). Further, we extrapolated the doses at the boundaries using an exponential fit across the dose values inside of the VCs. This estimation showed the ratio of the doses at the water-PPSU boundary for the MC over TG43 results were 0.945, 0.987, and 0.941 for the 20-mm, 25-mm, and 30-mm diameter VCs, respectively (on average, 4.17% reduction in dose at the boundry). The maximum/average dose reductions at the prescription points (i.e, 5 mm beyond the surface), excluding the curved portion of the VCs at the apex, were 4.49%/0.8%, 3.46%/1.09%, and 4.58%/2.53% for the 20-mm, 25-mm, and 30-mm diameter VCs, respectively. The size of the anisotropy dips at the apex location (i.e., distance from the lowest 100% dose point at the apex in the dip to the 5-mm prescription line) was about 1 mm smaller for the MC results comparted to the TG43, as well. A detailed analysis at the apex region will be given in the following sections.

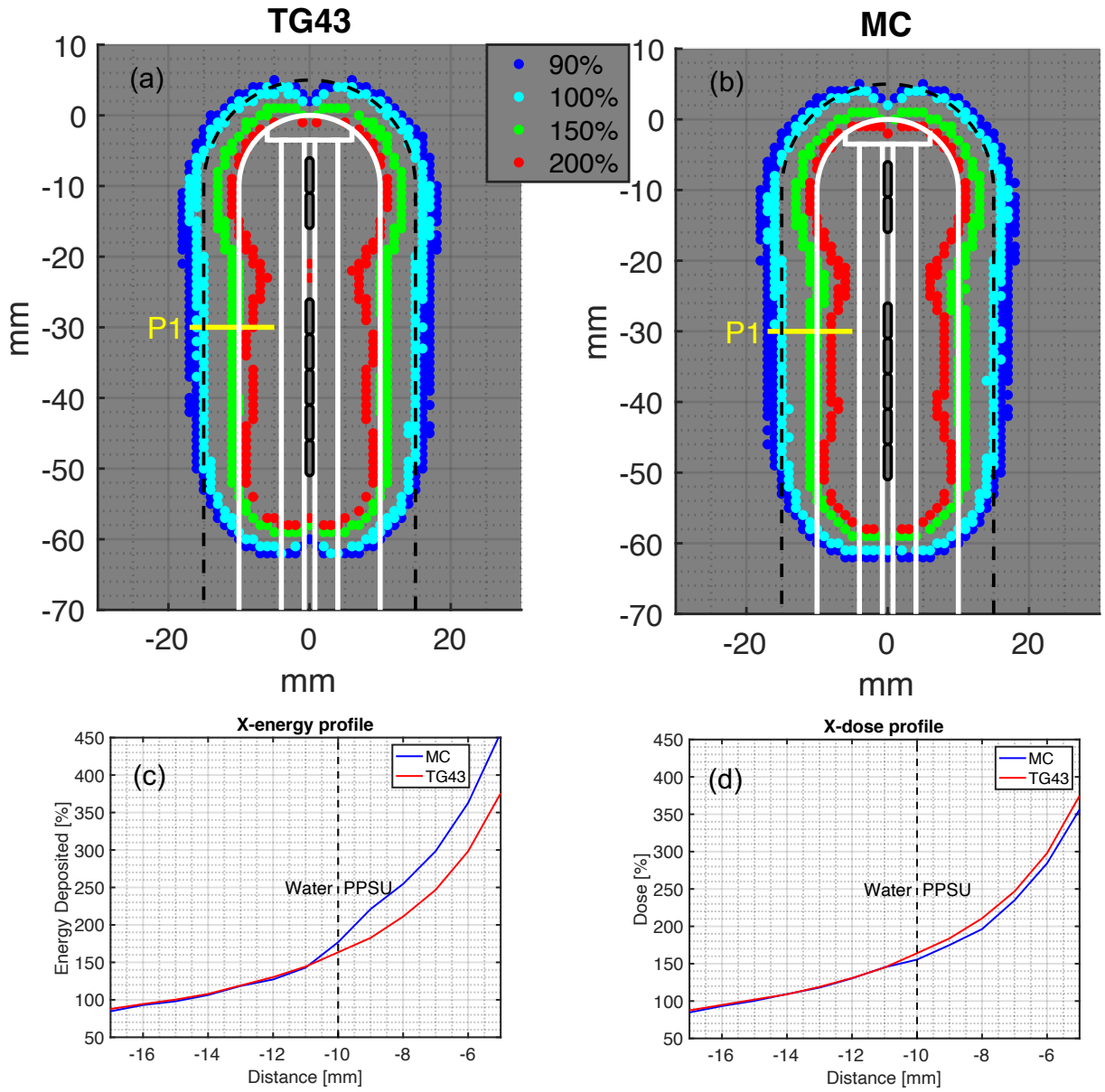

Figure 3. 4. The outer contour of a 20-mm diameter VC applicator (solid white lines), along with the dwell positions (solid black lines) utilized to optimize the plan, is shown. The prescription line, which is 5 mm beyond the VC surface, is shown in dashed black line. The various colored dots are the respective isodose lines calculated with the (a) TG43 and (b) MC. Also, the X-directional profiles of energy and dose deposited along the P1 solid yellow line are plotted in (c) and (d), respectively.

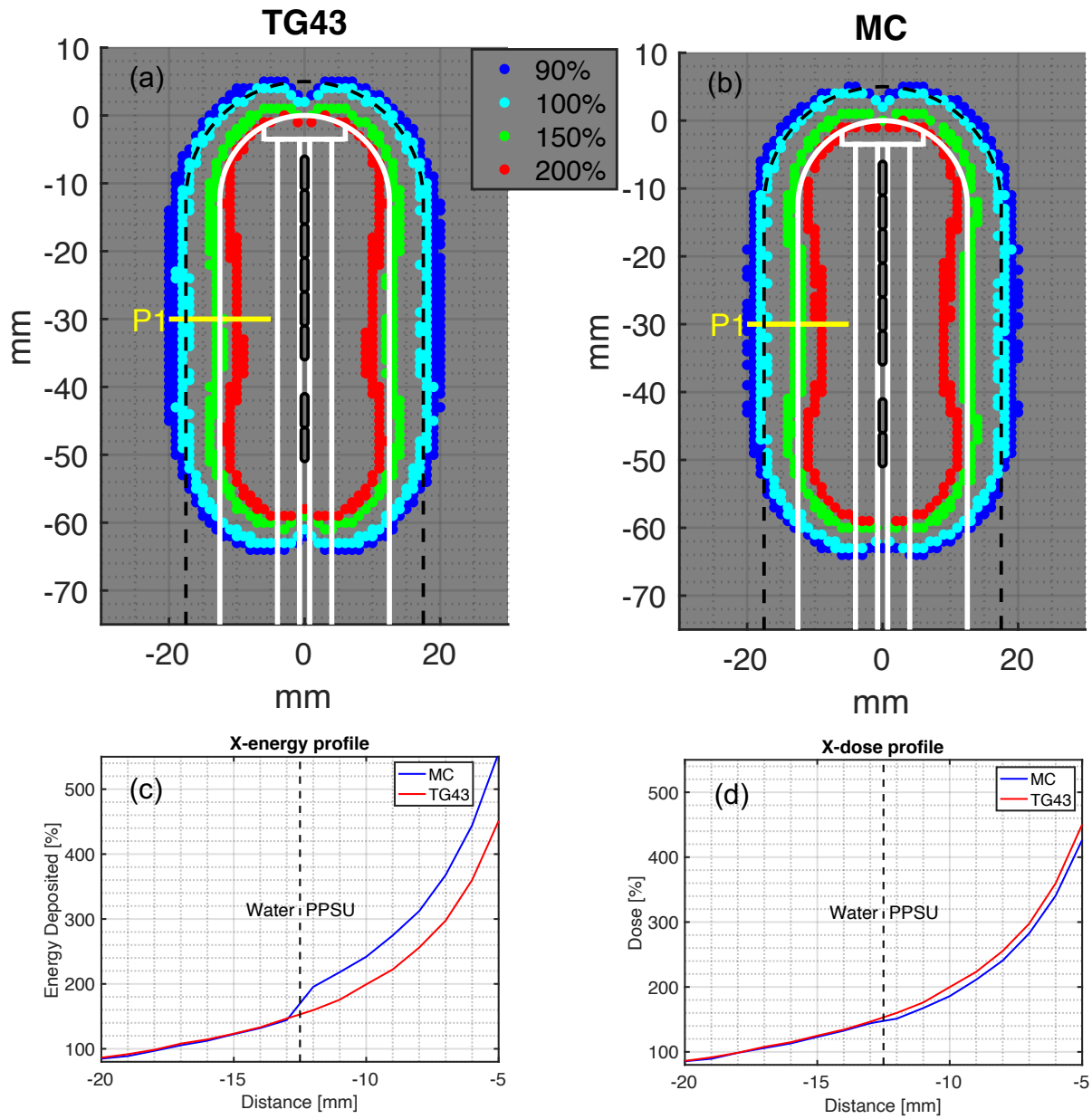

Figure 3. 5. The outer contour of a 25-mm diameter VC applicator (solid white lines), along with the dwell positions (solid black lines) utilized to optimize the plan, is shown. The prescription line, which is 5 mm beyond the VC surface, is shown in dashed black line. The various colored dots are the respective isodose lines calculated with the (a) TG43 and (b) MC. Also, the X-directional profiles of energy and dose deposited along the P1 solid yellow line are plotted in (c) and (d), respectively.

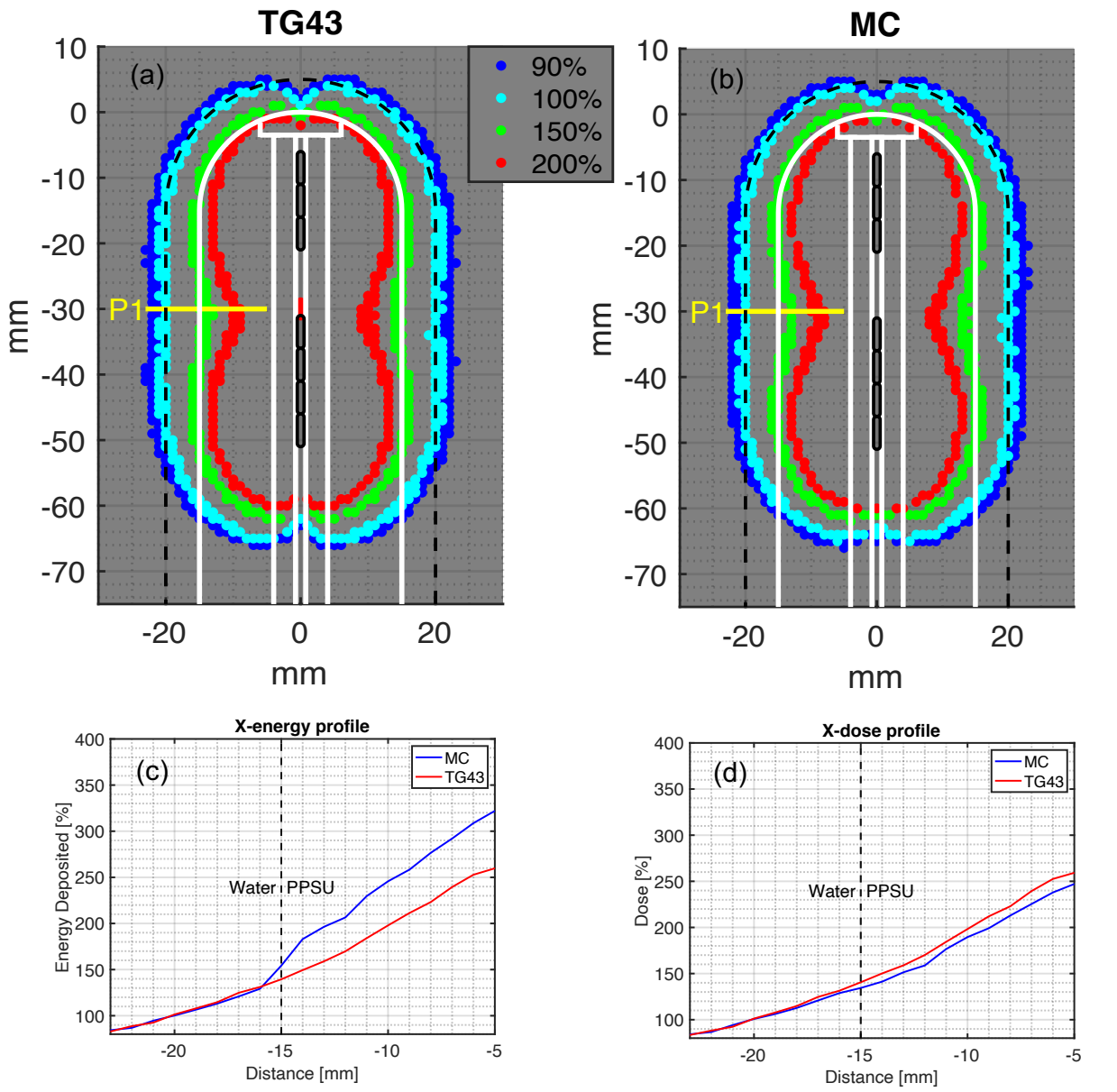

Figure 3. 6. The outer contour of a 30-mm diameter VC applicator (solid white lines), along with the dwell positions (solid black lines) utilized to optimize the plan, is shown. The prescription line, which is 5 mm beyond the VC surface, is shown in dashed black line. The various colored dots are the respective isodose lines calculated with the (a) TG43 and (b) MC. Also, the X-directional profiles of energy and dose deposited along the P1 solid yellow line are plotted in (c) and (d), respectively.

3.3.2 BrachyVision ACUROS™ vs Monte Carlo simulations

3.3.2.1 Prescription point: VC surface

Figures 3. 7 and 8 show the dose distributions and line profiles for the 35-mm diameter VC, comparing the GEANT4 MC and BVA algorithms against TG43, respectively. The prescription point is at the surface of the applicator and the 100% isodose line indicates a dose of 2,100 cGy (3 fxs × 700 cGy). Compared to the TG43 protocol (Figure 3. 7a), the MC results (Figure 3. 7b) show up to 1 mm of isodose line shrinkage starting just inside the applicator (Figure 3. 7c), i.e., the water-PPSU boundary, with the maximum/average dose values of 8.10%/6.42%, resulting in 6.15% (extrapolated) lower dose at the applicator surface. The maximum (extrapolated) dose reduction across the peripheral surface was 8.24%, located between the 5^{th} and the 6^{th} dwell positions from the tip of the VC. To evaluate the heterogeneity effect at the apex region (i.e., applicator's tip), the dose distribution was sampled across the line P2 (Y-dose profile), which crosses three different mediums: (1) water, (2) PEEK, and (3) part of the lumen filled with air. The Y-dose profile (Figure 3. 7d) exhibited an increase in the dose values, by the MC results, of 10.28%, 2.59%, and 34.56% inside water, PEEK, and air, respectively, compared to the TG43 results.

The same analysis was performed on the data extracted from the commercial BVA algorithm. The dose distributions from the TG43 protocol (Figure 3. 8a) and the BVA algorithm (Figure 3. 8b) look very much similar at the periphery (Figure 3. 8c). As can be seen from the X-dose profile (Figure 3. 8c), plotted from the P1 line, indicated a just slightly higher doses from the TG43 over the BVA results, with the maximum/average values of 1.77%/0.00% and 1.77%/1.56%, areas inside and outside of the VC, respectively. The BVA's Y-dose profile (Figure 3. 8d), also exhibited an average increase of 17.44%, 23.02%, and 35.38% in water, PEEK, and air, respectively, over the TG43 results.

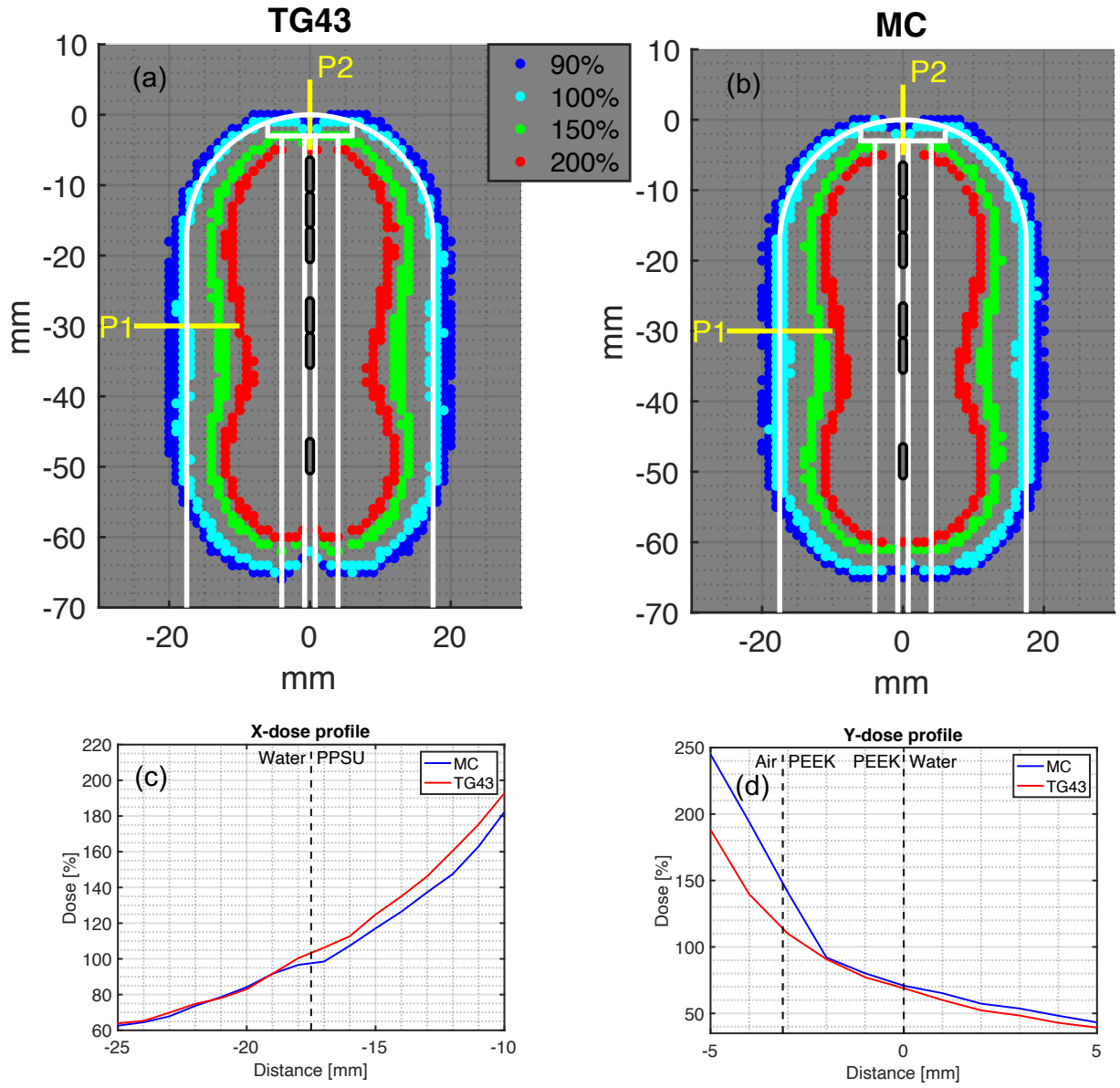

Figure 3. 7. The outer contour of a 35-mm diameter VC applicator (solid white lines), along with the dwell positions (solid black lines) utilized to optimize the plan, is shown. The prescription line is at the VC surface. The various colored dots are the respective isodose lines calculated with the (a) TG43 and (b) MC. Also, the X- and Y-directional profiles of dose deposited along the P1 and P2 solid yellow lines are plotted in (c) and (d), respectively.

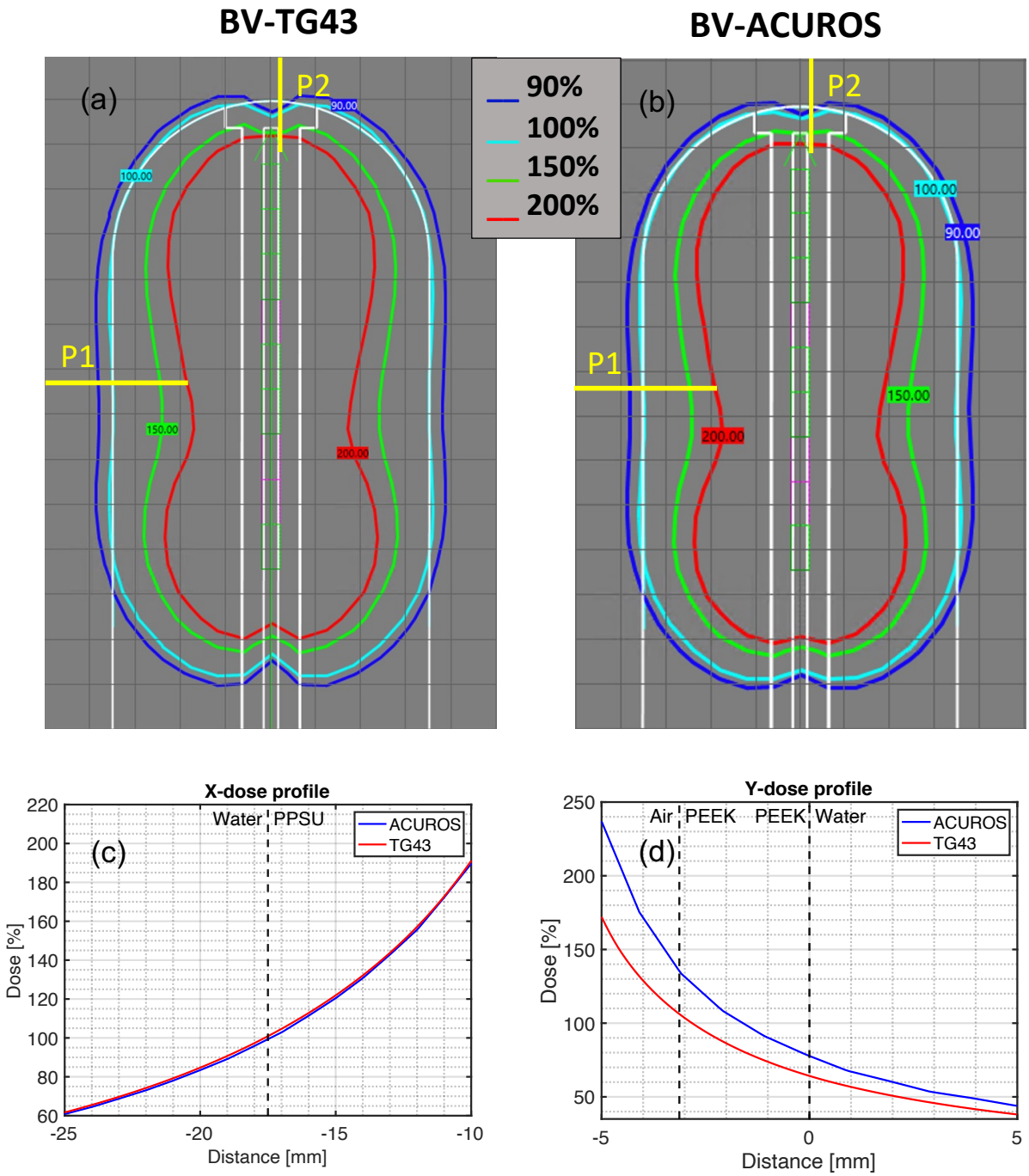

Figure 3. 8. The outer contour of a 35-mm diameter VC applicator (solid white lines), along with the available dwell positions (solid green) utilized to optimize the plan, is shown. The prescription line is at the VC surface. The various solid-colored lines are the respective isodose lines calculated with the (a) TG43 and (b) BVA. Also, the X- and Y-directional profiles of dose deposited along the P1 and P2 solid yellow lines are plotted in (c) and (d), respectively.

3.3.2.2 Prescription point: 5 mm beyond the VC surface

Figures 3. 9 and 3. 10 show the dose distributions and line profiles for the 35-mm diameter VC, comparing the GEANT4 MC and BVA algorithms against TG43, respectively. The prescription point is at 5 mm beyond the applicator's surface and the 100% isodose line indicates a dose of 2,100 cGy (3 fxs × 700 cGy). The same analysis was performed as in the Figures 3. 7 and 3. 8. Similarly, the MC results (Figure 3. 9b) show up to 1 mm of isodose line shrinkage starting just inside the applicator (Figure 3. 9c), (i.e., the water-PPSU boundary) with the maximum/average dose reductions of 8.65%/6.23% and 4.52%/1.80%, inside and outside the regions of the applicator, respectively. The maximum/average dose reductions by the MC results, compared to the TG43 protocol, at the prescription point were 3.46%/1.54% with the maximum reduction occurring between the 3rd and 4th dwell positions from the tip of the VC. The Y-dose profile (Figure 3. 9d), plotted from the P2 line, exhibited an average increase of 9.96%, 0.53%, and 29.80% in water, PEEK, and air, respectively, over the TG43 results.

The dose distributions generated were close in agreement between the TG43 (Figure 3. 10a) and the BVA algorithm (Figure 3. 10b), as can be seen from the X-dose profile plot (Figure 3. 10c), with just slightly higher doses from the TG43 with maximum/average increases of 1.91%/1.27% and 1.95 %/1.74%, inside and outside regions of the VC, respectively. The BVA's Y-dose profile (Figure 3. 10d), also exhibited an average increase of 16.70%, 24.82%, and 44.24% in air, PEEK, and water, respectively, over the TG43 results.

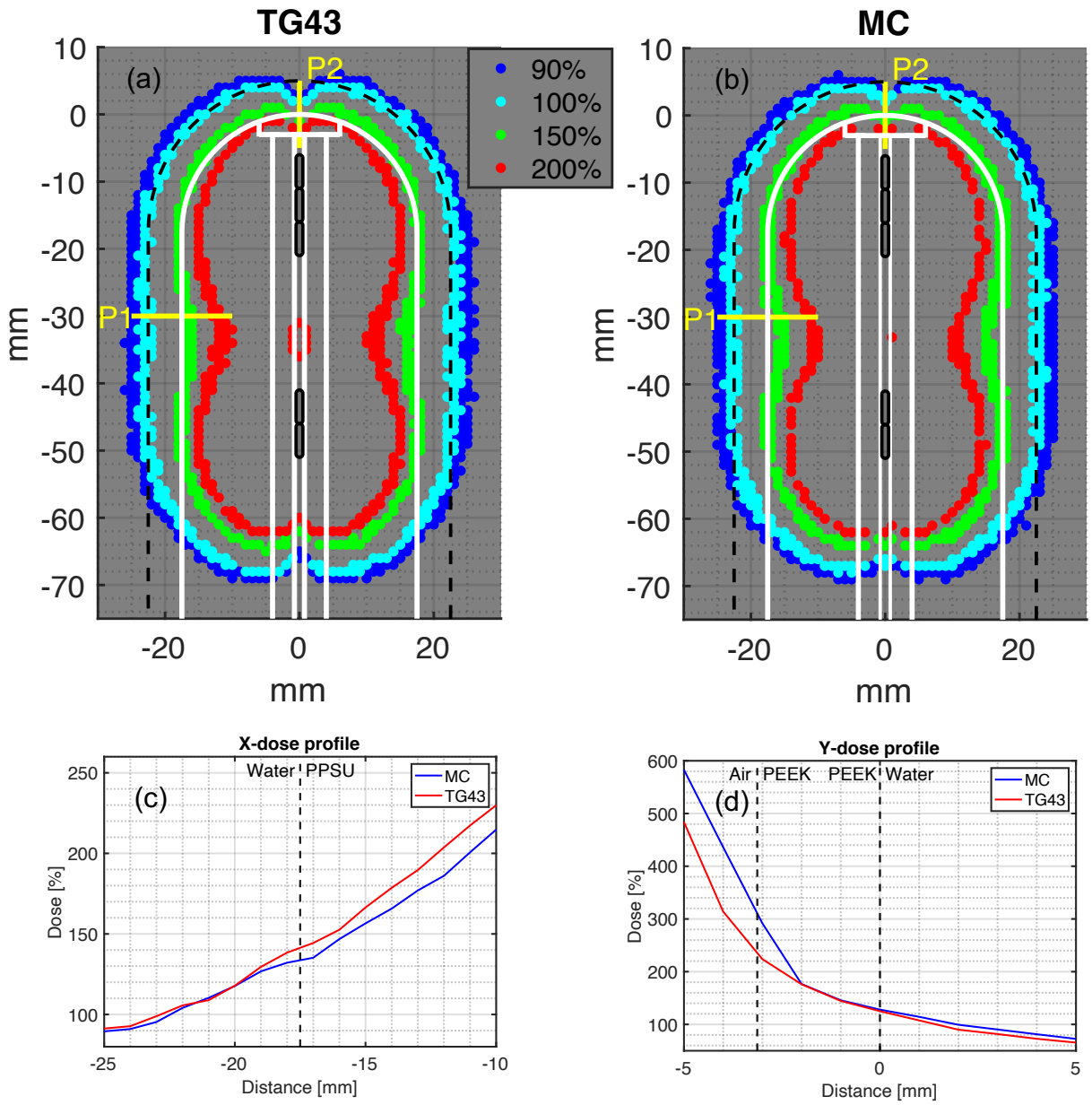

Figure 3. 9. The outer contour of a 35-mm diameter VC applicator (solid white lines), along with the dwell positions (solid black lines) utilized to optimize the plan, is shown. The prescription line, which is 5 mm beyond the VC surface, is shown in dashed black line. The various colored dots are the respective isodose lines calculated with the (a) TG43 and (b) MC. Also, the X- and Y-directional profiles of dose deposited along the P1 and P2 solid yellow lines are plotted in (c) and (d), respectively.

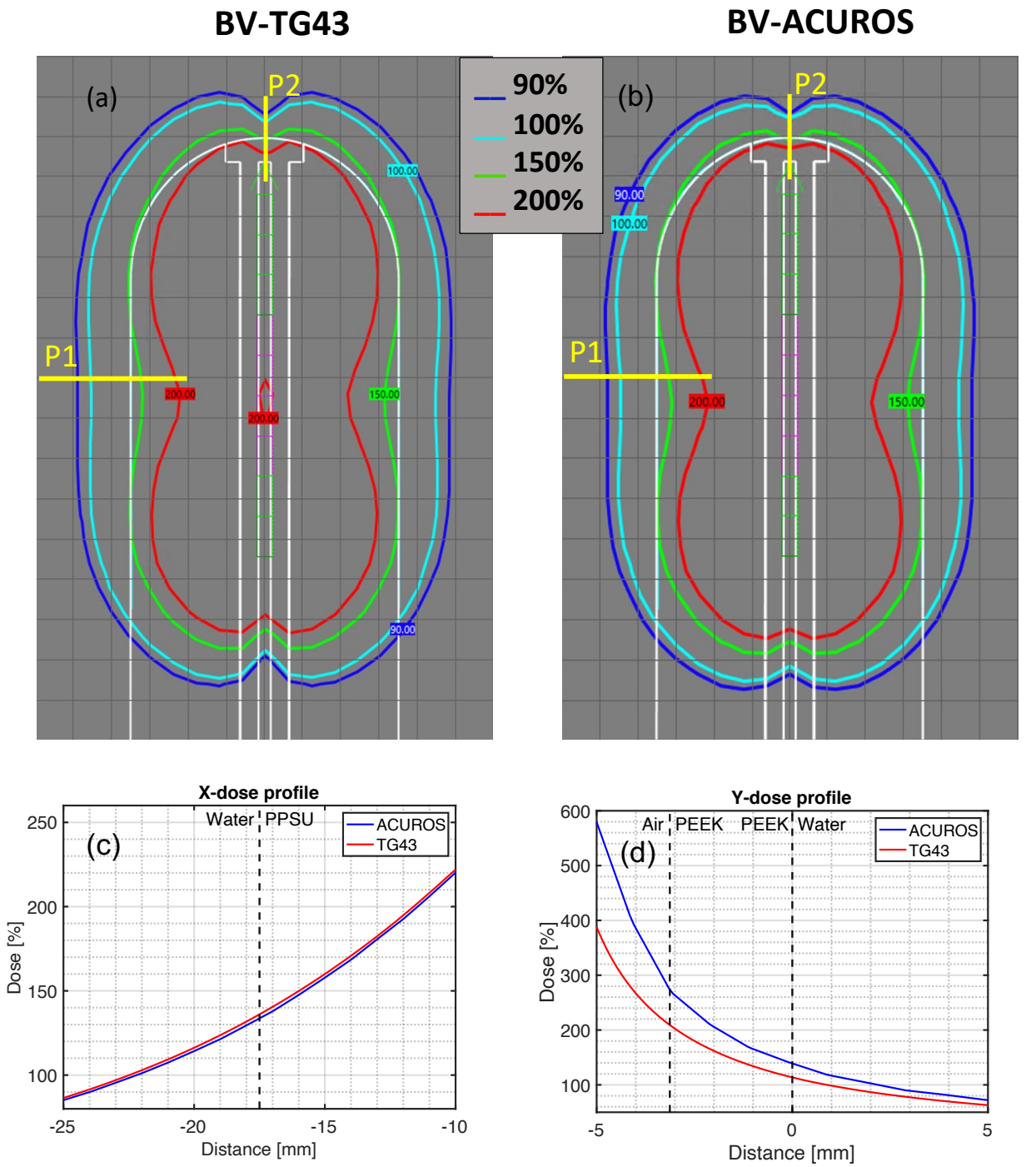

Figure 3. 10. The outer contour of a 35-mm diameter VC applicator (solid white lines), along with the available dwell positions (solid green) utilized to optimize the plan, is shown. The prescription line is 5 mm beyond the VC surface. The various solid-colored lines are the respective isodose lines calculated with the (a) TG43 and (b) BVA. Also, the X- and Y-directional profiles of dose deposited along the P1 and P2 solid yellow lines are plotted in (c) and (d), respectively.

3.3.2.3 BrachyVision ACUROS™ vs Monte Carlo simulations

Since both the MC simulations and the BVA algorithm can account for the heterogeneity effects, we directly compared the dose profiles from the Figures 3. 7-3. 10 with the following results:

1) *Prescription Point: VC Surface*

   The X-dose profile comparison (Figure 3. 11a) resulted in average/maximum difference values of 0.01%/1.35% and 4.54%/6.00%, in water and PPSU, respectively. The Y-dose profile comparison (Figure 3. 11b) resulted in average/maximum differences of 1.3%/3.89%, 12.11%/13.56%, and 8.37%/13.37%, in water, PEEK, and air, respectively. Also, the absolute average dose differences between the two dose calculation techniques were 4.49% at the water-PPSU boundary (i.e., prescription point) and 8.31% at the water-PEEK boundary.

2) *Prescription Point: 5 mm Beyond the VC Surface*

   The X-dose profile comparison (Figure 3. 11c) resulted in average/maximum difference values of 2.49%/4.90% and 2.25%/3.85%, in water and PPSU, respectively. The Y-dose profile comparison (Figure 3. 11d) resulted in average/maximum differences of 0.00%/2.29%, 13.54%/14.57%, and 6.92%/15.06%, in water, PEEK, and air, respectively. Also, the absolute average dose differences between the two dose calculation techniques were 0.00% and 2.77%, at the periphery and apex regions, respectively, of the prescription point.

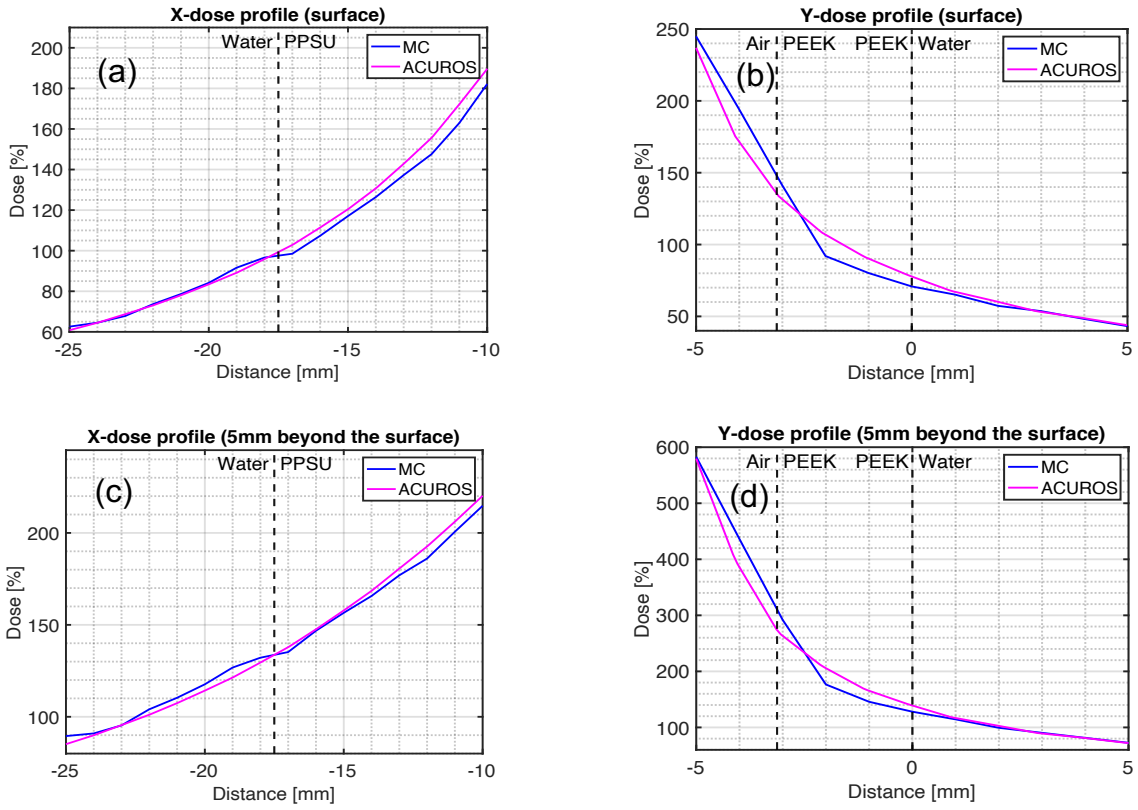

Figure 3. 11. The comparison between the MC and BVA generated dose profiles for the VC with a diameter of 35 mm. The dose is volume-averaged for the MC models at the boundaries between different mediums.

3.4 DISCUSSION

3.4.1 Monte Carlo simulations

All of the MC simulation results (Figures 3. 4b, 3. 5b, and 3. 6b) shown in this study exhibited consistent dose reductions at the applicators' surface (water-PPSU boundary), compared to the TG43 protocol, with an average reduction of about 4%. This can be better understood by examining the energy and the dose profiles plotted in the Figures 3. 4c-d, 3. 5c-d, and 3. 6c-d. With respect to the energy profiles, we can see a consistent increase in energy deposited inside the applicators, which gets higher as the VC diameter increases. This phenomenon arises from having more interactions of X- and gamma rays inside the applicators due to the higher density of the plastic materials (~1.3 g/cm^3) than that of water. Therefore, the bigger the applicator size, the higher the number of atoms and consequently the more interactions. This increases the energy deposition, of course,

with up to 22% increase observed for the 30-mm diameter VC. However, this does not translate to increase in dose deposited inside the applicators because the increase in energy deposition is counteracted by about 30% higher mass of the plastics than water, where the dose is defined as energy deposited per unit mass [J/kg]. Therefore, as a result, we saw consistently less dose deposited, overall, inside the cylinders (Figures 3. 4d, 3. 5d, and 3. 6d). Since the X- and gamma rays will interact and deposit their energies more in each layer of the plastic materials than water, the dose deposition will also occur at shorter distances from the source (dwell positions). Consequently, the shrinkage of the isodose lines will naturally occur (~1 mm) and has been captured well by the MC simulations in the figures. The radiation fluence will also get slightly less intense after exiting the VCs, hence the dose values will decrease beyond the VCs' surface. The maximum dose reductions at 5 mm beyond the surface (a prescription point) was smaller for the 25-mm VC (3.46%) compared to the 20-mm VC (4.49%). The reason for this is due to the difference in the number of dwell positions used, which were 8 and 7, respectively, and their locations (Figure 3. 4b vs 3. 5b). The regions without any dwell positions provide additional room for oblique filtration (attenuation) inside the VCs, potentially causing increased dose reductions in the 20-mm VC case. The dwell time variations play a role in this discrepancy, as well.

3.4.2 BrachyVision ACUROS™ vs Monte Carlo simulations

For the GEANT4 MC data, similar trends of dose deposition are observed in Figures 3. 7 and 3. 9 as compared to the Figures 3. 4-3. 6. A major difference, however, is the additional variable of the prescription point's location (surface vs 5 mm), which in turn affected the dwell positions' locations as well, in order to generate optimal plans. Looking at the lateral periphery of the VCs, the difference between the MC and TG43 data is bigger when the prescription point is the surface vs 5 mm (6.15% vs 1.54%). This is due to the different densities inside and outside of the VCs, as discussed above. Also, the maximum difference occurred in the region where there were no dwell positions (e.g., between the 5^{th} and 6^{th} dwell position - Figure 3. 7), due to the oblique filtration.

The Y-dose profiles showed an increase in dose in both the water and PEEK at the apex region of the applicators. This is because of the lumen, which is filled with air, and hence

the X- and gamma interactions are much less compared with assuming all-water by the TG43 protocol. Thus, the reduction of dose shown in the periphery of the VCs (Figures 3. 7c and 3. 9c) would be compensated for in the apex region, and hence the difference in dose is much smaller there (Figures 3. 7d and 3. 9d). The amount of difference in Figure 3. 7d vs 3. 9d is due to the difference in the dwell positions. Also, it is important to note that the apex surface dose is about 30% and 25% less than the prescription dose, when prescribed to the surface and 5 mm, respectively. This is due to the filtration inside the iridium core and the capsule, leading to a well-known anisotropic dip at the VCs' tip (e.g., Figures 3. 7b). Since the central PEEK tube design is universal across all of the commercial VCs studied in this work, the results of the Y-dose profiles should be similar for all VC sizes.

Based on the results presented, it is now apparent that the VCs' heterogeneities can significantly alter the dose distribution around the applicators, including the tip/apex and the lateral peripheral regions. This effect is more severe when prescribing to the applicators' surface than at 5 mm distance. The dosimetric disturbance effect, due to such high density plastics, also translates to a much higher dosimetric uncertainty level (8.65% based on the MC results) than the 1% set by the AAPM and GEC-ESTRO guidelines [62]. A good approach may be to reducing this uncertainty could be to use all of the available dwell positions and avoid large gaps between their positions when optimizing the plans.

The dose distributions generated by the BVA algorithm showed minimal differences to TG43 in the X-dose profile direction (lateral periphery), whether inside or outside of the VCs, where the average difference was less than 1% (Figures 3. 8c and 3. 10c) regardless of the location of the prescription point. Such was not the case in the Y-dose profile direction (tip/apex), however, where large differences were observed in the water and PEEK regions (Figures 3. 8d and 3. 10d). This, of course, is inconsistent with the MC-TG43 comparison results (Figures 3. 7d and 3. 9d), where in the water and PEEK regions, the two results are generally in agreement. Thus, it may not be completely reliable to review the effects of large plastic heterogeneities with the BVA algorithm alone, contrary to what others may claim [43], and that MC simulations or other forms of reference dosimetry may be required, as emphasized by TG 229 [13]. To this end, Figure 3. 11 showed the direct comparison between the MC simulations and the BVA algorithm. The

difference between the two results, inside the water, falls within 5% for both prescription points (surface vs 5 mm). However, the difference was up to 15% inside the plastics and air regions. Although there is no clinical concern for the dose differences inside the applicators, the accurate estimation of the dose at the VCs' surface would be concerning as it is a popular prescription/normalization point. Our analysis showed that the BVA algorithm overestimates the dose by 5.00% and 8.31% at the surface of the periphery and the apex regions, respectively, hence the potential for actual systematic under irradiation when prescribing to the surface exists (Figure 3. 11a-b). In the case of the 5 mm prescription point, however, the differences between the two dose calculation techniques are near negligible (Figure 3. 11c-d). In other words, the BVA algorithm does not provide enough dosimetric accuracy at the boundaries of mediums. This cannot be contributed solely to the volume averaging effect, as described in the BVA algorithm reference guide [7], since the volume averaging of the MC results are performed here as well. Other uncertainties and over estimations could have also been introduced by the BVA algorithm during the implementation of the discretization of the solution variables in space, angle, and energy [7]. These sources could be the root causes of the discrepancies between the MC and BVA algorithm results.

The study by Semeniuk *et al.* [26] produced similar dose distributions and dose profiles for plastic materials as well as in water, using one dwell position inside a 36-mm diameter VC. This study, however, didn't expand to include cases with multiple dwell positions, which is more typical clinically. In addition, they scored the dose only outside the VC. Another study, by Petrokokkinos *et al.* [58], benchmarked the BVA (version 8.8) against MC simulations for multiple dwell positions inside a 20-mm diameter VC, made of PMMA plastic (density = 1.19 g/cc), with a 180^{o} partial shielding. They studied the difference between the MC simulations and the TG43 protocol, as well. Although they showed some differences for MC vs TG43 as well as for MC vs BVA using 2D colormaps, the scored volume for the dose calculations were still limited to the outside of the VC. Additionally, the presence of metal shielding on one side can affect the dose distribution in all scored volume due to a different scattering condition in the medium. Therefore, the differences reported can't be attributed to the plastic heterogeneity alone. In contrast, the current study (1) provided a comprehensive dosimetry of the impact of the VC heterogeneity for

ranging sizes of a commercial VC model, based on standard clinical plans (i.e., multiple dwell positions), (2) revealed how the prescription locations can contribute to the effect, (3) provided a detailed explanation of how VC heterogeneity could affect the dose calculations using dose- and energy- deposited profiles, and (4) provided a site-specific benchmark study (MBDCA vs MC) which may further be available for correlation with known clinical outcomes [10].

This study focused on one particular commercial VC design, from a single vendor (Varian, Palo Alto, CA), with a standard range of diameters (20-35 mm), made from PEEK and PPSU plastic materials. Therefore, the results are limited to this commercial VC only, but perhaps translatable to other VCs using similar materials and designs. In addition, we only studied the dosimetric heterogeneity effect arising from the VCs. In the clinic, variables such as air bubbles, sutures, etc. could also be present in the treatment area [35,38]. Therefore, the impact of the heterogeneity effect on the target coverage could be more complicated, especially when prescribing to the surface. For the BVA algorithm, careful evaluation in the apex/tip region would be prudent then as there are already multiple heterogeneities there (e.g., water, PEEK, air, etc.), along with frequent air bubbles and sutures (left in post hysterectomy) present within the treatment area. A further work to closely examine the effect of the combined heterogeneities of the VCs and air bubbles-sutures could be valuable.

Finally, the type of the commercial VC design studied here (called the Stomp VC) aims to provide maximum coverage at the vaginal apex region (the site of surgery). However, both the MC and BVA (and even TG43) results showed large loss of coverage at the apex due to the anisotropy effect of the source design (~25-30% underdosage, e.g., see dosimetric dips around “P2” in Figure 3. 10). Such a loss of coverage is concerning but can be improved through a design modification via Direction Modulated Brachytherapy (DMBT) concept approach, as recently published [5].

CONCLUSIONS

We studied the effect of heterogeneities of high-density plastic materials used for the fabrication of commercial VC applicators on dose calculations, using the GEANT4 MC and BVA algorithms. The effect on dose calculations depended on the VC materials &

designs, and the prescription point's location (surface vs 5 mm). The existence of air bubbles and sutures around the applicators could add to the complexity, which needs further study.

Chapter 4. The design of a novel direction modulated brachytherapy ‘honeycomb’ tandem applicator for the optimized coverage of nonuniform targets in cervical cancer

BACKGROUND AND MOTIVES

The coverage of non-uniform targets is a challenging issue in cervical cancer brachytherapy and takes development of the (hybrid) intracavitary (IC)/interstitial (IS) applicators. This study aims to introduce a non-invasive IC applicator that could provide optimized coverage for the lateral extension of the tumor.

The standard IC applicators such as the tandem applicator can’t address the issue since the dose distribution of such applicator is symmetrical. However, IMBT technique could help this situation, such that a novel IMBT tandem applicator has been previously introduced. Although offering promising results in terms of better coverage and organs at risk (OAR) sparing, this design suffers from fundamental limitations.

The applicator is made of a tungsten alloy rod with six grooves for housing the radiation source (Figure 4.1). However, these grooves leave room for a substantial amount of radiation leakage as well, such that the shielding characteristic of the design is mainly limited to the central part of the tandem. In addition, this tandem applicator is only able to yield one type of dose distribution (Figure 4.9 a), limited to six directions where grooves face.

A novel concept design tandem has been introduced in this study, that offers (1) an optimized shielding design to reduce radiation leakage, (2) improve beam directionality, (3) provide room for transition of radiation source in all direction around the tandem, (4) and provide a variety of dose distributions as desired.

Detail of the study has been discussed in the following sections.

Abstract

Purpose: The intracavitary brachytherapy is an integral part for the treatment of the cervical cancer. However, the coverage of nonuniform target is a very challenging for this modality when dealing with the lateral extension of tumor and requires development of interstitial/ intercavitary state-of-the-art applicators. In this study we aim to introduce a novel tandem applicator design for direction modulated brachytherapy (DMBT), called 'honeycomb', to address this important issue.

Method and Materials: The novel 'honeycomb' tandem applicator was designed using GEANT4 Monte Carlo simulations to consist of a base with 19 channels, in a honeycomb arrangement, and a sheath of plastic to cover the base. The design also incorporated 18 iridium wires that can actively enter the channels to provide intensity/directional modulation. Three different MR compatible materials were studied for the base part, including the PEEK plastic, tungsten alloy, and iridium. A dosimetry study was then performed with different configurations of the HDR source and up to 18 iridium wires inside the bases. The previous innovation, namely DMBT tandem, was also reproduced and compared to the honeycomb design.

Results: The honeycomb design could produce a variety of dose distributions with different degree of the extended lateral coverage. However, the MR compatible tungsten alloy found to be the optimal base material, in terms of the radiation leakage and desired intensity/direction modulations while improving the lateral coverage. In addition, the honeycomb design showed superiority over the DMBT tandem in terms of back spillage and beam directionality, with more flexibility for coverage at different directions around the tandem.

Conclusion: The results indicated that the honeycomb tandem design, as a noninvasive approach, could be promising for the coverage of tumors with the lateral extension. Further study is needed for manufacturing of a prototype, the development of a dedicated treatment planning system and the required software/hardware for the radiation delivery.

Keywords

Direction Modulated Brachytherapy Honeycomb Tandem Applicator, Coverage of Nonuniform Targets, Monte Carlo Simulations

4.1 INTRODUCTION

The standard of care for the treatment of locally advanced cervical cancer (LACC) is external beam radiotherapy (EBRT) with concurrent (cisplatin-based) chemotherapy followed by brachytherapy (BT).[63–65] Typically, BT is employed after EBRT, but it can also be combined with surgery pre- or post-operatively as an essential part of treatment [34,66]. Thanks to the fast absorbed-dose fall-off, BT allows dose escalation to the primary tumor while sparing the organs at risk (OAR), including bowel and bladder [67–69]. Consequently, introduction of image-guided adaptive brachytherapy (IGABT), which enables the integration of 3D images such as MRI into treatment planning, and a set of recommendations from the Groupe Européen de Curiethérapie and European Society for Radiotherapy and Oncology (GEC-ESTRO) [66,70–72] have led to a notable improvement in clinical outcomes such as substantial benefit in local control and overall survival in last two decades [11,28,73,74].

According to the GEC-ESTRO guidelines, the high-risk clinical target volume (CTV_{HR}) should include the whole cervix at any stage and the extent of the tumor, whether in the parametrium, vagina or corpus uteri [34]. This implies the deviation from the typical symmetrical (pear shape) coverage of the target in the presence of the OARs that requires the development of the interstitial (IS) / intercavitary(IC) applicators [11]. Although helpful, the application of IS needles requires adequate training of physicians such that the plan quality depends on skill and experience of the physician inserting the needles into the appropriate positions. In the IC applications, the target can be in a position too far in the superior direction to be covered by the dose from the ovoids (or rings) (e.g., extended disease at the time of BT). That necessitates the whole coverage from the single-channel tandem, which suffers from extremely limiting fluence modulation capability. This would lead to complicated situations, in which satisfying the dose constraints to OARs, especially the bladder and sigmoid, becomes quite challenging. Innovations such as the Fletcher-Williamson applicator, (balloon) spacers, and rectal retractors [75] can help reduce the dose to OARs, but these technologies typically assist in dose limitations from the vagina, thus mostly benefiting the rectal dose at and below the cervix only. To address the latter challenge, a direction modulated brachytherapy (DMBT) tandem applicator was proposed[12]. The DMBT concept, first introduced in 2013 for the treatment of rectal cancer

[27] and later adopted for cervical cancer [12,28,34,64,76–78], is generating directional radiation beams in the area of interest through the application of high-density materials imbedded inside the applicator, which further increases the capacity for dose modulation and OARs sparing. The DMBT tandem is made of an MR compatible tungsten alloy with 6 grooves for advancing HDR sources [34], as shown in Figure 4. 1. This tandem applicator (together with ring applicator) was shown to notably improve OARs sparing [28], particularly with HDR sources with lower average energy, such as ^{169}Yb [64]. However, this design has also limited (shielding/delivery) capacity for the dose modulation and OAR sparing, because the grooves are symmetrically positioned in a fixed arrangement around the tandem (Figure 4. 1a), which further limits the maximum possible shielding/intensity modulation when treating one side due to the presence of other grooves. To overcome these limitations, we aim to propose a novel multi-channel DMBT tandem design, called *honeycomb DMBT tandem*, which allows dynamic dose delivery in a wide range of directions and provides better shielding capacity to improve coverage of nonsymmetric target and OARs sparing. In this article, we will go over the design of the honeycomb tandem and investigate the dosimetric characteristics of different (shielding) materials using Monte Carlo (MC) Simulations.

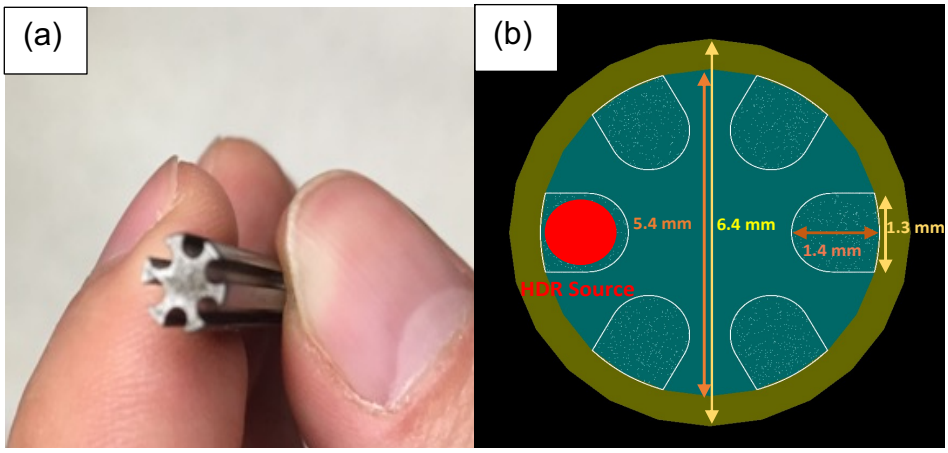

Figure 4. 1. The DMBT tandem applicator design. A successfully machined-to-specifications tungsten alloy piece (a). The transverse view of the simulated DMBT applicator in GEANT4 MC code (b), with tungsten alloy (shown in blue) covered by a sheath of PEEK (shown in yellow).

4.2 METHOD AND MATERIALS

4.2.1 The HDR source

The Varian popular widely used afterloader, namely GammaMedplus (GMP) HDR source, was modeled in the GEANT4 MC Simulation Code Toolkit 10.06, using the Boolean operations. Figure 4. 2 shows the physical dimensions and fabricating materials of the GMP source [7] and the simulated source constructions in GEANT4. As depicted, we accounted for 2 mm of wire at the distal end of the HDR sources. The ^{192}Ir source was defined based on all its significant gamma-ray and X-ray radiations [30,31]. To get the dose distribution, the source was virtually placed inside a standard water phantom 30×30×30 cm^3 and dose deposited was scored. Further details are given in section 4.2.3.

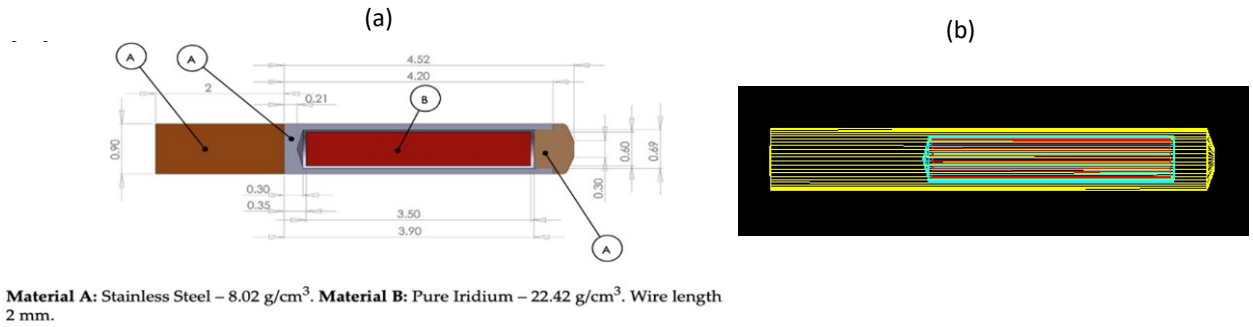

Figure 4. 2. GMP source I [7], and simulated GMP source in GEANT4 (D). The unit for the dimensions is in millimeters [mm].

4.2.2 The Honeycomb Tandem: Design and Materials

The tandem was designed using GEANT4 MC simulations to have 19 channels, each 1.1 mm in diameter and with an interchannel space of 0.1 mm, in a honeycomb arrangement inside a base with a diameter of 5.9 mm and a length of 60 mm. Three different materials were considered for the tandem base, including polyether ether ketone (PEEK) plastic, MR compatible tungsten alloy (percentage weight: 95% of pure tungsten, 3.5% nickel, and 1.5% copper) [34], and iridium. To provide dynamic directional modulation, up to 18 iridium wires with the diameter of 0.9 mm were added to the simulations to fill the channels inside the base simultaneously while allocating one channel for rooming the ^{192}Ir source

(i.e., the 19th channel). Further, a 0.3 mm crust of PEEK was considered to cover the tandem. The simulated DMBT honeycomb tandem is shown in Figure 4. 3. Physical properties and relevant information about materials used in the simulations are also given in the Table 4. 1. In addition, the attenuation characteristics of these materials were obtained from National Institute of Standards and Technology (NIST) database, using XCOM software [79].

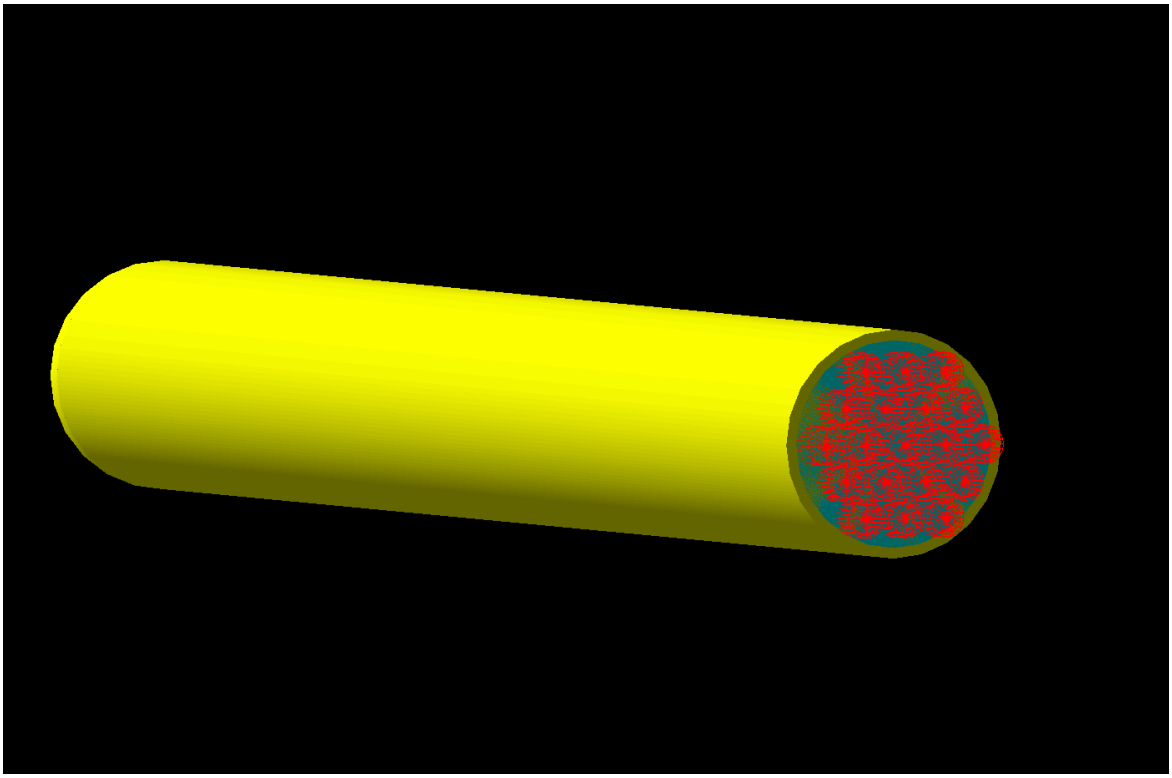

Figure 4. 3. The simulated DMBT honeycomb tandem applicator in the GEANT4 MC simulations code. The tandem base, iridium wires, and PEEK crust are shown in blue, red, and yellow, respectively.

Table 4. 1. Physical properties and relevant information about materials used in this study [77]

Materials	Atomic Number	Density (g/cm^3)	Magnetic Susceptibility (ppm)	Price/gram (USD/g)
PEEK	-	1.31	-9.33	-
Tungsten Alloy	72.77	18.01	-	0.6
Iridium	77	22.42	36.6	32.15
Water (37^o)	-	0.993	-9.05	-

4.2.3 The honeycomb tandem: dosimetry study

Three DMBT honeycomb tandems were placed virtually inside a standard water phantom with the dimension of 30×30×30 cm^3. Different arrangements of the iridium wires and GMP source inside three different bases (i.e., PEEK, tungsten alloy, and iridium) were considered, as well. To simplify the problem, for each scenario the iridium wires were considered either with their maximum possible length inside the channels (i.e., 6 cm) or out. Therefore, the number of iridium wires for each simulation varied between 0 to 18. For each configuration of the GMP source and iridium wires inside the tandem bases, 10^9 particle histories were generated and dose deposition inside the water phantom was scored with a uniform mesh size of 1 mm^3. The DMBT tandem design was also reproduced (See Figure 4. 1b) and compared to the honeycomb design.

4.3 RESULTS

4.3.1 The HDR source

The typical dose distribution of the simulated GMP ^{192}Ir source inside the water phantom is shown in Figure 4. 4, including the coronal view (Figure 4. 4a) and transvers view (Figure 4. 4b). The normalization point is 1 cm away from the center of the iridium core perpendicular to the source axis.

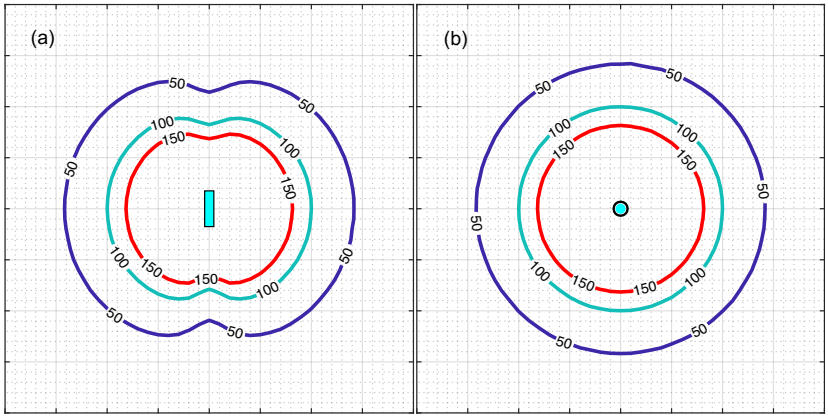

Figure 4. 4. The normalized dose distribution of the GMP ^{192}Ir source inside the water phantom, including the coronal view (a) and transverse view (b). The normalization point is 1 cm away from the center of the iridium core perpendicular to the source axis.

4.3.2 The Honeycomb Tandem: Design and Materials

The mass attenuation coefficient (MAC) of the different materials used in the simulations is also presented in Figure 4. 5. The graph shows that the MAC of iridium and tungsten alloy is similar for the photon energy higher than 300 keV. However, there is notable difference around the characteristic edges for the lower energies. It also demonstrates that the MAC of PEEK and water are similar for the photons with energy higher than 100 keV.

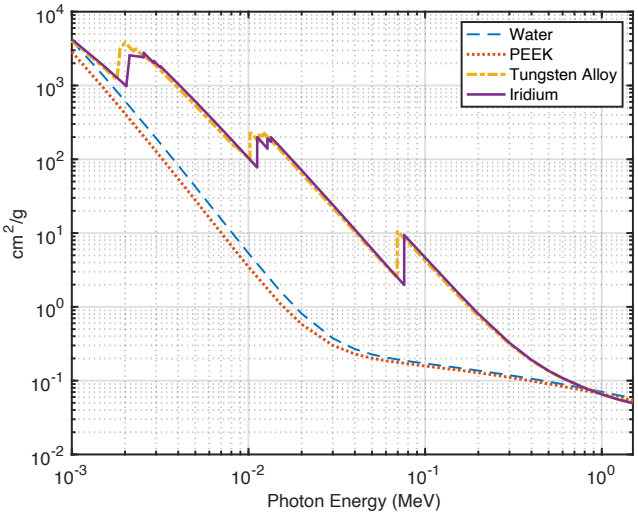

Figure 4. 5. The mass attenuation coefficient of materials used in the MC simulations

4.3.3 The honeycomb tandem: dosimetry study

Several normalized dose distributions of the honeycomb tandem with the PEEK base and different configurations of the GMP HDR source and iridium wires are given in Figure 4. 6. Each dose distribution shows a transverse plane cutting the middle of the source centered at the middle of the applicator. The normalization points are also considered to be 1 cm from the center of the applicator at a direction with the least distance from the HDR source. For each configuration, the channels are either filled with iridium wires (shown in pink) or left empty (shown in white) to achieve a variety of modulations. For example, Figure 4. 6a presents the dose distribution of the HDR source (shown in cyan) inside the honeycomb tandem applicator with PEEK base without any iridium wires. In contrast, Figure 4. 6b shows the dose distribution after inserting 18 iridium wires inside the channels, resulting in a directional modulation to the right side of the applicator. Like the tandem with the PEEK base, the normalized dose distributions of the tandem with the tungsten alloy and iridium bases are presented in Figure 4. 7 and Figure 4. 8, respectively.

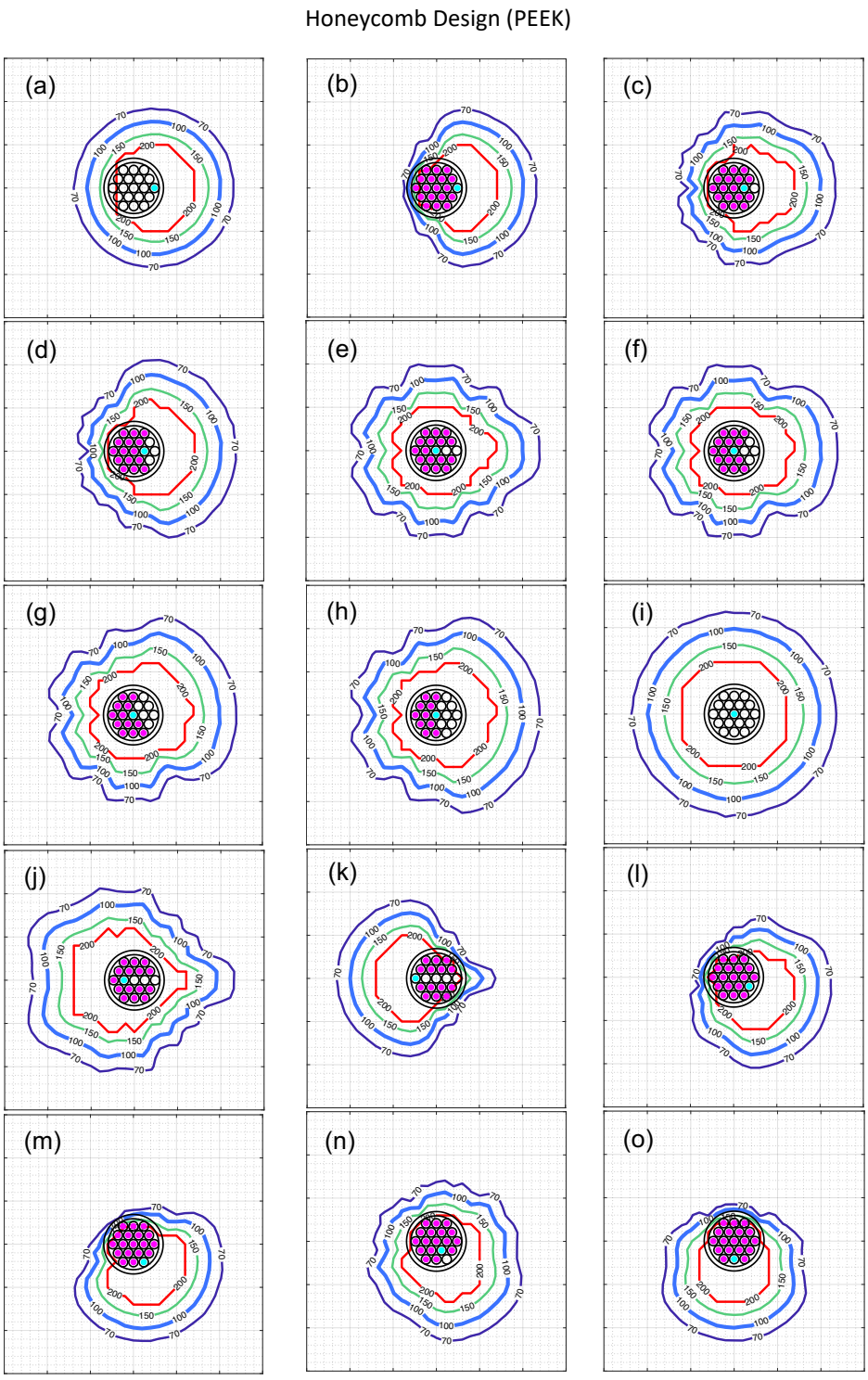

Figure 4. 6. The transverse dose distributions of the GMP source inside the honeycomb tandem with the PEEK base. The iridium wires and GMP source are demonstrated in pink and cyan, respectively. The 100 % isodose line is also shown in blue.

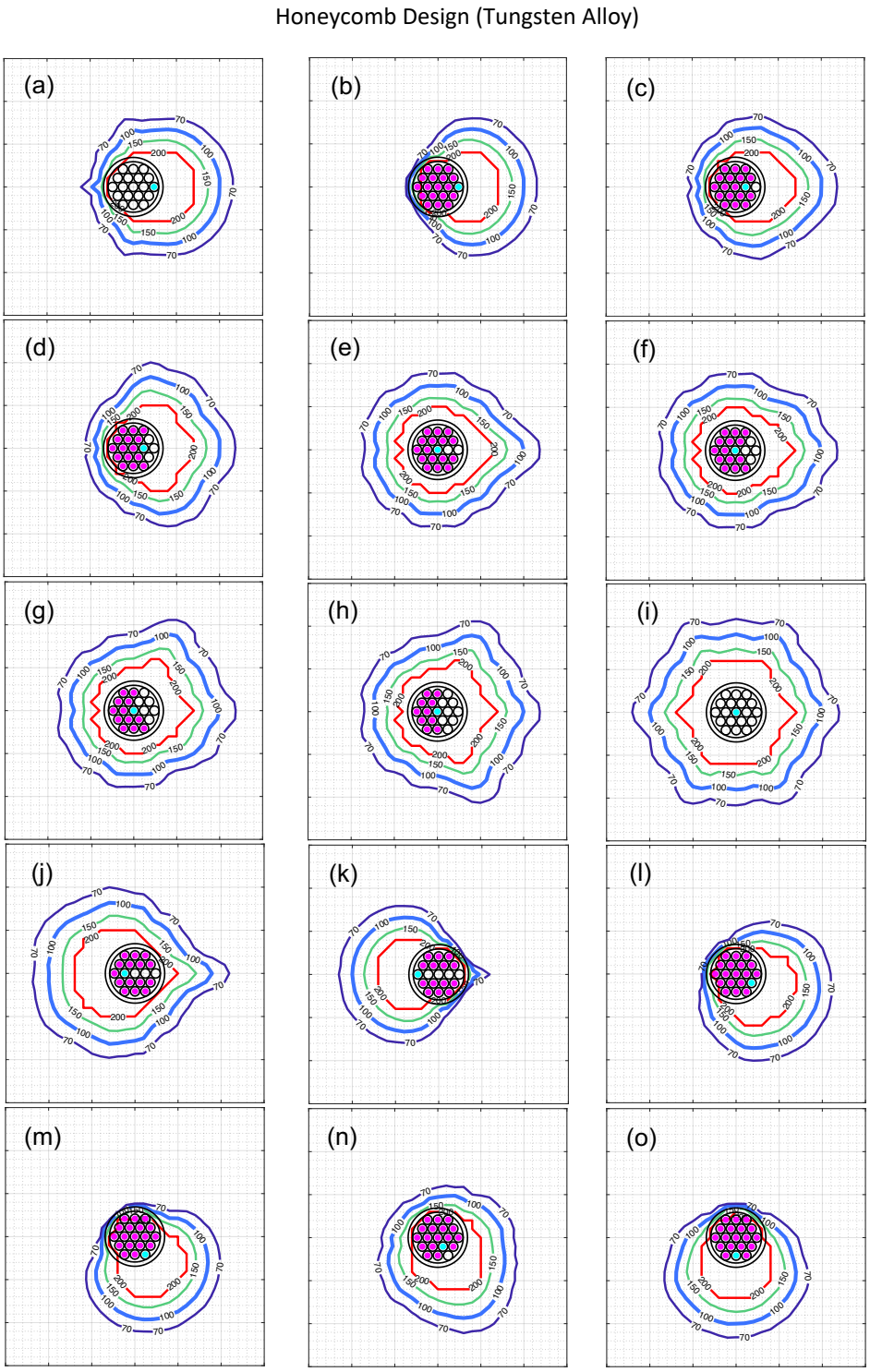

Figure 4. 7. The transverse dose distributions of the GMP source inside the honeycomb tandem with the tungsten alloy base. The iridium wires and GMP source are demonstrated in pink and cyan, respectively. The 100 % isodose line is also shown in blue.

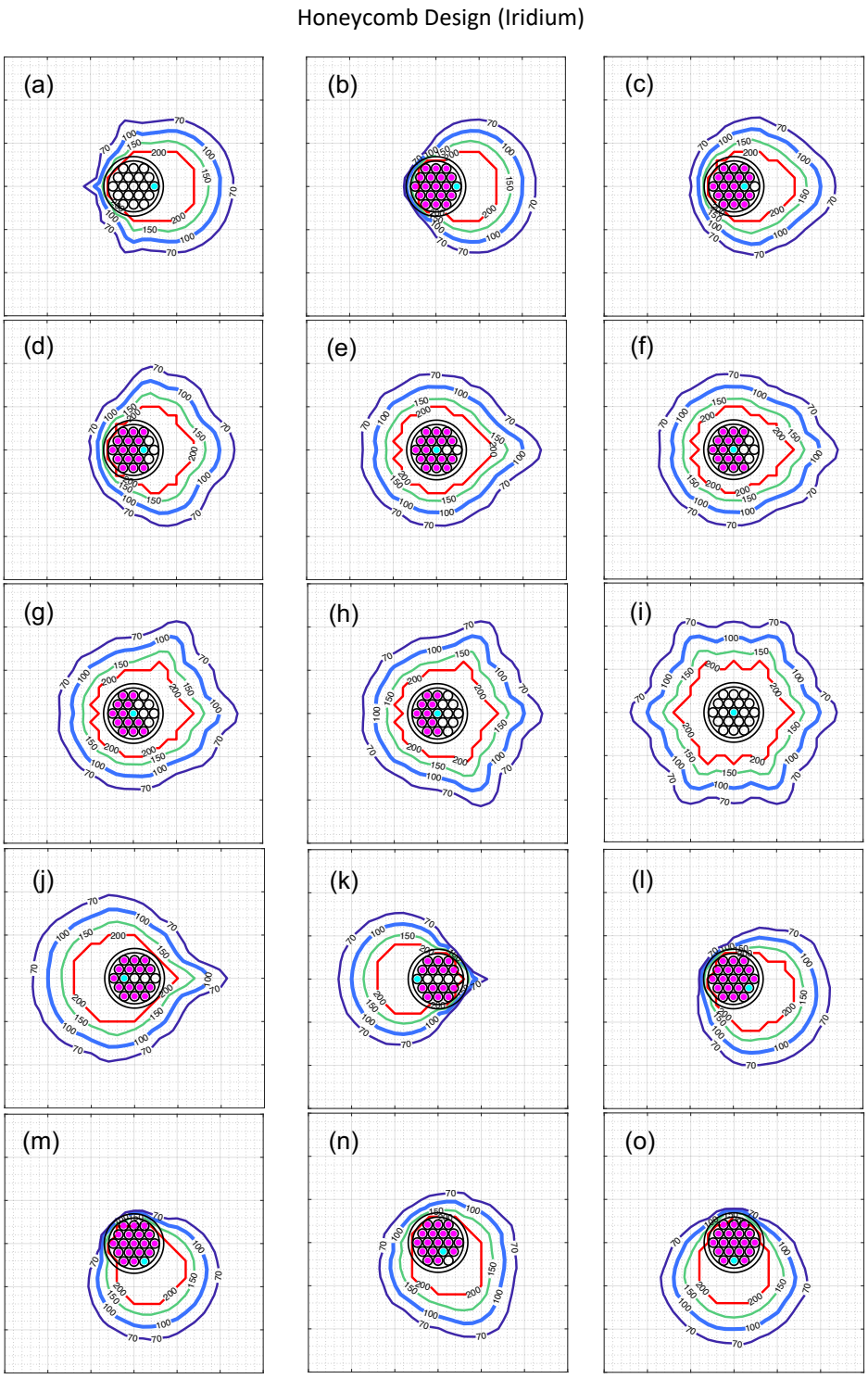

Figure 4. 8. The transverse dose distributions of the GMP source inside the honeycomb tandem with the iridium base. The iridium wires and GMP source are demonstrated in pink and cyan, respectively. The 100 % isodose line is also shown in blue.

The comparison between back spillage (radiation leakage) of the DMBT tandem design to that of the honeycomb design is also provided in Figure 4. 9. As can be observed, the backward radiation leakage has remarkably been improved in the honeycomb design (Figure 4. 9b-d). Nonetheless, the tungsten alloy (Figure 4. 9c) and iridium (Figure 4. 9d) bases rendered the least amount of the back spillage.

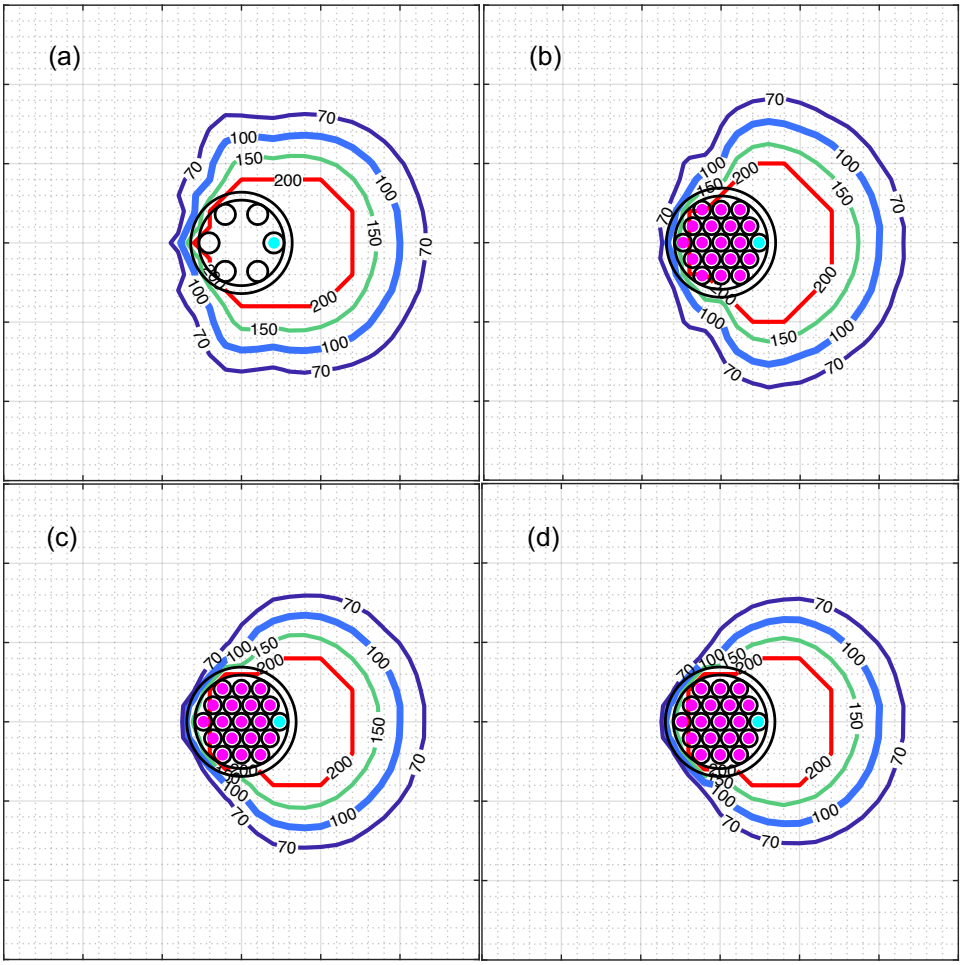

Figure 4. 9. The comparison between the back spillage of the DMBT tandem to that of the honeycomb design

The comparison between the beam directionality of the DMBT tandem to that of the honeycomb design is presented in Figure 10. As displayed, the honeycomb design with the PEEK base could slightly improve the beam directionality (Figure 4. 10b), leading to severe back spillage, in addition. However, the design with the tungsten alloy (Figure 4. 10c) and iridium (Figure 4. 10d) could outstandingly improve the beam directionality with comparable backward leakage to the DMBT design (Figure 4. 10a).

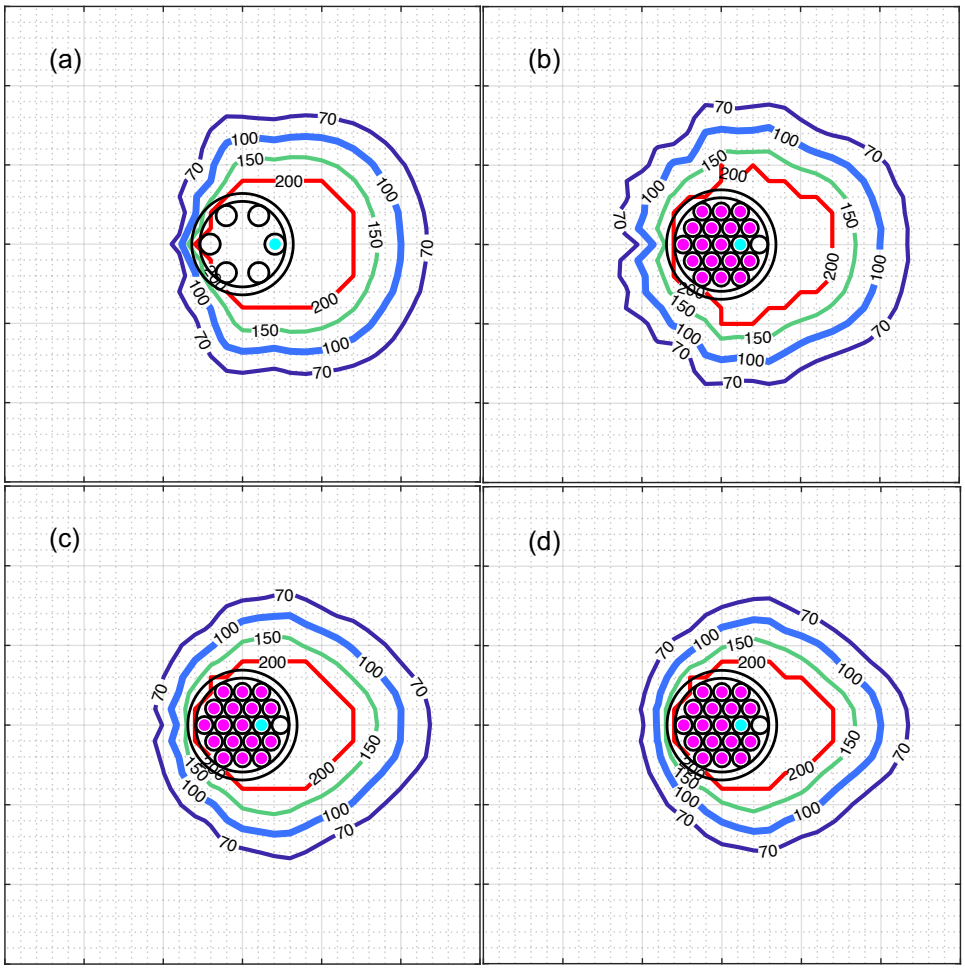

Figure 4. 10. The comparison between the beam directionality of the DMBT tandem to that of the honeycomb design

4.4 DISCUSSION

Development of the DMBT technique has been shown to be promising for the better patient care for different cancer sites including cervical cancer [5,27,28]. In this study, we introduced a new DMBT concept design (honeycomb) tandem applicator which provides a non-invasive approach for coverage of nonsymmetric target in cervical cancer. The honeycomb tandem applicator offers dynamic directional modulations through lively insertion/removal of iridium wires inside the tandem base to ultimately improve the lateral coverage of the tumor extension.

This novel design is initially a multichannel tandem applicator with 19 channels (Figure 4. 3). Therefore, considering the channel size (1.1 mm) and interchannel space (0.1 mm), there is room for shifting (the HDR source and hence) isodose lines up to 4.8 mm, from one side to the other side of the tandem at desired direction (Figures 4. 6a/4. 7a/4. 8a) compared to the traditional tandem applicator (Figure 4. 4b). Furthermore, the honeycomb pattern allows the most optimal configuration for the shielding with a minimal transmission when needed by insertion of all iridium wires while the source is located at the periphery sides, offering treatment of one side while cutting the radiation in the other side. In other words, these properties help the coverage of nonsymmetric target without overdosage of the OARs (Figures 4. 6b/4. 7b/4. 8b). Moreover, plenty of conformal dose distributions for coverage of tumor extension is achievable through the different configurations of the HDR source and the iridium wires inside the bases (Figures 4. 6-4. 8). The honeycomb design allows dose distribution of the traditional tandem applicator (Figure 4. 4b) using the PEEK base (Figure 4. 6i), as well. This is not exactly the case with the tungsten alloy and iridium bases yet, due to partial attenuation inside those materials used in the interchannel spaces and near the base periphery (Figures 4. 7i/ 4. 8i). However, this type of dose distribution has been shown to be achievable using the DMBT tandem (Figure 4. 1), through placement of the HDR source in 6 peripheral grooves [55]. Thus, according to similarity of the honeycomb design (Figure 4. 3) to the DMBT tandem at periphery sides (Figure 4. 1), tungsten alloy and Iridium bases can yield the traditional symmetrical dose distribution using the same strategy, incase needed.

Physical and dosimetric properties of three different materials used as the tandem base were also given in Table 4. 1 and Figure 4. 5. Iridium and PEEK have magnetic

susceptibility close to water, hence exhibit less artifact in MRI imaging [77]. The tungsten alloy has also been shown to have acceptable MR compatibility up to 3 T, as studied by Soliman. *et al* [34]. Therefore, there should be minimal artifacts in T2-weighted images used in clinical practice [34] with either of these materials. The tungsten alloy and iridium bases, however, showed to be significantly superior to the PEEK base for providing deeper/directional lateral coverage due to the higher density and atomic number. This characteristic can be well understood through the comparison of Figures 4. 6b/c to Figures 4. 7b/c and Figure 4. 8b/c, for example. Furthermore, beam directionality and (backward) transmission highly varies as the HDR source is placed in different peripheral channels inside the PEEK base (e.g., Figure 4. 6b versus Figure 4. 6l), because the distribution of the iridium wires inside the base is not similar in all directions. This results in an outstanding leakage through the PEEK and interchannel space for the directions with smaller numbers of iridium wires to reduce (backward) transmission. Due to excellent shielding characteristics, however, this dependence is minimal with the tungsten alloy and iridium bases, as shown in Figure 4. 7b (or 4. 8b) as opposed to Figure 4. 7l (or 4. 8l), for instance. Nevertheless, iridium offers better shielding characteristics than the tungsten alloy. Two points can help to explain this case. First, the MAC of the two is very close over the energy range from 300 keV to 1.5 MeV, as shown in Figure 5. However, since the density of the iridium (22.42 g/cm^3) is ~25% higher than the density of the tungsten alloy (18.01 g/cm^3), the total attenuation would be ~25% higher for a given thickness of iridium compared to the tungsten alloy. Second, the MAC of the iridium is notably higher near the 77 keV due to the K-edge absorption, which can effectively suppress the related X-rays in the ^{192}Ir spectrum. Therefore, iridium is a more favorable shielding material than the tungsten alloy when dealing with the ^{192}Ir source. The latter also explains the logic for utilizing the iridium wires in this study. However, iridium has inferior manufacturing properties to the tungsten alloy due to its stiffness [77]. As a result, making 19 small channels with small intervals can be really challenging on an iridium base. Besides, iridium is much more expensive than the tungsten alloy (Table 4. 1). Furthermore, iridium wires mainly regulate the shielding properties and hence intensity modulation. Consequently, the dose distributions from the honeycomb tandem with the tungsten alloy

base (Figure 4. 7) are comparable to that with the iridium base (Figure 4. 8). Thus, the tungsten alloy seems to be an optimum option for the tandem base.

The honeycomb design is also superior to the DMBT tandem. Figure 4. 9 shows that the honeycomb tandem with all bases would result in less back spillage (transmission) rather than the DMBT tandem due to better shielding design using iridium wires. However, with the PEEK tandem base (Figure 4. 9b) there would be a notable transmission in superior/ inferior directions to the HDR source, where filled with PEEK. Nonetheless, with the proposed tungsten alloy there is no such a problem as demonstrated in Figure 4. 9c. Therefore, this novel design offers treatment of the tumor extension in one lateral side, with a minimal radiation leakage in other side. Further, better beam directionality is achievable through the configuration presented in Figure 4. 10. Nevertheless, with the PEEK base there is a considerable amount of radiation leakage that limits the functionality (Figure 4. 10b). The tungsten alloy (and iridium base), however, would mitigate this problem, as demonstrated in Figure 4. 10c (and Figure 4. 10d), yielding a narrower radiation in one side with comparable leakage compared to the DMBT tandem (Figure 4. 10a). The honeycomb design would also offer 12 channels distributed out around the periphery for advancing the HDR source as opposed to the DMBT tandem with 6 fixed grooves, allowing more flexibility for the target coverage at different directions with a more effective shielding design. This characteristic would be optimal with the tungsten alloy base, allowing the similar dose distributions around the periphery, as discussed before. Therefore, the honeycomb design offers a dynamic intensity modulation all around the tandem periphery with more achievable dose distribution (Figure 4. 7), better shielding characteristics (Figure 4. 9), and beam directionality (Figure 4. 10) compared to the DMBT tandem.

The honeycomb tandem, however, is tied with complexity in the treatment planning and delivery. The treatment planning using this novel applicator can involve a lot of different configurations of iridium wires and the HDR source, each with different length of the wires inside the tandem and around the source in order to achieve the most optimal plan. In this study, we limited the configurations to either the iridium wires are inside the tandem or out, to help this issue. In addition, treatment delivery would take additional software and hardware. The treatment delivery with the honeycomb tandem would need a

dedicated patient specific QA procedure and may increase the treatment time in certain clinical scenarios, as well. Furthermore, the current design has been optimized based on the GMP source size, with a 0.9 mm diameter (Figure 4. 2). A new design would then be desirable for the other widely used Varian HDR source, namely VS2000 with a diameter of 0.6 mm, to avoid unnecessary leakage around the source. This could take a different number and/ or size of iridium wires.

Future works may include (1) the development of a knowledge-based treatment planning algorithm based upon previous clinical cases and additional/ more complex configurations of the source and iridium wires to facilitate the treatment planning, (2) manufacturing of a prototype with a tungsten alloy base and iridium wires for clinical end-to-end testing, and (3) design and manufacturing of the required hardware and software that allow the QA and radiation delivery for the clinical plans using the DMBT honeycomb tandem applicator.

4.5 CONCLUSION

We introduced a novel DMBT honeycomb tandem applicator concept-design offering dynamic intensity/direction modulation for the optimum coverage of the nonuniform target in cervical cancer. We further showed that the design would be optimum through the combination of an MR compatible tungsten alloy base and iridium wires. In addition, we indicated the honeycomb tandem superiority to a previous innovation (DMBT tandem) in terms of beam directionality and radiation leakage. Therefore, this noninvasive approach is hoped to further improve the lateral coverage, where the tumor extension might present, and the OAR sparing. The next step in the advancement of the applicator would include manufacturing of a prototype, and development of a dedicated treatment planning and delivery system.

Chapter 5. Dosimetry accuracy of a model-based dose calculation algorithm in modeling a novel direction modulated brachytherapy tandem applicator for the cervical cancer

BACKGROUND AND MOTIVES

The necessity of providing coverage for non-uniform target in cervical cancer was explained in the previous chapter. In addition, a DMBT tandem applicator was introduced as a novel non-invasive approach to address the issue while offering better OAR sparing. This tandem applicator has been recently incorporated in a model base dose calculation algorithm (MBDCA) for clinical translational research. This project aims to perform a comprehensive benchmark study to evaluate the accuracy of the TPS in modeling the DMBT tandem in dose calculations.

Per AAPM working group TG229 recommendation, there is a big need to benchmark the accuracy of such TPS against reference dosimetry. Such study would help to evaluate the uniform clinical implementation and robustness of these advance dose calculation algorithms. Moreover, it provides site specific data that may be further available for correlation with known clinical outcome.

For performing this project, a track length estimator was (TLE) develop using GEANT4 MC code for fast dose calculations. Detail of this project comes in the following sections.

Abstract

Purpose: A novel shielded tandem applicator for the direction modulated brachytherapy (DMBT) was previously introduced, which showed capability to improve the coverage of nonuniform targets and organs at risk in cervical cancer. This applicator has been recently modeled in a commercial treatment planning system (TPS - BrachyVision ACUROS^{TM} (BVA)), a Model based Dose Calculation algorithm (MBDCA), for the clinical research. In this study, we aim to benchmark the accuracy of the TPS in modeling the DMBT tandem using Monte Carlo (MC) simulations.

Methods: The DMBT tandem applicator, made of an MR compatible tungsten alloy with six symmetrical grooves covered by a sheath of PEEK plastic, was simulated in GEANT4 MC code. Subsequently, two scenarios were created using the BVA TPS and reproduced by GEANT4 MC simulations, including '*source at the center of the water phantom'* and '*source at the middle of the applicator'* for the cubical phantoms with dimensions of $(20\ cm)^3$, $(30\ cm)^3$, and $(40\ cm)^3$. A track length estimator (TLE) was then utilized to estimate the dose deposited inside the water phantoms and 2D/3D scoring were performed. Volumetric dose comparisons of the TPS against MC results were further implemented.

Results: There were different level of agreements between the TPS and MC results for the different phantom sizes. The best agreement, however, was achieved for the phantom $(40\ cm)^3$, such that the dose difference fell in the intervals [0% 8.5%] and [-6.5% 6.5%] in 95% of the voxels, for the 'source at the center of the water phantom' and 'source at the middle of the applicator', respectively. In addition, the dose difference was within 5% for all phantoms, within 5 cm from the center of the HDR sources.

Conclusion: The results of this study indicated that the accuracy of the TPS in dose calculation depends on the phantom size. Nevertheless, it seems the TPS could still provide satisfactory accuracy inside the area of clinical importance.

Keywords

Direction Modulated Brachy Therapy Tandem Applicator, Model Based Dose Calculation Algorithm, Monte Carlo Simulations

5.1 INTRODUCTION

High-Dose Rate (HDR) brachytherapy is an integral part of the standard treatment for the patients suffering from locally advanced cervical cancer, which allows dose escalation to the primary tumor, while sparing the organs at risk (OARs) including the bladder, rectum, and sigmoid because of the fast absorbed-dose fall-off [66–69.] In recent years, transition from 2D imaging and classical standard brachytherapy approaches to image guided adaptive brachytherapy (IGABT) has led to a significant change of practice, resulting in major advantages in local control and overall survival [11,63,66,70,72,80,81].

Besides the promising results, the coverage of nonsymmetric CTV_{HR} in large tumors (CTV_{HR} >30 cm^3) while sparing OARs has remained a challenging issue for performing IGABT. Consequently, the intracavitary (IC)/ interstitial (IS) brachytherapy has been considered part of the rationale for changing practice in the EMBRACE II study, leading to an emphasis on developing the state-of-the-art IC/IS applicators [11]. One of the previously proposed solely-IC solutions to this issue was a novel direction modulated brachytherapy (DMBT) tandem applicator.

The DMBT concept, first introduced in 2013 for the treatment of rectal cancer [27] and later adopted for cervical cancer [12,28,34,64,76–78], is generating directional radiation beams in the area of interest through the application of high-density materials imbedded inside the applicator, which further increases the capacity for dose modulation and OARs sparing. Therefore, the DMBT tandem (together with ring applicator) was found to decrease the D_{2cc} by up to (average) 20.1% (5.6%) for the rectum, 32.4% (2.8%) for the bladder, and 19.7% (5.4%) for sigmoid compared with standard tandem (and ring) plans, given the same target coverage [28]. The capacity for the OARs sparing was shown to be even notably improved using HDR sources with lower photon energies such as ^{169}Yb (average E=92keV) while covering the larger (CTV_{HR}>30cm^3) and irregular shape target volume[64]. Together with favorite characteristics such as MR-compatibility [34,76], clinically manageable metal artifacts in CT images [78], plan quality, affordability and machineability [77], the DMBT tandem applicator has been deemed to be the closest to clinical application for improving the cervical cancer brachytherapy [14].

This tandem applicator was also successfully modeled in the Oncentra Brachy advanced collapsed cone engine, a commercial MBDCA TPS [55]. A MBDCA offers departing from TG43 [42] water-assumed geometries by modeling radiation transport in the actual media, including tissues, applicators, and other heterogeneities resulting in a much more physically accurate reconstruction of the dose distribution actually delivered to the patient [82]. Recently, the DMBT tandem applicator has been incorporated in the BrachyVision ACUROS^{TM} (BVA) TPS, also a MBDCA, for conducting clinical research. In this work, we aim to benchmark the accuracy of the BVA in modeling the novel DMBT tandem applicator against Monte Carlo (MC) simulations, as a necessary step for the clinical research and implementation [13].

5.2 METHODS AND MATERIALS

5.2.1 The DMBT tandem: material and structure

The DMBT tandem is made of an MR compatible [34] tungsten alloy rod (percentage weight: 95% of pure tungsten, 3.5% nickel, and 1.5% copper) with a density of 18.0 g/cm^3, a thickness of 5.4 mm, and a length of 8 cm, housing 6 symmetrical peripheral grooves with 1.4 mm depth and 1.3 mm diameter. A 0.5 mm sheath of PEEK plastic covers the whole rod, in addition, such that the whole tandem applicator is 6.4 mm in diameter (Figure 5. 1).

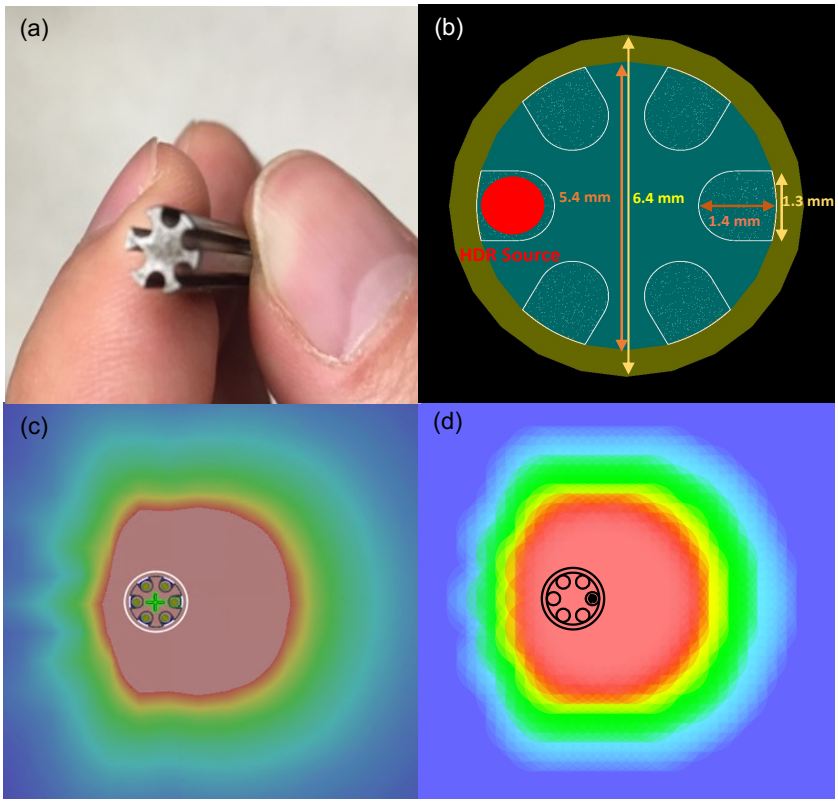

Figure 5. 1. The DMBT tandem applicator design. A successfully machined-to-specifications tungsten alloy piece (a). The transverse view of the simulated DMBT applicator in GEANT4 (b) with the corresponding dose distribution from BVA TPS (c) and MC simulation(d).

5.2.2 BrachyVision ACUROS™

In this study, BrachyVision ACUROS version 16.1 was used. In brief, ACUROS deterministically solves the linear Boltzmann transport equation (LBTE) for photons on a locally adaptive Cartesian grid [43] through fine discretization of spatial, angular, and energy variables, and then the average photon energy-fluence distribution is obtained and further converted to a dose distribution [56]. The detail information about BVA dose calculation can be found elsewhere [7,57–59].

5.2.3 Dose calculation approach

5.2.3.1 BVA set up

In BVA, three cubical digital water phantoms with the dimensions of 20 x 20 x 20 cm^3, 30 x 30 x 30 cm^3, and 40 x 40 x 40 cm^3 were created, with the intention to provide different

scattering conditions. For the benchmarking purpose, we used the popular ^{192}Ir GammamedPlus (GMP) (2012) source and considered two scenarios for three abovementioned phantoms:

(1) source at the center of the water phantom (Case 1-3)

(2) source at the middle of the applicator (Case 4-6); for this scenario the DMBT applicator was inserted from the Solid Applicator library inside each phantom separately such that the length of the applicator was along the Z axis and channels (grooves) 1 and 4 were bisected by the XZ plane, with channels 1 and 4 located in positive and negative X directions, respectively. Subsequently, the applicator was translated along Z axis such that the middle of the tungsten alloy rod was placed at the origin. In the applicator property window, the GMP (2012) source was selected as the after-loader and the source step size was set to 0.5 cm. The source was then placed at the middle of the channel 1, with first and last positions set to 3.6 cm and 3.8 cm, respectively. For an arbitrary dwell time and a source activity of 10 Ci the dose calculations were performed using ACUROS on a grid size of 201 x 201 x 201 mm^3 (mesh size of 1 mm^3) centered at the origin and the RD DICOM files were subsequently exported for the analysis. The calculation time was about 35 s for all cases.

5.2.3.2 MC simulations

The GEANT4 MC package version 10.6 was utilized for all the simulations. The Livermore physics was selected to model the electromagnetic interactions with a cut value of 0.05 mm. Detailed information about GEANT4 MC simulations and physics models can be found elsewhere [48–52]. Further, we simulated GMP(2012) as described in the BV ACUROS Algorithm reference guide [7].

The geometry of the applicator was created using the Boolean operation. The simulated GMP source and the DMBT applicator were then placed inside virtual water phantoms with the same condition as described in the ‘BVA set up’ section to reproduce the two scenarios. The collision KERMA was used to estimate dose in each voxel utilizing a linear track length estimator (TLE)[83] and 2D and 3D scoring were performed. The number of particle histories were 3×10^8 and 4×10^9, for 3D and 2D scoring, respectively.

Consequently, the statical uncertainty on average were 1% and less than 1% in 5 cm from the center of the source, for 3D and 2D scoring, respectively.

5.2.3.3 Data analysis

A 3D dose comparison was performed to assess the potential difference between the MC and ACUROS results. We first normalized the dose values of each dose matrix to the dose value at 1 cm away from the center of the source on the positive X axis. Subsequently, the dose difference in each voxel was obtained as $\Delta D = \frac{D_{\text{Acurous}} - D_{\text{MC}}}{D_{\text{MC}}} \times 100$. Histograms, scatter plots, and 2D colormap of ΔD (%) were then generated.

5.2.3.4 Scatter analysis

To compare the scattering condition, we also extracted the radial dose function, a TG43 parameter [42], based on the results from Case 1-3.

5.3 RESULTS

5.3.1 Source at the center of the water phantom (SACWP)

5.3.1.1 Case 1

Figure 5. 2 compares the MC to BVA TPS results for the phantom 20 x 20 x 20 cm^3. The ΔD (%) ranged [-7% 110%], as illustrated in the histogram (Figure 5. 2a) and scatter (Figure 5. 2b) plots. Additionally, the histogram presented a significant tendency (tail) toward the higher positive difference with a peak value around 10%. The scatter plot denoted that the dose difference goes higher for the points with the bigger distance to the center of the source (i.e., bigger r). Further, the dose difference fell inside [-1.5% 40.5%] for 95% of all voxels. The 2D color map at the XZ plane (y=0) (Figure 5. 2c) followed the same trend. Here, we limited the range of display to [-5% 50%] to allow more detail to show up in the colormap since the frequency of dose difference values above 50% were inconsequential. As presented, the dose difference fell inside the range [-5% 5%] for the region limited to [-5cm 5cm] across both the X and Z axes.

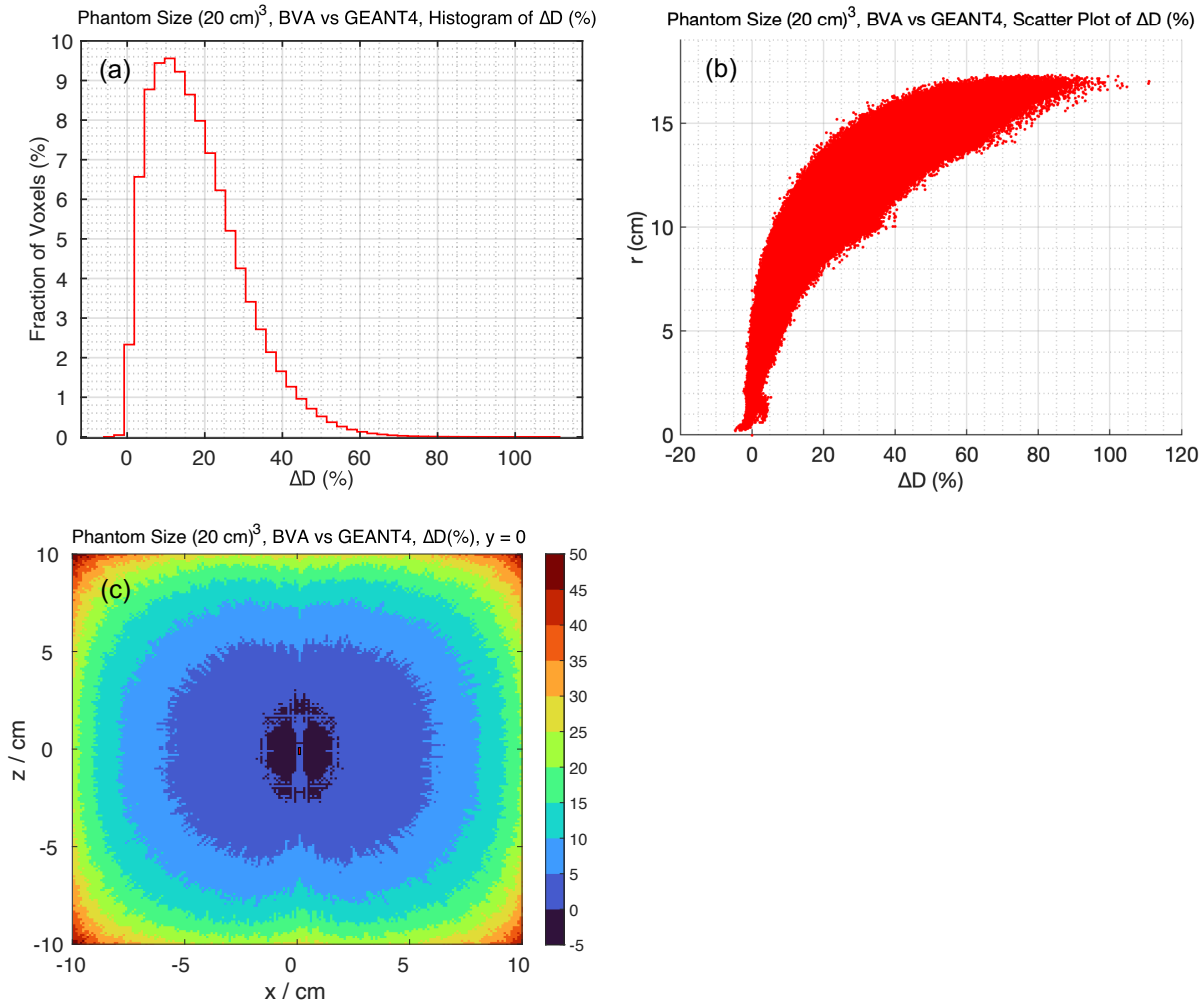

*Figure 5. 2. Dose difference, ΔD (%), between BVA TPS and GEANT4 MC simulations for the source centered at the water phantom 20 * 20 * 20 cm^3, as histogram (a), scatter plot (b), and colormap map (c) of ΔD (%).*

5.3.1.2 Case 2

The comparison between the MC and BVA TPS results for the phantom 30 x 30 x 30 cm^3 is also given in Figure 5. 3. The histogram plot (Figure 5. 3a) presented smaller tail and a shift toward the zero compared to Case 1, with a peak value around 5%. In addition, the scatter plot (Figure 5. 3b) indicated less dispersion in agreement with the histogram. Consequently, the ΔD (%) ranged [-7% 38%]. However, the TPS dose values were mostly bigger than their MC counterparts. Moreover, the dose difference fell inside the range

[0.5% 13.5%] for 95% of all voxels. The 2D color map at the XZ plane (y=0) for this case (Figure 5. 3c) showed a better agreement compared to Case 1, such that the ΔD (%) fell inside the range [-5% 5%] for the area limited to [-8cm 8cm] across the X and Z axes.

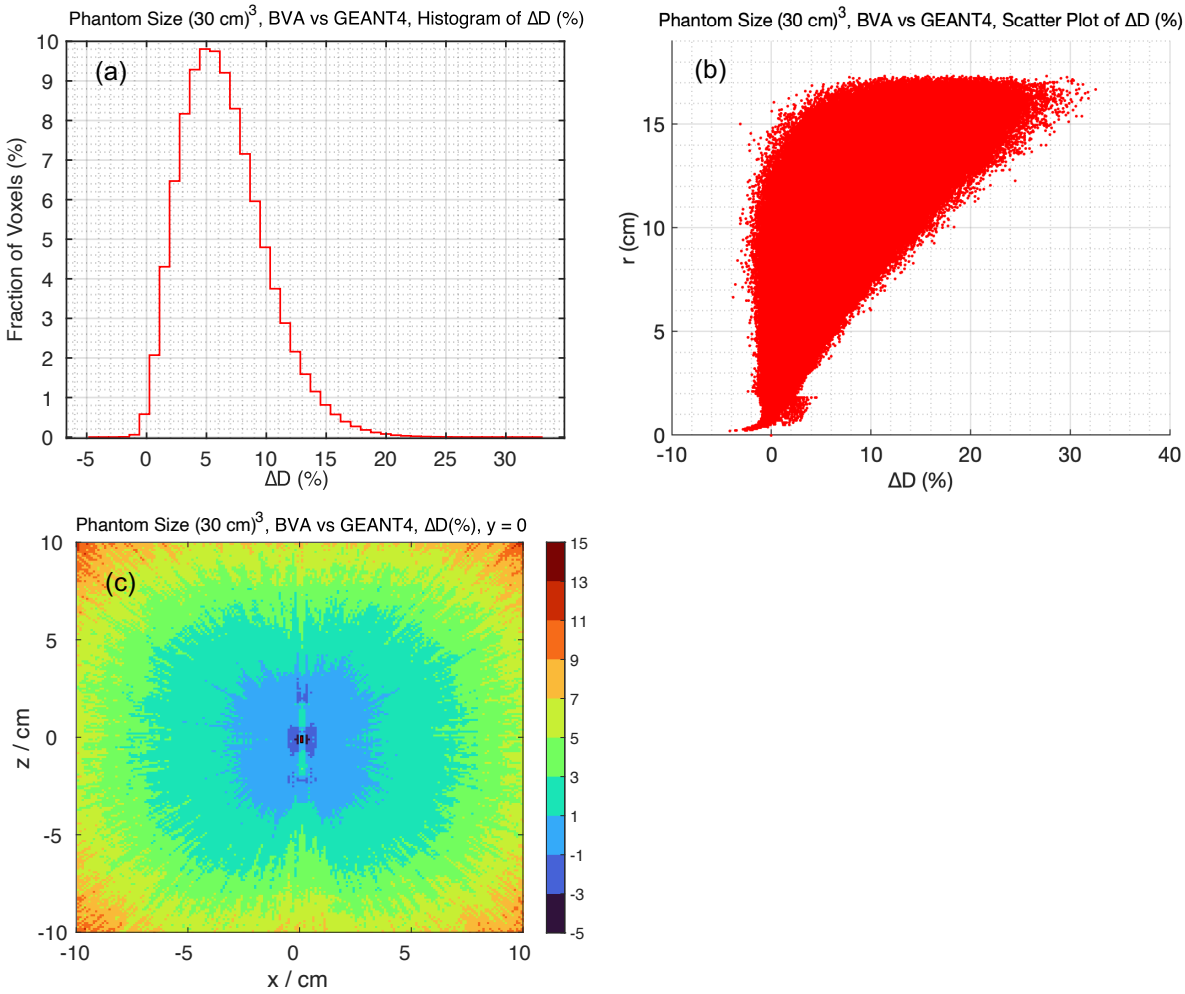

Figure 5. 3. Dose difference, ΔD (%), between BVA TPS and GEANT4 MC simulations for the source centered at the water phantom 30 x 30 x 30 cm^3 as histogram (a), scatter plot (b), and colormap map (c) of ΔD (%).

5.3.1.3 Case 3

The comparison between MC and BVA TPS for the phantom 40 x 40 x 40 cm^3 is demonstrated in Figure 5. 4. The ΔD (%) ranged [-7.5% 26%], as given in the histogram (Figure 5. 4a) and the scatter (Figure 5. 4b) plots. Unlike Case 1 and Case 2, the histogram formed a gaussian shape, with the peak value around 3%. Additionally, the

scatter plot was symmetric with less dispersion. Further, the dose difference fell inside the range [0.0% 8.5%] for 95% of all voxels. The 2D color map at the XZ plane (y=0) (Figure 5. 4c) agreed the trend as well, such that the dose difference fell inside the range [-5% 5%] for the whole plane (i.e., [-10cm 10cm]) across X and Z axes.

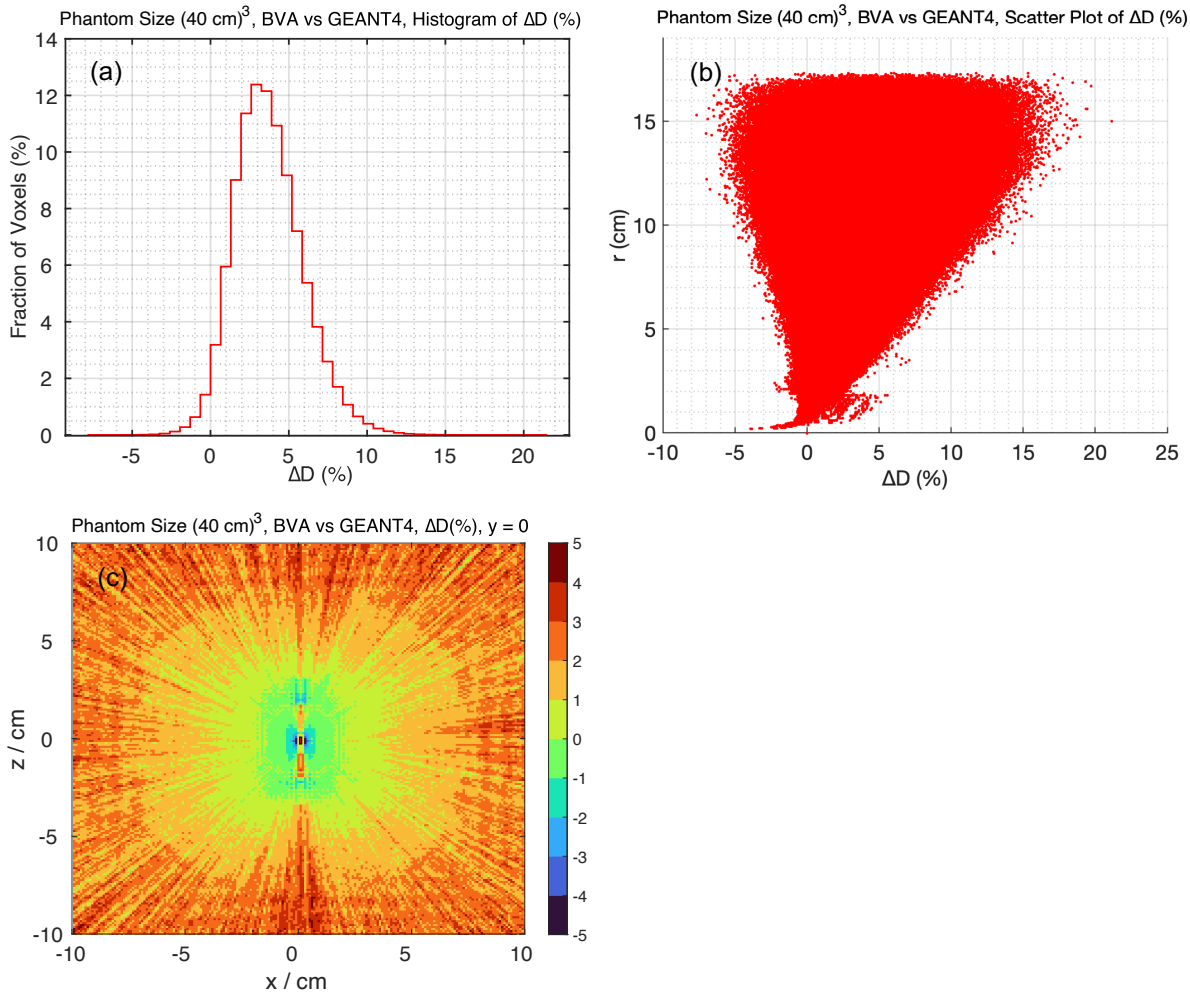

Figure 5. 4. Dose difference, ΔD (%), between BVA TPS and GEANT4 MC simulations for the source centered at the water phantom 40 x 40 x 40 cm^3, as histogram (a), scatter plot (b), and colormap map (c) of ΔD (%).

5.3.2 Source at the middle of the applicator (SAMA)

5.3.2.1 Case 4

Figure 5. 5 compares MC to BVA TPS results for the phantom 20 x 20 x 20 cm^3. The ΔD (%) ranged [-46% 125%] for both the histogram (Figure 5. 5a) and scatter (Figure 5. 5b)

plots. The histogram showed a tail toward positive values. The scatter plot indicated that the dose difference is bigger for the bigger r, as well. Yet, the agreement between MC and TPS was better for the unshielded part (black dots) compared to the shielded part (red dots).

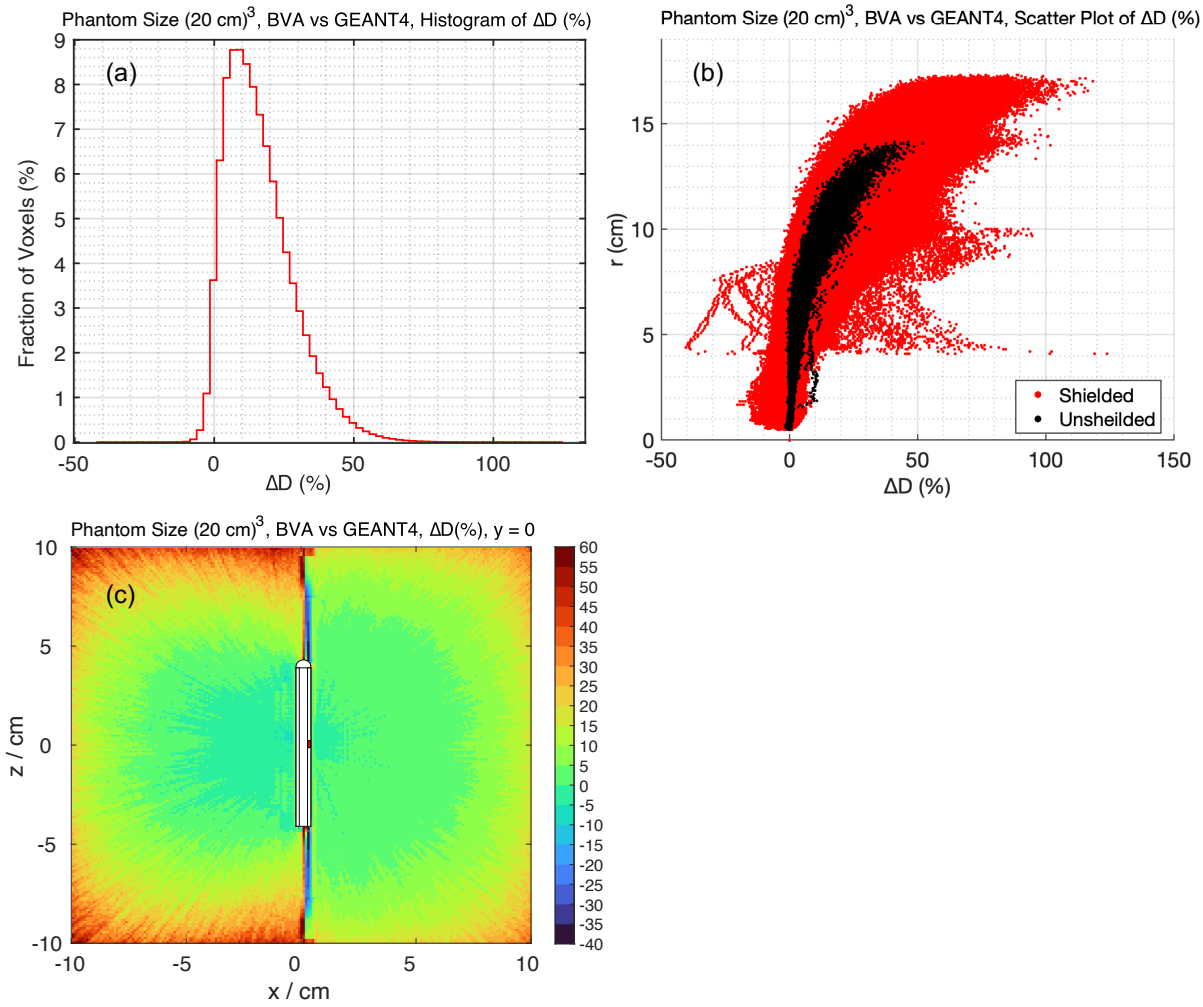

Figure 5. 5. Dose difference, ΔD (%), between BVA TPS and GEANT4 MC simulations for source at the middle of the DMBT applicator inside a water phantom 20 x 20 x 20 cm^3, as histogram (a), scatter plot (b), and colormap map (c) of ΔD (%).

In addition, the dose difference fell inside the range [-2% 41.5%] for 95% of all voxels. The 2D color map at the XZ plane (y=0) (Figure 5. 5c) followed the histogram and scatter plots of dose difference. For the shielded part, the dose difference fell inside the range [-5% 5%] for the region limited to [-5cm 0cm] and [-5cm 5cm] across the X and Z axes, respectively. For the unshielded part, however, the dose difference fell inside the range

[-5% 5%] for the region limited to [0cm 7cm] and [-7cm 7cm] across the X and Z axes, respectively. There were also two regions above and below the applicator along the channel 1 (i.e., the channel housing the HDR source), which presented notable dose differences as light/dark blue (up to -40%) followed by light/dark red (up to 60%) at the vicinity.

5.3.2.2 Case 5

The comparison between the MC and BVA TPS results for the phantom 30 x 30 x 30 cm^3 is presented in Figure 5. 6. The ΔD (%) interval included [-46% 107%], as illustrated in the histogram (Figure 5. 6a) and scatter (Figure 5. 6b) plots. The histogram had a gaussian shape with the peak around 4%. In addition, the dose difference fell inside the range [-3% 14%] for 95% of all voxels. The scatter plot indicates less dispersion for both shielded and unshielded parts, compared to Case 4, as well. Nonetheless, the agreement between MC and TPS was still better for the unshielded part (black dots). The 2D color map at the XZ plane (y=0) (Figure 5. 6c) was consistent with the histogram and scatter plots of the dose difference. For the shielded part, the dose difference fell inside the range [-5% 5%] for the region limited to [-10cm 0cm] and [-7cm 7cm] across X and Z axes, respectively. For the unshielded part, however, the dose difference ranged [-5% 5%] for the region limited to [0cm 10cm] and [-9cm 9cm] across X and Z axes, respectively. There were also two regions above and below the applicator along the channel 1, which indicated notable dose differences as light/dark blue (up to -40%) followed by light/dark red (up to 60%) at the vicinity, like Case 4. Nevertheless, the area covered by light/dark red was smaller in size compared to Case 4.

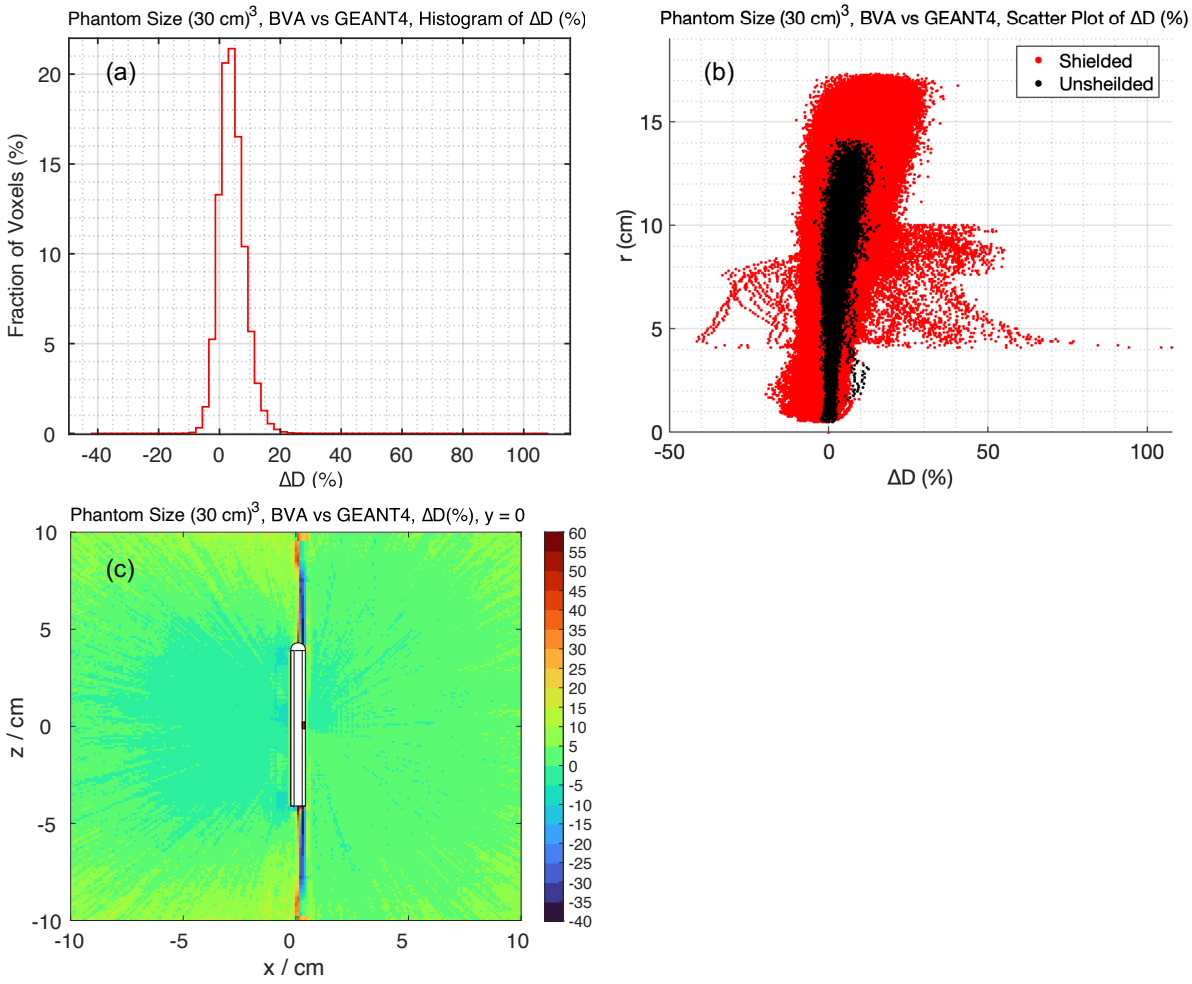

*Figure 5. 6. Dose difference, ΔD (%), between BVA TPS and GEANT4 MC simulations for source at the middle of the DMBT applicator inside a water phantom 30 * 30 * 30 cm^3, as histogram (a), scatter plot (b), and colormap map (c) of ΔD (%).*

5.3.2.3 Case 6

The comparison between MC and BVA TPS results for the phantom 40 x 40 x 40 cm^3 is presented in Figure 5. 7. The ΔD (%) interval was [-46% 107%] as given in the histogram (Figure 5. 7a) and scatter (Figure 5. 7b) plots. The histogram had a gaussian shape with the peak around 1%. In addition, the dose difference fell inside the range [-6.5% 6.5%] for 95% of all voxels. The scatter plot indicated less dispersion for both shielded and unshielded parts compared to both Case 4 and Case 5. However, the agreement between

MC and TPS was better for the unshielded part (black dots) compared to the shielded part (red dots).

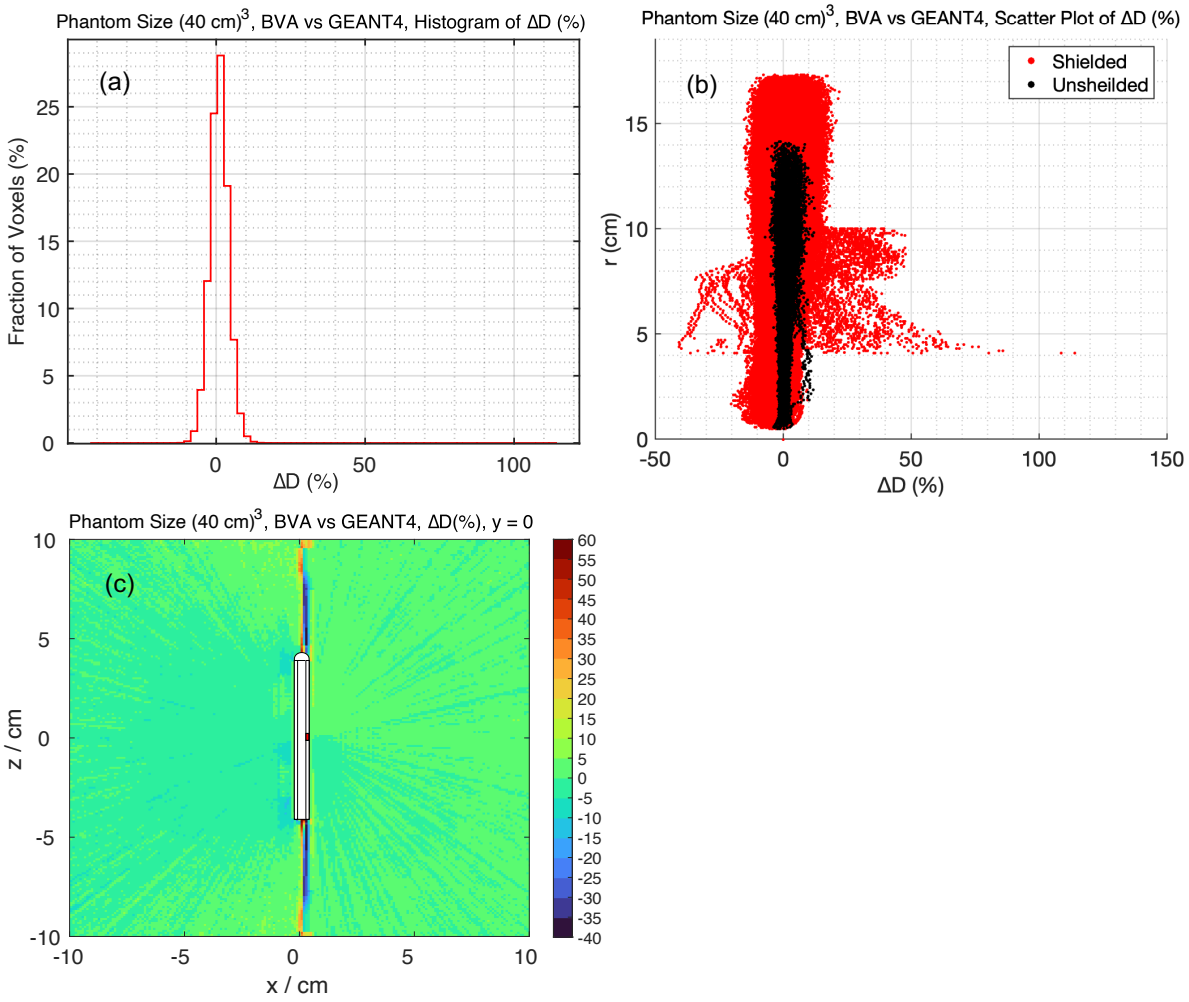

*Figure 5. 7. Dose difference, ΔD (%), between BVA TPS and GEANT4 MC simulations for source at the middle of the DMBT applicator inside a water phantom 40 * 40 * 40 cm^3, as histogram (a), scatter plot (b), and colormap map (c) of ΔD (%).*

The 2D color map at the XZ plane (y=0) (Figure 5. 6c) agreed with the histogram and scatter plots of the dose difference. The dose difference fell inside [-5% 5%] for the whole plane across X and Z axes, but there were regions above and below the applicator along the channel 1, which showed notable dose differences as light/dark blue (up to -40%) followed by light/dark red (up to 60%) at the vicinity, like Case 4 and Case 5.

Nevertheless, the area covered by light/dark was smaller in size compared to both Case 4 and Case 5.

5.3.2.4 Scatter analysis

The radial dose function, g(r), obtained from the Case 1-3 results, is given in Figure 8. As displayed, there was no difference in g(r) for the data from the BVA TPS.

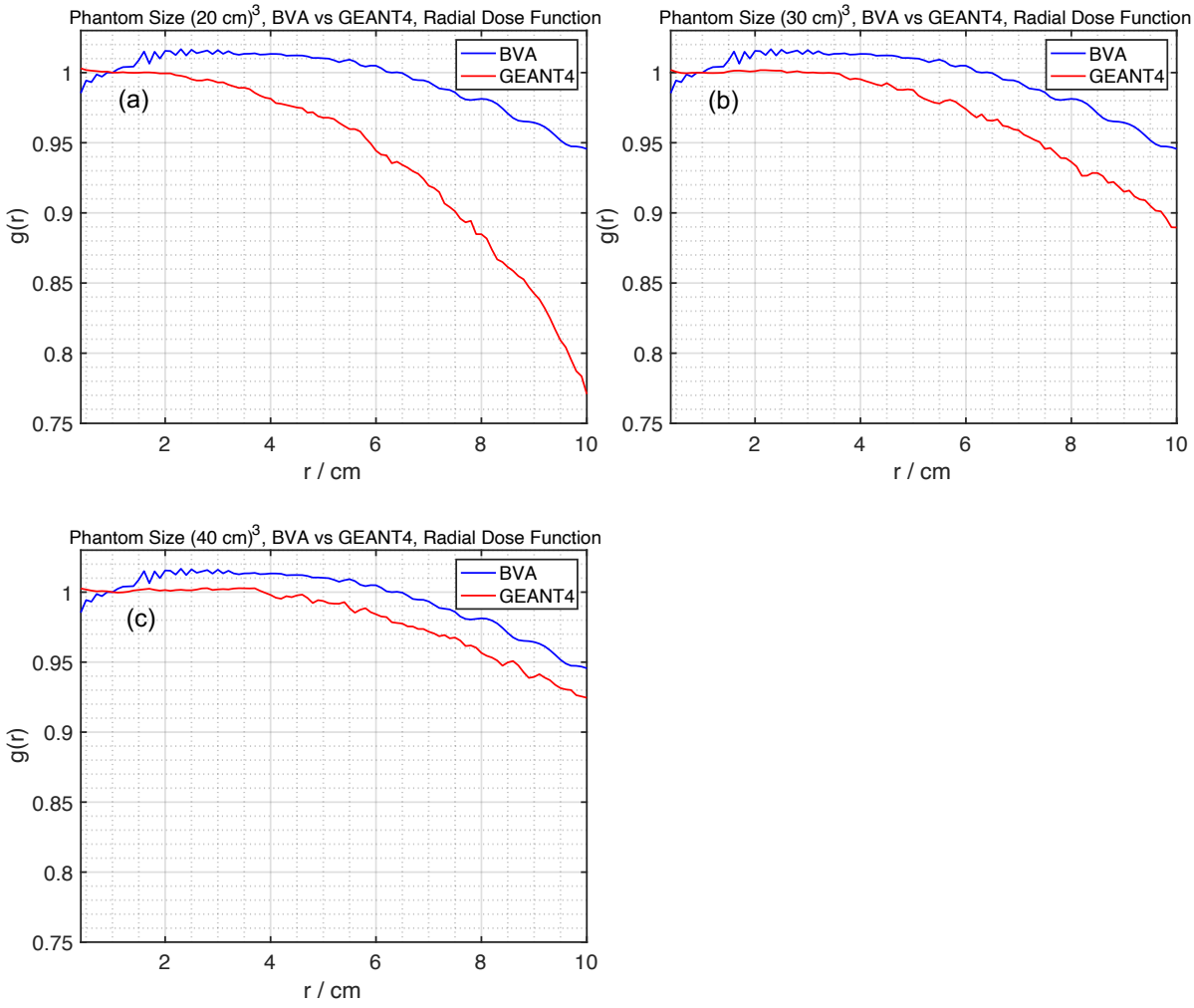

Figure 5. 8. Radial dose function, g(r). Comparison between BVA and GEANT4 for the phantom sizes, 20 x 20 x 20 cm^3, (a), 30 x 30 x 30 cm^3, (b), and 40 x 40 x 40 cm^3, (c).

However, g(r) varied significantly among the different phantoms (with different sizes) for the data extracted from GEANT4 MC simulations. The point of consideration is that as the size of the phantoms increases, g(r) shows a notable growth for r > 2 cm. Furthermore, the maximum difference between the two data set (i.e., MC vs BVA) at r = 10 cm was approximately 19%, 6%, and 2% for the phantoms 20 x 20 x 20 cm^3, 30 x 30 x 30 cm^3, and 40 x 40 x 40 cm^3, respectively.

5.4 DISCUSSION

In this study, we benchmarked the accuracy of the MBDCA BVA TPS in modeling the novel DMBT tandem applicator. Although such MBDCAs can account for heterogeneity and deliver fast dose calculations for clinical purposes, the lack of related extensive dosimetric data for different sites (hence applicators) has been a limiting factor, such that TG43 formalism is still widely used for the dose specifications. That necessitates collecting site-specific dosimetric data for correlation with known clinical outcomes[10], mainly when dealing with shielded applicators such as the DMBT tandem.

Here, we studied two different scenarios which allowed to assess the accuracy of the BVA TPS in two different conditions: (1) when dealing with the TG43 approach (i.e., the SACWP scenario) and (2) when accounting for the DMBT tandem (Figure 5. 1) heterogeneity, which includes the MR compatible tungsten alloy, the air inside the grooves, and the PEEK plastic sheath (i.e., the SAMA scenario). We also investigated the different phantom sizes to benchmark the accuracy of the TPS when dealing with different scattering conditions.

5.4.1 The SACWP Cases

We achieved different levels of agreement between the TPS and MC simulation results for the different phantom sizes. The worst agreement was for the phantom 20 x 20 x 20 cm^3 (Figure 5. 2), in which the dose difference showed a notable tendency toward the positive values (Figure 5. 2a&b). In other words, ΔD was strongly dependent on the

distance from the HDR source, r, such that for r > 5 cm, the dose difference exceeded 5 %. Consequently, ΔD recorded 20% at r = 10 cm (Figure 5. 2c). However, there was a substantial improvement in the agreement between the TPS and MC results for the phantom sizes 30 x 30 x 30 cm^3 (Figure 5. 3) and 40 x 40 x 40 cm^3 (Figure 5. 4). The histograms formed a Gaussian shape (Figures 5. 3a & 5. 4a), and the scatter plots showed less dispersion (Figures 5. 3b & 5. 4b). The 2D color plots presented a better agreement for the voxels far from the source, in addition, such that at r = 10 cm, the dose differences were 7% and 3% for Case 2 and Case 3, respectively (Figures 5. 3c & 5. 4c). Therefore, the general trend denoted a severe phantom size dependency when comparing the TPS and MC results. This dependence can be explained using the scatter analysis given in this study (section 5.3.2.4). The scattering condition depends on the phantom size and can be well examined using the radial dose function, g(r) [13,42,57]. While the TPS results rendered no difference in the radial dose function for the different phantom sizes, the MC results led to prominent changes in g(r) for the three phantoms (Figure 5. 8). The difference in g(r)/ ΔD between the TPS and MC at r = 10 cm were also 19% / 20%, 6% / 7%, and 2% / 3% for the phantom sizes $(20\ cm)^3$, $(30\ cm)^3$, and $(40\ cm)^3$, respectively. In addition, the best agreement between the TPS and MC was obtained for the phantom with side length of 40 cm, which yields 'quasi' full scattering condition [13] (Figure 5. 4). This indicates that the BVA TPS considers a full/fixed scattering condition for dose calculations. However, there was still few percent difference between the TPS and MC results near the cube sides, for the phantom size $(40\ cm)^3$ (Figure 5. 8c). This discrepancy could also be in part due to deviation from an ideal scattering condition inside a phantom with infinite size that affects interactions near the cube sides. Statistical uncertainty could be the other contributor, as well.

5.4.2 The SAMA Cases

There was close similarity between these cases and the SACWP ones, such that the agreement between the TPS and MC results implied a significant phantom size dependence (Figures 5. 5-5. 7). Nevertheless, there were a few differences as following: First, there was a better agreement between the TPS and MC results for the unshielded part compared to the shielded part as mentioned in the result section (Figures 5. 5b & 5.

6b & 5. 7b). Furthermore, the areas covering the range [-5% 5%] of dose difference across the X and Y axes in the unshielded parts were bigger than those in the shielded parts and their SACWP counterparts, particularly for the phantom sizes $(20\ cm)^3$ and $(30\ cm)^3$ (compare Figure 5. 5c to Figure 5. 2c, for example). Here, the point of consideration is that the scattering condition is quite different for the SAMA cases as opposed to SACWP ones, due to the presence of high-density tungsten alloy in the virtual water phantoms. Further, the primary beam exiting from the shielded part is different from the unshielded part. Since BVA utilizes a preset configuration to discretize energy (i.e., to put the radiation beam into the different energy bins (groups) and weight them), any change in scattering/ primary beams can affect average energy on the energy bins, and hence the calculated dose values. Therefore, these changes have somehow improved the agreement in the unshielded parts and worsened the agreement in the area far from the source in the shielded area compared to the SACWP counterparts (for example, compare the red/green areas between Figure 5. 2c and Figure 5. 5c). Nevertheless, since the overall agreement improves as the phantom sizes increase, as shown in Figure 5. 5c compared to Figure 5. 6c and Figure 5. 7c, the root cause of this discrepancy should be mainly due to difference in the scattering condition.

Second, there were two regions located superiorly/ inferiorly to the applicator along the channel 1 for the SAMA cases, showing a remarkable ΔD as blue (cold, up to -40) and red (hot, up to 60%) for all phantom sizes (Figures 5. 5c & 5. 6c & 5. 7c). There are two points for this inconsistently. (1) There were no such regions for the SACWP counterparts which represent a TG43 environment for the dose calculations (Figures 5. 2c & 5. 3c & 5. 4c). (2) These regions are located near the applicator (made of tungsten alloy with a cover of PEEK plastic) along the channel 1 which is very small in size (1.3 mm * 1.4 mm) and filled with the air. Therefore, it seems the TPS results suffer from a systematic error due to one or more discretization that BVA utilizes, in a very heterogenous environment such that the cold and hot regions are in close proximity. These regions have also shown up with very low frequency on the histograms and scatter plots (see Figures 5. 7a & 5. 7b, for example).

Third, the SAMA histograms (also scatter plots) displayed more converged ΔD compared to the SACWP counterparts with less tendency toward the higher positive results,

regardless of very low frequency regions (compare Figure 5. 3a to Figure 5. 6a, for example). The reason for this issue is also related to the difference in the scattering condition as explained before. Therefore, as the size of the phantoms increase and scattering condition approaches the full scatter condition, the SAMA histograms demonstrates better agreement between the TPS and MC results versus the SACWP counterparts (compare Figures 5. 3a/ 5. 4a to Figures 5. 6a / 5. 7a). Consequently, for the phantom 40 x 40 x 40 cm^3, with a quasi-full scattering condition, the SAMA / SACWP histograms have gaussian shapes with peak values at 1% / 5%. Although the deviation from 0% could be in part due to statistical uncertainty, the bigger dose difference for the SACWP (i.e., 5%) should be mainly due to deviation from a real full scattering condition. Results presented in this study demonstrated a remarkable discrepancy compared to the previous studies by Ma *et al* [56] and Ballester *et al* [9], in which they benchmarked the accuracy of the BVA TPS in modeling a generic HDR source and applicator using a phantom with a side length of 20 cm. Two scenarios introduced in this study have been taken care of in those two studies. Although there are few differences in the methodologies including the difference in the particle histories for MC simulations and the analysis methods, there should have been some agreement in the (local) dose difference within the uncertainty levels between Case 1 (i.e., SACWP, 20 cm) and Case 4 (i.e., SAMA, 20 cm) from this study compared to 'source centered in water' and 'source centered in applicator' from those studies, respectively. There is, however, a difference in the TPS version utilized in this study (version 16.1) versus those studies (version 13.0). The average time for dose calculation in this version for all the cases was ~ 35 s compared to ~ 120 s mentioned by Ballester *et al* [9]. The calculation time has been reported in study by Zourari *et* al, as well [57], in which they stated the TPS (version 8.8) calculation times on the order of 2 min (120 s) on a Quad-Core Xeon E5420/2.5 GHz processor for a dose reporting grid covering a 30 cm diameter sphere with the voxel size of 1 mm^3. The calculations in this study were performed on a Dual-Core Xeon Silver 4110/2.1 GHz. Therefore, the calculation time is much faster (~ 4 times) for the latest version (16.1). Additionally, the scatter analysis presented in this study indicated that the scattering condition is quite similar among all phantom sizes for the data obtained from the BVA TPS. A as result, this disagreement could be due to the difference in the TPS version with

different preset configurations for the dose calculations. In other words, the version 16.1 provides much faster dose calculation, but also assumes a fixed full scattering condition, which can compromise the accuracy (i.e., $|\Delta D\ (\%)| > 5$) when dealing with the smaller phantom (or patient) size (i.e., length side (size) of 20 cm) for the area far from the center of the HDR source (i.e., r >=5), as demonstrated in Figures 5. 2c & 5. 5c.

The current study presented a thorough assessment of the BVA TPS in the modeling of the DMBT tandem applicator. Nonetheless, the results are limited to the given specific conditions (and scenarios). Therefore, a future study may include multiple dwell positions inside the DMBT tandem based on the clinical plans. Such a study may result in less phantom size dependency and improve the overall agreement including the above-mentioned systematic errors between the TPS and reference data.

5.5 CONCLUSION

The comparison between the BVA TPS and MC results for different scenarios indicated that the accuracy of the TPS in dose calculation notably depends on the phantom size. However, even for the worst-case scenario (i.e., phantom size $(20\ cm)^3$) there was an agreement range [-5% 5%] within 5 cm from the center of the HDR source. Therefore, it seems the TPS could still render sufficient accuracy for the region of clinical importance.

Chapter 6. Future works

Future works have been specifically mentioned at the end of chapters 2-5. Nonetheless, it is worth stating/emphasizing on another area of research that can be very helpful for supporting the DMBT/IMBT technique in GYN BT.

All the applicators discussed in this dissertation were designed based on ^{192}Ir HDR sources. Since the size of shielding materials in DMBT applicators, such as honeycomb design, is very limited (up to some millimeters), research focusing on development of new HDR sources with lower photon energies can be valuable. Such novel BT sources may improve the beam directionality and radiation leakage in DMBT applicators, resulting in better target coverage and potentially less radiation toxicity.

Reference:

1. Centers for Disease Control and Prevention (CDC). What Is Gynecologic Cancer? https://www.cdc.gov/cancer/gynecologic/basic_info/what-is-gynecologic-cancer.htm.
2. JOHNS HOPKINS MEDICINE. Gynecologic Cancers. https://www.hopkinsmedicine.org/health/conditions-and-diseases/gynecologic-cancers.
3. Medicine, S. O. F. & Oncology, R. Intracavitary Brachytherapy for Gynecologic Malignancies: Applications and Innovations. (2015).
4. Khan, F. M. & Gibbons, J. P. *Khan's the Physics of Radiation Therapy*. *Oral and Maxillofacial Surgery* (Wolters Kluwer, 2014). doi:10.1016/B978-1-4160-4389-8.50098-4.
5. Meftahi, M., Fields, E., Guy, C. & Song, W. Y. The Design of a Novel Direction Modulated Brachytherapy Vaginal Cylinder Applicator for Optimizing Coverage of the Apex. *Med. Phys.* 1–10 (2022) doi:10.1002/mp.15666.
6. Dagli, A., Yurt, F. & Yegin, G. Evaluation of BrachyDose Monte Carlo code for HDR brachytherapy: Dose comparison against Acuros®BV and TG-43 algorithms. *J. Radiother. Pract.* **19**, 76–83 (2020).
7. Varian Medical Systems. Acuros BV Algorithm Reference Guide- B504878R01A. *Varian Med. Syst. Palo Alto, CA2013* 1–33 (2013).
8. Guy, C. L. *et al.* The vaginal cylinder: Misunderstood, misused, or trivial? An in-depth dosimetric and multiinstitutional outcome investigation. *Brachytherapy* **18**,

763–770 (2019).

9. Ballester, F. *et al.* A generic high-dose rate 192Ir brachytherapy source for evaluation of model-based dose calculations beyond the TG-43 formalism. *Med. Phys.* **42**, 3048–3062 (2015).
10. Morcos, M., Viswanathan, A. N. & Enger, S. A. On the impact of absorbed dose specification, tissue heterogeneities, and applicator heterogeneities on Monte Carlo-based dosimetry of Ir-192, Se-75, and Yb-169 in conventional and intensity-modulated brachytherapy for the treatment of cervical cancer. *Med. Phys.* **48**, 2604–2613 (2021).
11. Pötter, R. *et al.* The EMBRACE II study: The outcome and prospect of two decades of evolution within the GEC-ESTRO GYN working group and the EMBRACE studies. *Clin. Transl. Radiat. Oncol.* **9**, 48–60 (2018).
12. Han, D. Y. *et al.* Direction-modulated brachytherapy for high-dose-rate treatment of cervical cancer. I: Theoretical design. *Int. J. Radiat. Oncol. Biol. Phys.* **89**, 666–673 (2014).
13. Perez-Calatayud, J. *et al. Dose calculation for photon-emitting brachytherapy sources with average energy higher than 50 keV: Report of the AAPM and ESTRO*. *Medical Physics* vol. 39 (2012).
14. Cunha, J. A. M. *et al.* Brachytherapy Future Directions. *Semin. Radiat. Oncol.* **30**, 94–106 (2020).
15. Small, W. *et al.* American Brachytherapy Society consensus guidelines for adjuvant vaginal cuff brachytherapy after hysterectomy. *Brachytherapy* **11**, 58–67 (2012).

16. Demiral, S. Evaluation of Organ-At-Risk (OAR) Sparing in Vaginal Cuff Boost Treatment for Endometrial Cancer using Stereotactic Body Radiotherapy (SBRT) and Brachytherapy. *Cancer Ther. Oncol. Int. J.* **7**, 52–57 (2017).

17. Alban, G. M. *et al.* Low-Dose Adjuvant Cylinder Brachytherapy for Endometrioid Endometrial Cancer. *Pract. Radiat. Oncol.* **10**, 95–103 (2020).

18. Petereit, D. G., Tannehill, S. P., Grosen, E. A., Hartenbach, E. M. & Schink, J. C. Outpatient vaginal cuff brachytherapy for endometrial cancer. *Int. J. Gynecol. Cancer* **9**, 456–462 (1999).

19. Zhang, H., Donnelly, E. D., Strauss, J. B. & Qi, Y. Therapeutic analysis of high-dose-rate 192Ir vaginal cuff brachytherapy for endometrial cancer using a cylindrical target volume model and varied cancer cell distributions. *Med. Phys.* **43**, 483–494 (2016).

20. Sorbe, B. *et al.* External pelvic and vaginal irradiation versus vaginal irradiation alone as postoperative therapy in medium-risk endometrial carcinoma - A prospective randomized study. *Int. J. Radiat. Oncol. Biol. Phys.* **82**, 1249–1255 (2012).

21. Wortman, B. G. *et al.* Ten-year results of the PORTEC-2 trial for high-intermediate risk endometrial carcinoma: improving patient selection for adjuvant therapy. *Br. J. Cancer* **119**, 1067–1074 (2018).

22. Sharma, S. D., Bianchi, C., Conte, L., Novario, R. & Bhatt, B. C. Radiochromic film measurement of anisotropy function for high-dose-rate Ir-192 brachytherapy source. *Phys. Med. Biol.* **49**, 4065–4072 (2004).

23. Bahadur, Y. A. *et al.* Single versus multichannel applicator in high-dose-rate

vaginal brachytherapy optimized by inverse treatment planning. *J. Contemp. Brachytherapy* **6**, 362–370 (2014).

24. Sabater, S. *et al.* Vaginal cuff brachytherapy in endometrial cancer - a technically easy treatment? *Cancer Manag. Res.* **9**, 351–362 (2017).
25. Shin, S. M. *et al.* Use of a flexible inflatable multi-channel applicator for vaginal brachytherapy in the management of gynecologic cancer. *Front. Oncol.* **5**, 1–7 (2015).
26. Semeniuk, O., Cherpak, A. & Robar, J. Design and evaluation of 3D printable patient-specific applicators for gynecologic HDR brachytherapy. *Med. Phys.* 1–11 (2021) doi:10.1002/mp.14888.
27. Webster, M. J. *et al.* HDR brachytherapy of rectal cancer using a novel grooved-shielding applicator design. *Med. Phys.* **40**, 1–10 (2013).
28. Han, D. Y. *et al.* Direction Modulated Brachytherapy for Treatment of Cervical Cancer. II: Comparative Planning Study With Intracavitary and Intracavitary–Interstitial Techniques. *Int. J. Radiat. Oncol. Biol. Phys.* **96**, 440–448 (2016).
29. Safigholi, H. *et al.* Direction modulated brachytherapy (DMBT) for treatment of cervical cancer: A planning study with 192Ir, 60Co, and 169Yb HDR sources. *Med. Phys.* **44**, 6538–6547 (2017).
30. Chu, S. Y. ., Ekström, L. . & Firestone, R. . Table of Radioactive Isotopes. *The Lund/LBNL Nuclear Data Search* http://nucleardata.nuclear.lu.se/toi/nuclide.asp?iZA=770192 (1999).
31. X-ray and Gamma-ray Decay Data Standards for Detector Calibration and Other Applications. *IAEA* https://www-nds.iaea.org/xgamma_standards/ (2005).

32. Ababneh, E., Dababneh, S., Qatarneh, S. & Wadi-Ramahi, S. Enhancement and validation of Geant4 Brachytherapy application on clinical HDR 192Ir source. *Radiat. Phys. Chem.* **103**, 57–66 (2014).

33. Kim, Y., Cabel, K. & Sun, W. Does the apex optimization line matter for single-channel vaginal cylinder brachytherapy planning? *J. Appl. Clin. Med. Phys.* **19**, 307–312 (2018).

34. Soliman, A. S. *et al.* Quantitative MRI assessment of a novel direction modulated brachytherapy tandem applicator for cervical cancer at 1.5 T. *Radiother. Oncol.* **120**, 500–506 (2016).

35. Chapman, C. H. *et al.* MRI-based evaluation of the vaginal cuff in brachytherapy planning: Are we missing the target? *Int. J. Radiat. Oncol. Biol. Phys.* **95**, 743–750 (2016).

36. Ager, B. J. *et al.* Do vaginal recurrence rates differ among adjuvant vaginal brachytherapy regimens in early-stage endometrial cancer? *Brachytherapy* **18**, 453–461 (2019).

37. Chapman, C. H., Cunha, J. A. M., Littell, R. D., Chen, L. & Hsu, I.-C. J. High-dose-rate brachytherapy for vaginal endometrial cancer recurrence after surgery and prior radiotherapy. *Gynecol. Oncol.* **159**, e25 (2020).

38. Sapienza, L. G. *et al.* Detection of air gaps around the cylinder by postinsertion computed tomography in vaginal cuff brachytherapy: A prospective series, systematic review, and meta-analysis. *Brachytherapy* **18**, 620–626 (2019).

39. Skinner, L. B. *et al.* Intensity modulated Ir-192 brachytherapy using high-Z 3D printed applicators. *Phys. Med. Biol.* **65**, (2020).

40. Webster, M. J. *et al.* Dynamic modulated brachytherapy (DMBT) for rectal cancer. *Med. Phys.* **40**, 1–12 (2013).

41. Abe, K. *et al.* Impact of a commercially available model-based dose calculation algorithm on treatment planning of high-dose-rate brachytherapy in patients with cervical cancer. *J. Radiat. Res.* **59**, 198–206 (2018).

42. Rivard, M. J. *et al.* Update of AAPM Task Group No. 43 Report: A revised AAPM protocol for brachytherapy dose calculations. *Med. Phys.* **31**, 633–674 (2004).

43. Mikell, J. K. *et al.* Impact of heterogeneity-based dose calculation using a deterministic grid-based boltzmann equation solver for intracavitary brachytherapy. *Int. J. Radiat. Oncol. Biol. Phys.* **83**, e417–e422 (2012).

44. Rivard, M. J., Melhus, C. S., Granero, D., Perez-Calatayud, J. & Ballester, F. An approach to using conventional brachytherapy software for clinical treatment planning of complex, Monte Carlo-based brachytherapy dose distributionsa. *Med. Phys.* **36**, 1968–1975 (2009).

45. Rodrigues, S. S. O. F., Begalli, M., De Queiroz Filho, P. P. & De Souza Santos, D. Monte carlo simulation of an Ir-192 brachytherapysourcespectra, geometryand anysotropy factors using geant4 code. *IEEE Nucl. Sci. Symp. Conf. Rec.* 860–863 (2008) doi:10.1109/NSSMIC.2008.4774530.

46. Tian, Z. *et al.* Monte Carlo dose calculations for high-dose-rate brachytherapy using GPU-accelerated processing. *Brachytherapy* **15**, 387–398 (2016).

47. Mikell, J. K. & Mourtada, F. Dosimetric impact of an 192 Ir brachytherapy source cable length modeled using a grid-based Boltzmann transport equation solver. *Med. Phys.* **37**, 4733–4743 (2010).

48. Pérez-Calatayud, J., Lliso, F., Carmona, V., Ballester, F. & Hernández, C. Monte Carlo calculation of dose rate distributions around 0.5 and 0.6 mm in diameter 192Ir wires. *Med. Phys.* **26**, 395–401 (1999).

49. Arce, P. *et al.* Report on G4-Med, a Geant4 benchmarking system for medical physics applications developed by the Geant4 Medical Simulation Benchmarking Group. *Med. Phys.* **48**, 19–56 (2020).

50. Collaboration, G. *Book For Application Developers*. (2017).

51. Geant4 Collaboration. Guide For Physics Lists. 65 (2020).

52. Ballester, F., Granero, D., Perez-Calatayud, J., Venselaar, J. L. M. & Rivard, M. J. Study of encapsulated 170Tm sources for their potential use in brachytherapy. *Med. Phys.* **37**, 1629–1637 (2010).

53. Daskalov, G. M., Baker, R. S., Rogers, D. W. O. & Williamson, J. F. Dosimetric modeling of the microselectron high-dose rate 192Ir source by the multigroup discrete ordinates method. *Med. Phys.* **27**, 2307–2319 (2000).

54. Ballester, F., Hernández, C., Pérez-Calatayud, J. & Lliso, F. Monte Carlo calculation of dose rate distributions around 192Ir wires. *Med. Phys.* **24**, 1221–1228 (1997).

55. Safigholi, H., van Veelen, B., Niatsetski, Y. & Song, W. Y. Modeling of the direction modulated brachytherapy tandem applicator using the Oncentra Brachy advanced collapsed cone engine. *Brachytherapy* **17**, 1030–1036 (2018).

56. Ma, Y. *et al.* A generic TG-186 shielded applicator for commissioning model-based dose calculation algorithms for high-dose-rate 192Ir brachytherapy: *Med. Phys.* **44**, 5961–5976 (2017).

57. Zourari, K. *et al.* Dosimetric accuracy of a deterministic radiation transport based 192Ir brachytherapy treatment planning system. Part I: Single sources and bounded homogeneous geometries. *Med. Phys.* **37**, 649–661 (2010).

58. Petrokokkinos, L. *et al.* Dosimetric accuracy of a deterministic radiation transport based I 192 r brachytherapy treatment planning system. Part II: Monte Carlo and experimental verification of a multiple source dwell position plan employing a shielded applicator. *Med. Phys.* **38**, 1981–1992 (2011).

59. Zourari, K. *et al.* Dosimetric accuracy of a deterministic radiation transport based 192Ir brachytherapy treatment planning system. Part III. Comparison to Monte Carlo simulation in voxelized anatomical computational models. *Med. Phys.* **40**, 1–9 (2013).

60. Angelopoulos, A., Baras, P., Sakelliou, L., Karaiskos, P. & Sandilos, P. Monte Carlo dosimetry of a new 192Ir high dose rate brachytherapy source. *Med. Phys.* **27**, 2521–2527 (2000).

61. Taylor, R. E. P. & Rogers, D. W. O. EGSnrc Monte Carlo calculated dosimetry parameters for 192Ir and 169Yb brachytherapy sources. *Med. Phys.* **35**, 4933–4944 (2008).

62. Kirisits, C. *et al.* Review of clinical brachytherapy uncertainties: Analysis guidelines of GEC-ESTRO and the AAPM. *Radiother. Oncol.* **110**, 199–212 (2014).

63. Sturdza, A. *et al.* Image guided brachytherapy in locally advanced cervical cancer: Improved pelvic control and survival in RetroEMBRACE, a multicenter cohort study. *Radiother. Oncol.* **120**, 428–433 (2016).

64. Safigholi, H. *et al.* Direction modulated brachytherapy (DMBT) for treatment of cervical cancer: A planning study with 192Ir, 60Co, and 169Yb HDR sources: A. *Med. Phys.* **44**, 6538–6547 (2017).

65. Yip, W. W. L., Wong, J. S. Y., Lee, V. W. Y., Wong, F. C. S. & Tung, S. Y. Throwing the dart blind-folded: Comparison of computed tomography versus magnetic resonance imaging-guided brachytherapy for cervical cancer with regard to dose received by the 'actual' targets and organs at risk. *J. Contemp. Brachytherapy* **9**, 446–452 (2017).

66. Haie-Meder, C. *et al.* Recommendations from Gynaecological (GYN) GEC-ESTRO Working Group (I): Concepts and terms in 3D image based 3D treatment planning in cervix cancer brachytherapy with emphasis on MRI assessment of GTV and CTV. *Radiother. Oncol.* **74**, 235–245 (2005).

67. International Commission on Radiation Units and Measurements. *Prescribing, Recording, and ReporInternational Commission on Radiation Units and Measurements. (2013). Prescribing, Recording, and Reporting Brachytherapy for Cancer of the Cervix (ICRU report 89). Journal of the ICRU (Vol. 13). http://doi.org/10.1093/jic*. *Journal of the ICRU* vol. 13 (2013).

68. Han, K., Milosevic, M., Fyles, A., Pintilie, M. & Viswanathan, A. N. Trends in the utilization of brachytherapy in cervical cancer in the United States. *Int. J. Radiat. Oncol. Biol. Phys.* **87**, 111–119 (2013).

69. Banerjee, R. & Kamrava, M. Brachytherapy in the treatment of cervical cancer: A review. *Int. J. Womens. Health* **6**, 555–564 (2014).

70. Pötter, R. *et al.* Recommendations from gynaecological (GYN) GEC ESTRO

working group (II): Concepts and terms in 3D image-based treatment planning in cervix cancer brachytherapy - 3D dose volume parameters and aspects of 3D image-based anatomy, radiation physics, radiobiolo. *Radiother. Oncol.* **78**, 67–77 (2006).

71. Hellebust, T. P. *et al.* Recommendations from Gynaecological (GYN) GEC-ESTRO working group: Considerations and pitfalls in commissioning and applicator reconstruction in 3D image-based treatment planning of cervix cancer brachytherapy. *Radiother. Oncol.* **96**, 153–160 (2010).
72. Dimopoulos, J. C. A. *et al.* Recommendations from Gynaecological (GYN) GEC-ESTRO Working Group (IV): Basic principles and parameters for MR imaging within the frame of image based adaptive cervix cancer brachytherapy. *Radiother. Oncol.* **103**, 113–122 (2012).
73. Pötter, R. *et al.* Present status and future of high-precision image guided adaptive brachytherapy for cervix carcinoma. *Acta Oncol. (Madr).* **47**, 1325–1336 (2008).
74. Mazeron, R. *et al.* Dose–volume effect relationships for late rectal morbidity in patients treated with chemoradiation and MRI-guided adaptive brachytherapy for locally advanced cervical cancer: Results from the prospective multicenter EMBRACE study. *Radiother. Oncol.* **120**, 412–419 (2016).
75. Rai, B. *et al.* Bladder-rectum spacer balloon in high-dose-rate brachytherapy in cervix carcinoma. *Int. J. Radiat. Oncol. Biol. Phys.* **85**, e217–e222 (2013).
76. Soliman, A. S., Owrangi, A., Ravi, A. & Song, W. Y. Metal artefacts in MRI-guided brachytherapy of cervical cancer. *J. Contemp. Brachytherapy* **8**, 363–369 (2016).
77. Safigholi, H., Han, D. Y., Soliman, A. & Song, W. Y. Direction modulated

brachytherapy (DMBT) tandem applicator for cervical cancer treatment: Choosing the optimal shielding material. *Med. Phys.* **45**, 3524–3533 (2018).

78. Elzibak, A. H. *et al.* Quantitative CT assessment of a novel direction-modulated brachytherapy tandem applicator. *Brachytherapy* **17**, 465–475 (2018).
79. National Institute of Standards and Technology (NIST). XCOM. *https://physics.nist.gov/PhysRefData/Xcom/html/xcom1.html*.
80. Charra-Brunaud, C. *et al.* Impact of 3D image-based PDR brachytherapy on outcome of patients treated for cervix carcinoma in France: Results of the French STIC prospective study. *Radiother. Oncol.* **103**, 305–313 (2012).
81. Okazaki, S. *et al.* Dose-volume parameters and local tumor control in cervical cancer treated with central-shielding external-beam radiotherapy and CT-based image-guided brachytherapy. *J. Radiat. Res.* **60**, 490–500 (2019).
82. Beaulieu, L. *et al.* Report of the Task Group 186 on model-based dose calculation methods in brachytherapy beyond the TG-43 formalism: Current status and recommendations for clinical implementation. *Med. Phys.* **39**, 6208–6236 (2012).
83. Williamson JF. Monte Carlo evaluation of kerma at a point for photon transport problems.pdf. *Med. Phys.* **14**, 567–76 (1987).